Institut für Erd-und Umweltwissenschaften
Mathematisch-Naturwissenschaftliche
Fakultät Universität Potsdam

Geochemistry of Variscan lamprophyre magmatism in the Saxo-Thuringian Zone

Kumulative Dissertation
zur Erlangung des akademischen Grades
"doctor rerum naturalium"
(Dr. rer. nat.)
in der Wissenschaftsdisziplin " Geochemistry "

eingereicht an der
Mathematisch-Naturwissenschaftlichen Fakultät
der Universität Potsdam

von
Khaled Mohamed Abdelfadil

Potsdam, im June 2013

Published online at the
Institutional Repository of the University of Potsdam:
URL http://opus.kobv.de/ubp/volltexte/2013/6885/
URN urn:nbn:de:kobv:517-opus-68854
http://nbn-resolving.de/urn:nbn:de:kobv:517-opus-68854

Abstract

Lamprophyres are mantle-derived magmatic rocks, commonly occurring as dikes. They are readily identified from their field setting, petrography, chemical and mineralogical composition. These rocks not only provide important information on melting processes in the mantle, but also on geodynamic processes modifying the mantle. There are numerous occurrences of lamprophyres in the Saxo-Thuringian Zone of Variscan Central Europe, which are useful to track the variable effects of the Variscan orogeny on local mantle evolution.

This work presents and evaluates the mineralogical, geochemical, and Sr-Nd-Pb isotopic data of late-Variscan calc-alkaline lamprophyres, post-Variscan ultramafic lamprophyres, of alkaline basalt from Lusatia, and, for comparison, of pre-Variscan gabbros. In addition, lithium isotopic signatures combined with Sr-Nd-Pb isotopic data of late-Variscan calc-alkaline lamprophyres from three different Variscan Domains (i.e., Erzgebirge, Lusatia, and Sudetes) are used to assess compositional changes of the mantle during Variscan orogeny.

$^{40}Ar/^{39}Ar$ dating of Variscan calc-alkaline lamprophyres from Lusatia was performed to precisely define the ages of magmatic activity. The new ages show that the lamprophyres from Lusatia were emplaced during the late stage of the Variscan orogeny. Ages are in the same range as those for calc-alkaline lamprophyres from the adjacent Erzgebirge and Sudetes.

The pre- and late-Variscan mantle beneath Lusatia was sampled by gabbroic and calc-alkaline lamprophyric melts, respectively. The related magmatic rocks should record changes in mantle composition related to Variscan orogenic processes. Major and trace element compositions as well as isotopic compositions of pre-Variscan tholeiitic gabbros (c. 400 Ma) from Lusatia indicate that these rocks originated from a mantle source that had initially been modified by Cadomian subduction-related metasomatism at c. 570 Ma, which led to the enrichment of LREE and LILE relative to primitive mantle. Crustal contributions to the gabbro source in the mantle are also evident from certain trace element ratios (i.e., Nb/U, Ce/Pb, Th/La, Sm/La and Ba/Nb) which resemble crustal rather than mantle signatures.

The mantle beneath Lusatia has been metasomatised again during the Variscan orogeny. This is demonstrated by the Late Variscan calc-alkaline lamprophyres (spessartites) with strong crustal signatures as indicated by their contents and ratios of

incompatible elements, and their Sr-Nd-Pb isotopic compositions. These trace element and isotopic signatures depart markedly more from primitive mantle signatures than those of the pre-Variscan gabbros, indicating a repeated enrichment of the mantle source during the Variscan orogeny.

The post-Variscan ultramafic lamprophyre and alkaline basaltic dikes of Lusatia have been derived from an enriched mantle source and their trace-element patterns are similar to those of the Lusatian late-Variscan calc-alkaline lamprophyres. This shows that the Variscan mantle beneath Lusatia has been repeatedly reactivated in late- and post-Variscan time. Melting and re-melting of this metasomatised mantle source is related to large-scale reorganization of the local stress field and to crustal thinning and mantle upwelling in the waning stages of the Variscan orogeny.

The spatial variation of subducted material and the regionally contrasting tectonic regime during the Variscan orogeny have been traced using late-Variscan calc-alkaline lamprophyres from different domains of the northern Bohemian Massif (Erzgebirge, Lusatia, Sudetes). Li-Nd-Pb-Sr isotopic compositions, Li contents, and trace element signatures of these rocks document the heterogeneity of late-Variscan mantle sources. This heterogeneity is best explained by contrasting compositions of subducted material during the Variscan event. The new data indicate that the material subducted during the Variscan convergence is dominated by altered oceanic crust underneath Lusatia, by sediments underneath the Erzgebirge, and by a mixture of both end-member compositions in the Sudetes.

Zusammenfassung

Lamprophyre sind porphyrische, aus Mantelschmelzen gebildete Gesteine, die meist in Form von Gängen auftreten. Sie zeichnen sich durch auffällige und charakteristische texturelle, chemische und mineralogische Eigenschaften aus. Als ehemalige Mantelschmelzen liefern sie Information sowohl über Bedingungen der Schmelzbildung im Mantel als auch über geodynamische Prozesse, die zu metasomatischer Veränderung des Mantels geführt haben. Im Saxothuringikum Mitteleuropas, am Nordrand des Böhmischen Massivs, gibt es zahlreiche Lamprophyrvorkommen, die hier zur Charakterisierung der Mantelentwicklung während der variszischen Orogenese dienen.

Die vorliegende Arbeit befaßt sich mit den mineralogischen, geochemischen und isotopischen (Sr-Nd-Pb) Signaturen von spätvariszischen kalkalkalischen Lamprophyren, von postvariszischen ultramafischen Lamprophyren, von Alkalibasalten der Lausitz und, zum Vergleich, von prävariszischen Gabbros. Darüberhinaus nutzt die Arbeit Lithium-Isotopensignaturen kombiniert mit Sr-Nd-Pb–Isotopendaten spätvariszischer kalkalkalischer Lamprophyre aus drei variszischen Domänen (Erzgebirge, Lausitz, Sudeten) zur Erkundung der lokalen Mantelüberprägungen während der variszischen Orogenese.

Zur genauen Festlegung der Intrusionsalter kalkalkalischer Lamprophyre der Lausitz wurden $^{40}Ar/^{39}Ar$-Datierungen durchgeführt. Die neuen Altersdaten zeigen, daß diese Lamprophyre in einem späten Stadium der variszischen orogenen Entwicklung gebildet wurden, und zwar praktisch gleichzeitig mit den kalkalkalischen Lamprophyren des Erzgebirges und der Sudeten.

In der Lausitz treten sowohl prävariszische Mantelschmelzen in Form von Gabbros als auch spätvariszische Mantelschmelzen in Form von kalkalkalischen Lamprophyren auf. Ein Vergleich der entsprechenden Gesteine sollte Hinweise auf eventuelle variszische metasomatische Überprägungen des Mantels liefern. Haupt- und Spurenelementdaten und isotopische Zusammensetzungen prävariszischer (~400 Ma) tholeiitischer Gabbros der Lausitz zeigen eine Anreicherung des prävariszischen Mantels an LREE und LILE. Diese Anreicherung geht auf eine cadomische (~570 Ma) subduktionsbezogene Metasomatose ehemals primitiven Mantels zurück. Spurenelementverhältnisse, die zur Unterscheidung von Krusten- und Mantelsignaturen dienen (Nb/U, Ce/Pb, Th/La, Sm/La und Ba/Nb), zeigen ebenfalls

eine signifikante Zufuhr von Material der Erdkruste zur Magmenquelle der Gabbros an.

Im Bereich der Lausitz ist der lokale Erdmantel während der variszischen Orogenese ein weiteres Mal chemisch überprägt worden. Hinweise darauf liefern spätvariszische kalkalkalische Lamprophyre (Spessatite). Diese belegen sehr deutliche krustale Beiträge zur Magmenquelle, mit stark krustal geprägten Sr-Nd-Pb-Isotopensignaturen und Spurenelementverhältnissen. Die krustale Signatur ist hier deutlich stärker ausgeprägt als in den prävariszischen Gabbros, was auf eine erneute subduktionsbezogene Zufuhr krustalen Materials während der variszischen Orogenese zurückzuführen ist.

Die postvariszischen ultramafischen Lamprophyre und Alkalibasalt-Gänge der Lausitz stammen ebenso wie die spätvariszischen kalkalkalischen Lamprophyre der Lausitz aus einer metasomatisch angereicherten Manteldomäne. Beide Gesteinsgruppen zeigen sehr ähnliche Spurenelementmuster. Offenbar sind aus dem lokalen Mantel unter der Lausitz mehrfach Teilschmelzen extrahiert worden. Diese wiederholte Schmelzbildung ist vermutlich das Ergebnis von Änderungen des lokalen Stressfeldes und von Druckentlastung im Übergang von spätvariszischen Bedingungen zu postvariszischer Extension.

Spätvariszische kalkalkalische Lamprophyre aus unterschiedlichen Krustendomänen des nördlichen Böhmischen Massivs (Erzgebirge, Lausitz, Sudeten) zeigen deutliche Unterschiede in ihrer Zusammensetzung. Diese Unterschiede belegen eine räumliche Variation der Zusammensetzung der krustalen Komponenten, die im Zuge der variszischen Subduktionsprozesse dem jeweiligen Mantel der drei Krustenabschnitte zugeführt worden sind. Lithium-Konzentrationen, Spurenelementsignaturen und Li-Sr-Nd-Pb-Isotopendaten zeigen, dass dem lokalen Mantel unter der Lausitz hauptsächlich alterierte ozeanische Kruste zugeführt worden ist, während unter dem Erzgebirge die Subduktion von Sedimentgesteinen überwogen hat. Der sudetische Mantel ist durch beide Komponenten beeinflußt. Unterschiedliche variszisch-tektonische Rahmenbedingungen und Mantelentwicklungen der drei Krustenblöcke werden demnach deutlich in Lamprophyr-Signaturen abgebildet.

Acknowledgments

First and foremost, I would like to thank my supervisor Prof. Dr. Rolf L. Romer for the support, advice, encouragement, suggestions, criticism, and guidance during this study, as well as giving me the opportunity to study and stay in Germany.

In addition, I would like to express my deepest thanks and appreciation to the academic and technical staff at German Research Centre for Geosciences (GFZ) for their help with the analytical work, as well as their financial support of field work, publishing, and conferences. Special thanks to the head of the Department of Inorganic and Isotope Geochemistry Prof. Dr. Jorg Erzinger for his continued support.

I am also grateful to Dr. Rudolf Naumann for the XRF analysis, Dr. Knut Hahne for trace element analysis, Sabine Tonn for REE data, Oona Appelt for support with the microprobe work, and Uwe Dittmann and Elke Lewerenz for their help with thin section preparation.

Special thanks to Anette Meixner, Cathrin Schulz, and Bettina Hübner for their assistance in training me in the Lab of isotope geochemistry. I also wish to thank PD Dr. Johannes Glodny, Dr. Robert Trumbull, Dr. Nicole Hoymann, Dr. Jochen Rötzler, Dr. Dr. Naser Meqbel, Dr. Helga Kemnitz, Dr. Mark Krienitz, Dr. Franziska Wilke, Jens Krüger and Christian Kujawa for their assistance and support. I am grateful to Marina Ospald and Hartmut Liep for guidance me in preparation of samples to analytical work.

I would like to acknowledge Dr. Masafumi Sudo from Potsdam University for his aid with the Ar-dating. My deepest thanks go to Prof. Dr. Ryszard Kryza and Dr. Awdankiewicz from University of Wroclaw and Dr. Reiner Lobst from Sächsisches Landesamt für Umwelt, Landwirtschaft und Geologie Pillnitzer for their guidance in field. Special thanks to Dr. Wolfgang Kramer for his support with some sample powders and in field work. I would like to thank the Ministry of Higher Education of Egypt, for their financial support of my studies and residence.

Finally, I would like to express my special appreciation to my mother for her support, patience, and care of my sibling during my stay in Germany.

Contents

1. Introduction

Lamprophyres are strongly porphyritic, with abundant phenocrysts of biotite and amphiboles. Feldspar is usually restricted to the ground mass. The term 'lamprophyre' comes from the Greek for "shining rock" in reference to amphibole and biotite crystals which often glisten on fresh surfaces (Rock, 1991). These rocks represent primitive, mantle-derived rocks as indicated from their major and compatible trace element contents (i.e., high MgO, Cr, and Ni) and high Mg# value. However, they have high incompatible trace element and rare earth element contents and the isotope composition of Sr, Nd, and Pb, which typically reflect a crustal source. These rocks can provide information on the lithosphere, deep mantle dynamics and contamination processes (e.g. AFC, FC, and mixing). Some of these rocks are associated with important mineral deposit of gold and diamond (Rock, 1991).

It has been known that the structural and stratigraphic data are commonly used to track the tectonic history, but the potential of lamprophyric and associated mafic magmatism to provide additional information has been little used. Literature indicates that different varieties of lamprophyres reflect of their tectonic environment and depth and temperature of crystallization. For example, the calc-alkaline lamprophyres are most characteristic lamprophyre types in convergent settings, whereas the ultramafic lamprophyre is characteristic of extensional tectonics (Turpin et al., 1988; Rock, 1991; Renno et al., 2003a; Awdankiewicz, 2007). However, the potentially powerful ability of compositional variation in lamprophyre suites to trace tectonic regime in time and space is little used. Recently, lamproites have been used to track the metasomatised mantle and source of metasomatism in a subducting setting (Prelevic et al., 2010). Thus, the combination of radiogenic isotope composition (Sr-Nd-Pb) with stable isotope (δ^7Li), in addition to major, trace and rare earth element data of lamprophyres of different emplacement age and tectonic regime may provide information on the mantle and the crustal material involved in tectonic events. The Saxo-Thuringian Zone is an appropriate situation to test wether there is a systematic relation between crustal source and metasomatic component in the lamprophyre source.

The Saxo-Thuringian zone is situated at the northern border of the Bohemian Massif and considered to be a part of the Pre-Gondwanan province that was affected by Cambro-Ordovician extensional tectonics. Cambrian to Ordovician rifting of the northern margin of Gondwana led to the formation of two types of continental crust of different thickness in Saxo-Thuringian Zone (Kroner and Romer, 2010). During the Variscan orogeny, blocks of thick Cadomian continental crust and zones of thinned continental crust behaved differently.

Blocks of thick crust (e.g., Lusatia) were not subductible and escaped significant Variscan deformation and metamorphism, whereas the areas of thin continental crust were subductible and strongly reworked (Kroner and Romer, 2010). The latter one are now exposed in high grade metamorphic areas like Erzgebirge and the Sudetes. Furthermore, the subducted materials during the Variscan orogeny are variable; include oceanic crust, thinned continental crust and its sedimentary cover (Kroner and Romer, 2013). The crust and its sedimentary cover subducted during the Variscan orogeny will provide the agents to metasomatize the mantle beneath the Saxo-Thuringian zone. Accordingly, the mantle beneath Variscan orogeny will produce rocks of different degree and/ signature of mantle metasomatism.

Calc-alkaline lamprophyres are widespread in Variscan Belt, particularly in Saxo-Thuringian zone. These rocks are typically emplaced late-Variscan collision. Based on the type of the phenocrysts and feldspar, the calc-alkaline lamprophyres are classified to four types (minettes, kersantite, vogesite, and spessartite). The estimated emplacement age of these rocks range between c. 300 and c. 330 Ma and they are often associated by microgabbro/microdiorite and granitoid rocks (Kramer, 1976; Turpin et al., 1988; Hegner et al., 1998; von Seckendorff et al., 2004; Awdankiewicz, 2007; Seifert, 2008; Krimicek, 2010). Previous studies indicate that crustal components of these rocks were introduced into the mantle probably during Variscan subduction event. Furthermore, the high compatible elements contents of these rocks (Cr, Ni, Co and Sc) and high Mg# of these rocks exclude significant crustal contamination as a source of this enrichment.

In Lusatia (northeastern part of Saxo-Thuringian Zone), beside the occurrence of late-Variation calc-alkaline lamprophyres, there occur early Cretaceous ultramafic lamprophyres and associated alkaline basalt. Previous studies of these rocks revealed that these rocks were emplaced in an extensional setting prior to the pre-rifting of the Eger Graben (Renno, et al., 2003a). Based on geochemical data (major, trace and rare earth elements), it is proposed that these rocks were extracted from an enriched mantle source (Renno, et al., 2003a). Furthermore, the comparison of the metasomatic components of these mantle-derived rocks with the late Variscan calc-alkaline lamprophyre allows constraining the persistence of metasomatic signatures in the mantle over extended periods of time.

To trace the compositional variation of the mantle beneath Saxo-Thuringian zone as a result of contrasting Variscan development and different subducted material during the Variscan orogeny, late Variscan calc-alkaline lamprophyre from different blocks of contrasting behavior during Variscan orogeny (e.g. Lusatia and Erzgebirge) will be used in our study. From the previous studies, it is notable that the number of lamprophyre dikes from

Lusatia is low relative to other parts of Variscan orogenic belt (Kramer et al., 1976; Awdankiewicz, 2007; Seifert, 2008). The regional distribution of calc-alkaline lamprophyres may reflect the distribution of Variscan subduction zones and the regional geochemical variation among these late-Variscan lamprophyres may trace the contrasting character of the subducted material.

Lusatia is a part of the Saxo-Thuringian Zone, dominated by Cadomian basement that largely escaped Variscan metamorphic reworking, whereas the adjacent Erzgebirge represents piles of metamorphic nappes. These nappes consist of Cadomian basement and its volcanosedimentary cover, which have been metamorphosed under medium to high grade conditions during the Variscan orogeny. Because of the contrasting behavior of Lusatia during the Variscan orogeny, it is possible that the mantle underlying Lusatia had experienced a fundamentally different Variscan geochemical development.

The Cadomian granodiorites in Lusatia (c. 550 Ma; Kröner and Hegner, 1998) had intruded by several stocks and dikes swarms of c. 400 Ma pre-Variscan gabbroic rocks. The gabbros comprise gabbro norite, olivine gabbro, and diorite (Kramer et al, 1977; Kindermann et al., 2003). The occurrence and setting of gabbroic rocks of c. 400 Ma in Lusatia are unusual relative to other parts of the Saxo-Thuringian Zone. Gabbroic rocks contain many xenoliths of pegmatitic gabbro. Previous studies indicate that these rocks have geochemical characteristic of within-plate setting (Kramer et al, 1977). However, there is no isotope data to give more detail information about the petrogenesis of these rocks. Isotopic signature of these rocks will also provide valuable information about the nature of the pre-Variscan mantle.

Lusatian calc-alkaline lamprophyres form NE to SW trending dikes which may reach 25 m width. Kramer et al. (1977) described these rocks as spessartites. There imprecise K/Ar age of c. 230 Ma is inconsistent with the emplacement age of calc-alkaline lamprophyres from other parts of Variscan Europe, e.g., the Sudetes, the Black Forest, the Erzgebirge, and the French Massif Central (Turpin et al., 1988; Hegner et al., 1998; Awdankiewicz, 2007; Seifert, 2008), all of which have been emplaced during the late stages of the Variscan orogeny (300 to 330 Ma). Hens, it is important to perform a precise age dating to calc-alkaline lamprophyre from Lusatia.

The late-Variscan calc-alkaline lamprophyres from the Erzgebirge form NW-SE trending dike swarms of kersantites, minettes and spessartites composition that cut the Variscan postkinematic granites and volcano-sedimentary sequences (von Seckendorff et al., 2004 and references therein). The calc-alkaline lamprophyres in the Gera Jachymov Zone form NW-SE trending dikes of kersantites composition. A cluster of shoshonitic-

trachyandesitic lavas are exposed in the Erzgebirge Basin. To the south of these Lavas a few dikes of kersantite (295 Ma) cut the Kirchberg granites, gneiss, mica schist and phyllites (von Seckendorff et al., 2004; Kramer, 1976).

Chapter 2 focuses in pre-Variscan gabbros and the late-Variscan calc-alkaline lamprophyre from Lusatia in order to characterize the effect of the Variscan orogeny on the mantle and to compare it with the metasomatized mantle beneath the Erzgebirge and Sudeten. In this study the gabbros and calc-alkaline lamprophyre have been used to trace the pre/late Variscan, respectively. The new geochemical and isotope data of the late Variscan calc-alkaline lamprophyre from Lusatia compared with existing data sets of late Variscan calc-alkaline lamprophyre from other parts of Variscan orogeny to achieve a better picture of geochemical evolution of late Variscan mantle in space. To attain that the following topics were investigated

1. Alteration and assimilation processes as a source of the crustal signature
2. Magma sources of the late-Variscan calc-alkaline lamprophyre and Pre-Variscan gabbros
3. Precise age dating for the calc-alkaline lamprophyre in Lusatia
4. Comparison of geochemical fingerprint and isotope signature of the pre/late Variscan of the mantle beneath Lusatia
5. Comparison of geochemical and isotope signature of the late-Variscan lamprophyre from Lusatia and adjacent areas in Saxo-Thuringian Zone

In this study, I used the most suitable methods available to determine contents of major, trace, and rare earth elements of the lamprophyre and gabbros. These analyses were done using techniques of X-ray fluorescence spectrometry, inductively coupled plasma- mass spectrometry and inductively coupled plasma-atomic emission spectrometry. Furthermore, the study was supported by microprobe analysis of major element composition of the minerals. The first Sr, Nd, and Pb isotopic composition on bulk rock which determined on a Triton and a Finnigan MAT262 multi-collector mass-spectrometer, respectively. Additionally, the age of the calc-alkaline lamprophyre was defined using ^{40}Ar–^{39}Ar hornblende age dating. The new age data imply that lamprophyric magmatism in Lusatia is coeval not only with lamprophyre emplacement in the adjacent areas of the Erzgebirge and Sudetes, but also with lamprophyres from other parts of the Variscan orogen, Accordingly, in this study lamprophyres of similar age from different parts of Saxo-Thuringian Zone were used to trace the contrasting

development of the Variscan orogen. The major element compositions of minerals were determined using electron microprobe analyses.

Chapter 3, I present the geochemical and first Sr-Nd-Pb isotopic data as well as mineral chemistry for Cretaceous ultramafic lamprophyre and alkaline basalt from Lusatia in order to characterize the mantle source of these rocks. These new data compared with existing geochemical and isotopic data sets of late Variscan calc-alkaline lamprophyre from Lusatia to accomplish a better view of geochemical evolution of post-Variscan mantle in time. The genetic relation between the ultramafic lamprophyre and alkaline basalt has been investigated. The emplacement age and geodynamic significance of the ultramafic lamprophyre from Lusatia with similar Cretaceous lamprophyres and associated volcanisms in central, western Europe as well as eastern north America were discussed.

Chapter 4, I present the Li-Sr-Pb-Nd isotopic composition and lithium content of the calc-alkaline lamprophyre from the Erzgebirge, Lusatia, and the Sudetes to in order to asses the compositional variations of the mantle associated the Variscan event. Li-isotope ratios were determined using a Thermo Finnigan NEPTUNE MC ICP-MS. We also presented Sr, Nd, and Pb isotope analyses for some lamprophyre samples from Erzgebirge. In this study three topic were discussed which include (1) spatial variation in δ^7Li and Li contents as well as Sr-Pb-Nd isotopic composition and fluid-mobile and fluid-immobile elements (2) Transfer of Li from the slab to the mantle wedge, and (3) Lamprophyres and the Li budget of the mantle

Chapter 2 ("*Calc-alkaline lamprophyres from Lusatia (Germany) – evidence for a repeatedly enriched mantle source"* by Khaled Abdelfadil. Rolf L. Romer, Thomas Seifert, and Reiner Lobst) is published in Chemical Geology. Chapter 4 (*"Enriched mantle beneath Lusatia, Germany: Evidence from alkaline basalt and ultramafic lamprophyre"* by Khaled Abdelfadil and Rolf L. Romer) will be submitted to International Journal of Earth Sciences. Chapter 3 (*"Fate of subducted Li-the lamprophyre connection"* by Khaled Abdelfadil, Rolf L. Romer, Johannes Glodny) will be submitted to Lithos.

Each manuscript represents a co-operation with a number of colleges; I initiated the ideas of the papers and I got help during writing from Mr. Romer to raise the quality of my papers and to make it possible to publish in high quality journals. Each manuscript was checked by R. Romer. All laboratory work has been done by me under supervision of R. Romer and J. Glodny. At the beginning I got support from A. Meixner C. Schulz, and B. Hübner as I did not work before in clean room laboratories. For major and trace elements as

well as microprobe analyses R. Naumann, S. Tonn, K. Hahne and O. Appelt guided me. U. Dittmann, E. Lewerenz, M. Ospald and H. Liep helped me during thin section preparation and sample preparation for geochemistry.

Th. Seifert, W. Kramer, R. Romer and R. Lobst guided excursions to Lusatia and the Erzgebirge while M. Awdankiewicz and R. Kryza guided an excursion to the Sudetes (SW Poland). All the analytical work has been done at GFZ except for Ar-Ar dating that was done at Potsdam University under guidance of M. Sudu.

2. Calc-alkaline lamprophyres from Lusatia (Germany) – evidence for a repeatedly enriched mantle source

Abstract

Pre-Variscan mantle derived gabbros (c. 400 Ma) and late-Variscan calc-alkaline lamprophyres (c. 330 Ma) were emplaced within the Cadomian basement of Lusatia. They were sampled to characterize the effect of the Variscan orogeny onto the mantle beneath Lusatia. The tholeiitic gabbros originated from a mantle source that had been metasomatized during subduction beneath the Cadomian magmatic arc at c. 570 Ma, which led to enrichment of LREE, Ba/Nb, and LILE relative to primitive mantle. The late-Variscan calc-alkaline lamprophyres (spessartites) have high MgO, Cr, and Ni contents reflecting the mantle source. The spessartites, however, have distinctly higher Rb, Ba, Pb, Sr, Th, and Cs contents, higher La/Yb, $^{87}Sr/^{86}Sr$, and $^{206}Pb/^{204}Pb$ ratios, and lower $^{143}Nd/^{144}Nd$ ratios than the gabbros, which indicates a second, Variscan event of mantle enrichment. In addition, the spessartites have trace element ratios (i.e., Ba/Nb, Nb/U, Th/U, and Th/Nb) that resemble continental crust and Sr, Nd, and Pb isotopic compositions that demonstrate involvement of crustal material by source enrichment during the Variscan orogeny. The calc-alkaline lamprophyres of the Lusatia occupy the same age range as calc-alkaline lamprophyres from the adjacent Erzgebirge and Sudetes. The trace-element signatures and Sr and Nd isotopic compositions of Lusatian spessartites, however, are less enriched than those of comparable dikes in the Sudetes and the Erzgebirge. This implies that the Variscan orogeny resulted in geochemically and isotopically heterogeneous lithospheric mantle on the regional scale, possibly reflecting the contrasting nature of the subducted rocks.

2.1. Introduction

Calc-alkaline lamprophyres are hypabyssal rocks that commonly form dikes and sills and that are characterized by a panidiomorphic porphyritic texture with abundant phenocrysts of amphibole and/or dark mica. Lamprophyres are widely considered to be primary mantle-derived magmas (e.g., Rock, 1991; Bedard, 1994) that provide not only important information for magma genesis in the mantle, but also on geodynamic processes modifying the mantle and leading to the extraction of lamprophyric melts. Although lamprophyres were long thought to sample a metasomatized mantle source, which may have been enriched during an ancient event, it has become increasingly obvious that the trace-element and isotopic signatures of old

crust-derived material equally well may have been introduced during geologically young events (e.g., Hegner et al., 1998; Hoch, et al., 2001; Prelević et al., 2005, 2012). The geochemical composition of lamprophyres shows an uncoupling of the major and compatible trace element contents (i.e., high MgO, Cr, and Ni) and high Mg# values, which reflect the mantle source, from the incompatible trace element and rare earth element contents and the isotope composition of Sr, Nd, and Pb, which typically reflect a crustal source. In previous studies, this geochemical uncoupling in lamprophyric magma has been variably linked to a low degree of partial melting of lithospheric mantle peridotites, metasomatised mantle sources in a subduction setting, mixing of mantle and crustal melts, and assimilation with fractional crystallization (e.g., Jones and Smith, 1983; Macdonald et al., 1985; Turpin et al., 1988; Stille et al., 1989; Rock, 1991; Currie and Williams, 1993; Prelević et al., 2004, 2007; Janoušek, et al., 2010). Prelević et al. (2005, 2010) noticed a close correspondence between the geochemical and isotopic signature of Mediterranean orogenic lamproites and the sediments in the trench and the sedimentary wedge. This indicates that the local geochemical signature of the material entering into the subduction zone resurfaces in the orogenic lamproites extracted from the mantle above the subducting plate (Prelević et al., 2005). This correspondence not only demonstrates that metasomatism of the mantle in the orogenic lamproite (and more generally in the lamprophyre) source may occur shortly before they are extracted, but also opens the possibility to use orogenic lamproites and lamprophyres to trace the composition of subducting plate in young and ancient orogens. The geochemical signature of orogenic lamproites and possibly also calc-alkaline lamprophyres may be used to trace post-collisional interaction between an orogenic lithospheric mantle and a shallow subducting plate (cf. Prelević et al., 2010).

The Variscan orogen resulted from the collision of Laurussia with Gondwana and several smaller crustal blocks (i.e., Bohemia, Brittany, Iberia) between them. These crustal blocks, dominated by Cadomian basement (c. 570 to 545 Ma), are bordered by belts Variscan high-grade metamorphic rocks (e.g., Erzgebirge, Sudetes, Vosges, Black Forest) that are interpreted to trace belts of Variscan subduction zones (e.g., Matte, 1991, 2001; Franke, 2000). The scarcity of subduction-related magmatism indicates that along these zones predominantly thinned continental crust – and its sedimentary cover – was subducted. These rocks are now largely preserved in Variscan high-grade metamorphic rocks. Post-collisional magmatism includes voluminous syn- and post-tectonic granitoids that are mostly derived from crustal melting (e.g., Turpin et al., 1990; Finger et al., 1997; Förster and Romer, 2010). Subduction of thinned continental crust and its sedimentary cover resulted in the

metasomatism of the mantle above the subducted plate. This metasomatized mantle was sampled by a suite of late-orogenic lamprophyre dikes, most importantly among them calc-alkaline lamprophyres (Turpin et al., 1988; Wenzel et al., 1991; Hegner et al., 1998; von Seckendorff et al., 2004; Awdankiewicz, 2007; Seifert, 2008). In analogy to the geochemical variability of the Mediterranean orogenic lamproites that reflect the regional variability of the subducted sediments, the regional distribution of calc-alkaline lamprophyres may reflect the distribution of Variscan subduction zones and the regional geochemical variation among these lamprophyres may trace the contrasting character of the subducted material.

Lusatia is one of these Cadomian blocks that largely escaped Variscan metamorphism and deformation and that differs from adjacent parts of the Bohemian Massif by the absence of piles of Variscan high-grade metamorphic rocks. The Cadomian basement of Lusatia (greywackes and granodiorites; Fig. 2.1) has been intruded by pre-Variscan gabbros and by late-Variscan lamprophyres. The compositional variations between the pre-Variscan gabbros and late-Variscan lamprophyres allow us to characterize the effect of material subducted during the Variscan orogeny on the mantle beneath Lusatia. Furthermore, the contrasting Variscan development of Lusatia and adjacent regions with Variscan high-grade metamorphic rocks may find its expression in contrasting metasomatism of the mantle source for the lamprophyric magmatism. In this paper, we present mineralogical, geochemical, and Sr, Nd, and Pb isotope data of pre-Variscan gabbros and late-Variscan calc-alkaline lamprophyres to characterize the geochemical and isotopic effect of the Variscan (and possibly Cadomian) orogeny on the mantle beneath Lusatia.

2.2. Geological setting

The Cambrian to Ordovician rifting of the northern margin of Gondwana, which eventually led to the opening of the Rheic Ocean, resulted in the formation of two types of continental crust, i.e., blocks with continental crust of normal thickness that are separated by thinned continental crust that developed into shelf areas with marine sedimentation (e.g., Linnemann et al., 2000, 2008, 2010a; Kroner et al., 2007; Kroner and Romer, 2010; Heuse et al., 2010). The blocks of normal crustal thickness are dominated by metamorphic and voluminous magmatic rocks of the former Cadomian magmatic arc (570 to 545 Ma, Linnemann et al., 2000, 2008). The areas of thinned continental crust developed into sedimentation areas that record the successive development of rift-bound sedimentation with siliciclastic debris from the Cadomian arc to shallow and eventually to deep shelf

sedimentation (Linnemann et al., 2004, 2010b). During the Variscan orogeny, these blocks of thick Cadomian continental crust and the zones of thinned continental crust behaved differently: The areas of thick crust were not subductible, whereas the areas of thin continental crust were subductible (cf. Kroner et al., 2007; Kroner and Romer, 2010). The closure of the Rheic Ocean initially was accomplished by consumption of oceanic crust beneath the Mid-German Crystalline Zone, eventually leading to the docking of Gondwana-derived blocks to Laurussia. Once a block of thick Cadomian continental crust had docked to Laurussia, a new subduction zone was initiated behind this block. In these later subduction zones, thinned continental crust and its sedimentary cover was subducted until the next block of thick Cadomian continental crust arrived and collided, resulting in the generation of yet another subduction zone. With the arrest of subduction, the subducted continental crust escaped from beneath the blocks of thick Cadomian continental crust – either by lateral escape or backflow in the subduction channel – and was emplaced as stacks of nappes of contrasting metamorphic history on adjacent terranes (cf. Kroner et al., 2007, 2010; Kroner and Romer, 2010). Subduction of thinned continental crust and formation of new subduction zones behind blocks of thick crust (i) explains the occurrence of high grade metamorphic rocks in close spatial association with areas of little Variscan overprint, (ii) accounts for the scarcity of subduction-related Variscan magmatism, and (iii) brings thinned continental crust and its sedimentary cover to mantle depth (e.g., Kroner et al., 2007, 2008; Kroner and Romer, 2010). Fluid-loss from these sediments and possible partial melting of the sediments and their crystalline substratum provides the agents that may metasomatize the mantle above the subducting plate.

The Bohemian Massif and in particular the Lusatian block are special as they are among the first Gondwana-derived blocks to collide with Laurussia. The approach of Bohemia and Laurussia resulted in the thrusting of the Tepla-Barrandian Unit onto other parts of the Bohemian Massif, the formation of the Sudetes, and in establishing a new subduction zone to the SW of the Bohemian Massif. Lusatia was at that time not a part of the Bohemian Massif and continued to move toward Laurussia. The strike slip zone between Bohemia and Lusatia later was reactivated during the subsequent lateral escape of subducted crustal rocks from beneath Bohemia and their emplacement onto the Saxo-Thuringian Zone to form the Erzgebirge (cf. Kroner et al., 2007, 2010; Kroner and Goerz, 2010; Kroner and Romer, 2010).

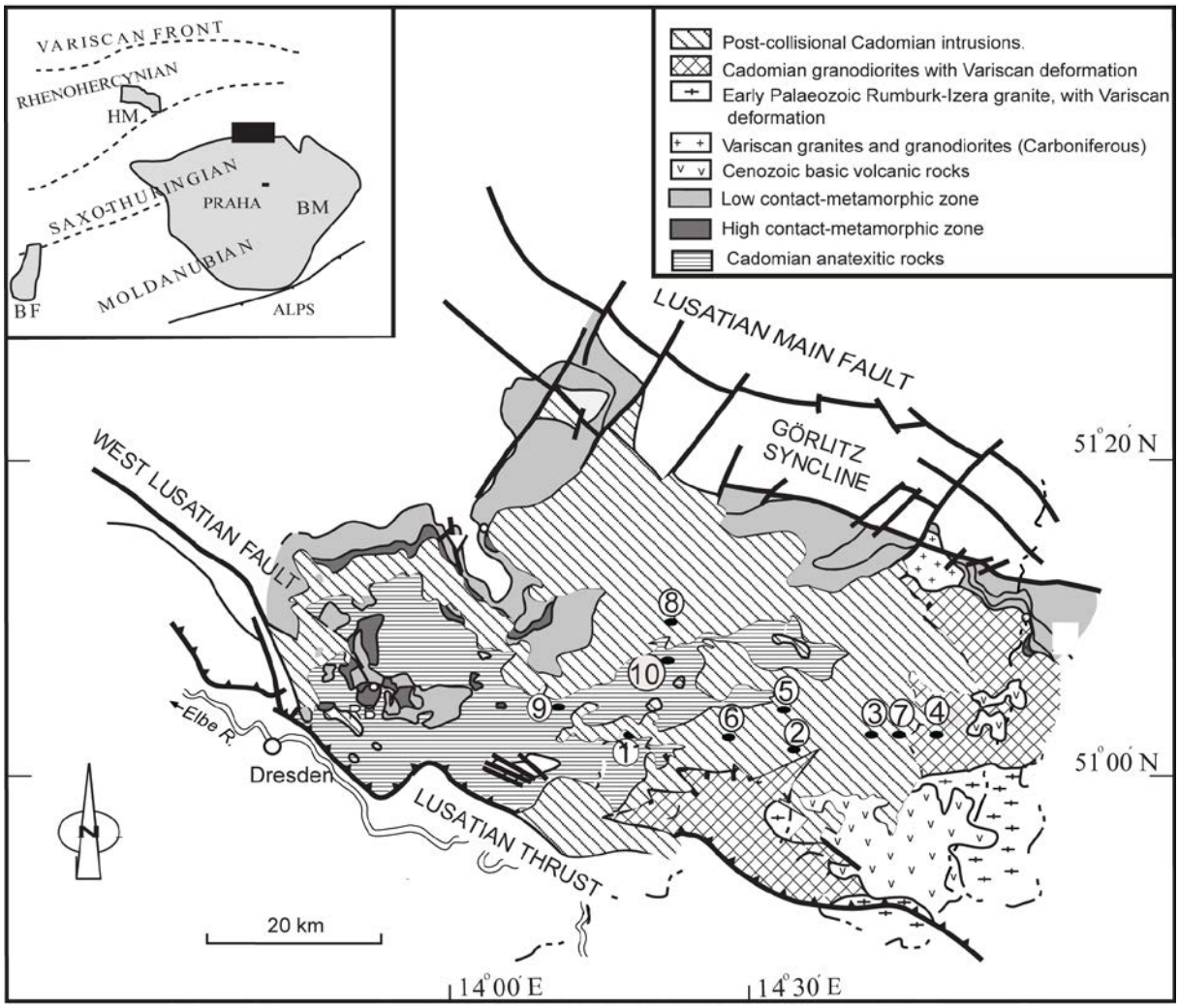

Fig. 2.1. Geological map of the Lusatian Block in the Saxo-Thuringian Domain (after Kemnitz, 2007). Sampling locations: 1- Valtengrund (51°04′ N, 14°17′ E), 2- Klunst Ebersbach (51°01′ N, 14°35′ E), 3- Das Gericht (51°02′ N, 14°41′ E), 4- Julienstein (51°02′ N, 14°44′ E), 5- Israel (51°04′ N, 14°32′ E), 6- Hutzelberg (51°02′ N, 14°32′ E), 7- Strahwalde (51°02′ N, 14°43′ E), 8- Bautzen-Stiebitz (51°10′ N, 14°23′ E), 9- Fichtenberg (51°05′ N, 14°13′ E), 10- Soraer Höhe (51°08′ N, 14°22′ E).The gabbro samples were collected at locations 1, 2, 8, 9, and 10, whereas the lamprophyre at 3, 4, 5, 6, and 7. Post-collisional Cadomian intrusions occur as plutons and are granodioritic in composition. Inset shows the position of Lusatia relative to major Variscan massifs and zones. BM: Bohemian Massif; BF: Black Forest; HM; Harz Mountains. Geological map is after Kemnitz (2007).

Lusatia, located at the northeastern margin of the Bohemian Massif, is bordered to the SW by the Elbe-Fault Zone and to the NE by faults paralleling the Görlitz slate belt (Fig. 2.1). These structural elements have been active during the Variscan orogeny and have been repeatedly reactivated since. To the south, Lusatia is bordered by the Tertiary Eger rift, which largely

follows the strike slip zone along which Lusatia had slipped by the Bohemian Massif during the Variscan orogeny. To the north Lusatia is separated from the Mid-German Crystalline Zone by a major shear zone. In the southern part of Lusatia, where Cadomian granodiorites predominate, several stocks and dikes swarms of gabbroic rocks, in particular gabbro norite, olivine gabbro, and diorite (Kramer et al, 1977), had intruded. Kramer et al. (1977) reported a K-Ar whole rock age of 400 Ma for the gabbros in Lusatia. This age later was confirmed by a Pb-Pb age of 390±8 Ma (zircon evaporation; Kindermann et al., 2003) for a gabbro near Valtengrund (Fig. 2.1). The gabbros have been emplaced in stable crust and show within-plate geochemical signatures (e.g., Peschel et al., 1973; Kramer, 1988; Heinrich, 1993). The occurrence of gabbroic rocks of this age and setting in Lusatia is unusual: In other parts of the Saxo-Thuringian Zone, gabbros are much older and related to the opening of the Rheic Ocean (e.g., Vesser Zone, Kemnitz et al., 2002; Münchberg, Stosch and Lugmair, 1990). In the West-Sudetes (i.e., at Braszowice and Sleza) occur gabbros of corresponding age, i.e., 400±10 Ma (Kryza and Pin, 2010) and 420±20 Ma (Oliver et al., 1993), but there, the gabbros are part of ophiolitic successions (Kryza and Pin, 2010).

The Cadomian granodiorites and greywackes and the pre-Variscan gabbros of Lusatia are intruded by (i) dike swarms of alkaline basalt with unknown – but pre-Variscan – age (Kramer, 1988) and (ii) late-Variscan dikes of older calc-alkaline lamprophyres (this study), and 315-304 Ma old post-Variscan granite intrusions (Eidam et al., 1995; Fig. 2.1), as well as post-Variscan dike swarms of (iii) andesites, rhyodacites, rhyolite, and younger lamprophyres (Eidam et al., 2001). The calc-alkaline lamprophyres are spessartites (amphibole and plagioclase dominant). They form NE to SW trending dikes that may reach 25 m width (Kramer et al., 1977). The age of these dikes is not well known and the K/Ar age of 230 Ma (Kramer et al., 1977) is inconsistent with the emplacement age of lamprophyres from other parts of Variscan Europe, e.g., the Sudetes, the Black Forest, the Erzgebirge, and the French Massif Central (Turpin et al., 1988; Hegner et al., 1998; Awdankiewicz, 2007; Seifert, 2008), all of which have been emplaced during the late stages of the Variscan orogeny.

The Palaeozoic (post-Cadomian and pre-Variscan) tholeiitic gabbros and the late-Variscan calc-alkaline lamprophyres (spessartite) sampled the mantle beneath Lusatia, which allows to characterize the effect of the Variscan orogeny on the mantle and to compare it with the metasomatized mantle beneath the Erzgebirge and the Sudetes. As the latter areas have been much more intensely involved into the Variscan orogeny, they may have a different extent and/or signature of mantle metasomatism.

2.3. Samples and analytical methods

We present data from eleven gabbro samples and eleven relatively fresh calc-alkaline lamprophyres collected from Lusatia. The gabbro samples were collected at five locations (Valtengrund, Fichtenberg, Soraer Höhe, Bautzen-Stiebitz, Klunst Ebersbach, Fig. 2.1) and the calc-alkaline lamprophyres were sampled from small dikes at five locations (Israel, Hutzelberg, Strahwalde, Julienstein, Das Gericht, Fig. 2.1). As the age of the lamprophyres was known only from K-Ar whole-rock dating, we separated amphibole from two spessartite samples collected at Das Gericht and Julienstein for Ar/Ar dating.

Amphibole Ar-Ar dating was performed at the geochronology laboratory of the University of Potsdam. Amphibole was separated from the 250 to 200 μm fraction and purified by hand-picking under a binocular microscope. The samples were irradiated at the Geesthacht Neutron Facility (GeNF), GKSS Research Center, Germany, for 96 h with a fast neutron flux of 1x1012 n/cm^2/s. As monitors for the neutron flux and the production of Ar from Ca and K, we used Fish Canyon tuff sanidine and crystals of CaF_2 and K_2SO_4, respectively. For the Fish Canyon tuff sanidine, we used an age of 27.5 Ma (Uto et al., 1997; Ishizuka, 1988; Ishizuka et al., 2002), which agrees with the one obtained by Lanphere and Baadsgaard (2001). The samples were analyzed by stepwise heating until total fusion, using a 50W CO_2 laser operated at a wavelength of 10.6 μm involved in the Dual Wave laser ablation system. The extracted gas was purified using cold traps and Zr-Al SEALS alloy getters and analyzed using a Micromass 5400 noble gas mass spectrometer with high sensitivity and low background. System blanks were measured after every three samples. The measured isotopic ratios were corrected for blank measurements, mass discrimination, interference of Ar isotopes derived from Ca and K by irradiation, and post irradiation decay of ^{37}Ar and ^{39}Ar. The final age calculation and errors follow the procedure of Uto et al (1997). The following three criteria were used to define a plateau for the dated samples; (1) The plateau has to include a series of adjacent steps that together comprise more than 50% of the released ^{39}Ar, (2) the ages of the steps should agree within two sigma (2σ) error, (3) each degassing step included in the plateau should have more than 3 % of the total ^{39}Ar released.

Mineral analyses were performed using a CAMECA SX100 electron microprobe operated at 15 kV accelerating voltage, a beam current of 20 nA, and a variable beam diameter of 1 to 15 μm. Peak counting times were 10-20 s for major and 30 s for minor elements; backgrounds were counted for 5-15 s. Data reduction used the PAP correction procedure implemented in the CAMECA software.

Major and trace element analyses were carried out at Deutsches GeoForschungZentrum (GFZ). Major element oxides and the trace elements Ba, Cr, Ga, Nb, Ni, Rb, Sr, V, Y, Zn, and Zr were analyzed by XRF on fused disks prepared from dried (105 °C) powders (< 60 μm) and Li tetraborate-metaborate (Fluxana FX-X65) at a sample-to-flux ratio 1:6. Concentrations were determined using a Panalytical Axios advanced wavelength-dispersive spectrometer and matrix correction programs. H_2O+ and CO_2 were determined using a Vario EL III using high-temperature catalytic combustion. Trace elements (Nb, Mo, Cd, Cs, Ti, Pb, Th, U, Sc, Co, Cu, Ga, Sb, and Sn) were determined by IC-MS using a VG Plasma Quad PG2. Sample powders were decomposed using HF, Aqua regia, and $HClO_4$. The dissolved samples were redissolved in HNO_3 and diluted to a volume of 50 ml for analysis. Rare earth element (REE) and Y contents were determined by inductively coupled plasma-atomic emission spectroscopy (ICP-AES) following the procedure of Zuleger and Erzinger (1988). The samples are decomposed using Na_2O_2 fusion and the REE are separated and concentrated chromatographically using ion-exchange methods.

Whole-rock Nd, Sr, and Pb isotopic compositions were analyzed at Deutsches GeoForschungZentrum. Samples were dissolved using concentrated HF for four days at 160°C on a hotplate. To transfer fluorides into nitrates, the digested samples were dried and taken up in HNO_3 and dried again. Hereafter, the samples were re-dissolved in 6N HCl and splitted for Pb and Sr-Nd ion-chromatographic separation. Pb was separated using the HCl-HBr ion exchange chemistry described by Romer et al. (2005). Pb was loaded together with H_3PO_4 and silica-gel on single Re-filaments and its isotopic composition was measured at temperatures between 1200–1250°C on a Finnigan MAT262 TIMS multi-collector mass spectrometer using static multicollection. Instrumental mass-fractionation was corrected using 0.1% per a.m.u. as determined from the repeated measurement of the NBS SRM 981 standard. Accuracy and precision of the Pb isotopic ratio is better than 0.1% at the 2σ level. Total procedural blanks are better than 15-30 pg Pb. Sr and Nd were separated using cation-exchange chromatographic procedures. The Sr and Nd isotopic composition was determined on a Triton and a Finnigan MAT262 multi-collector mass-spectrometer, respectively, operated in dynamic multicollection mode. $^{87}Sr/^{86}Sr$ and $^{143}Nd/^{144}Nd$ were normalized to $^{86}Sr/^{88}Sr = 0.1194$ and Nd $^{146}Nd/^{144}Nd = 0.7219$, respectively. During the period of analytical work the Sr reference material NBS987 gave $^{87}Sr/^{86}Sr = 0.710249 \pm 0.000005$ (n = 20) and the La Jolla Nd reference material gave $^{143}Nd/^{144}Nd = 0.511855 \pm 0.000006$ (n = 14). Total procedural blanks for Sr and Nd analyses are less than 50 pg Sr and less than 30 pg Nd.

2.4. Results

2.4.1 ^{40}Ar–^{39}Ar age dating of lamprophyres

The ^{40}Ar–^{39}Ar data are presented in Table 2.1 and Fig. 2.2. The Ar-release spectrum of hornblende from Julienstein (sample 2693) yields a plateau that is defined by five steps and more than 80% of ^{39}Ar-release. The low-temperature Ar-release, which encompasses only 3% of the spectrum and yields anomalously old apparent ages, and the last high-temperature step, which yields a slightly lower age than the plateau, have been excluded. The plateau corresponds to a ^{39}Ar–^{40}Ar age of 335.4 ± 1.2 Ma (Fig. 2.2a), which is within uncertainties identical with the 336.7 ± 3.9 Ma obtained from the ^{40}Ar/^{36}Ar vs. ^{39}Ar/^{46}Ar isochron with a mean square of weighted deviations (MSWD) of 0.88 (Fig. 2.2b). This total gas age of 339.2 ± 1.2 Ma is slightly older, reflecting the contribution of the small, but highly anomalous first release step.

The Ar-release spectrum of hornblende from the lamprophyre of the location Das Gericht (sample 2683) yields a three-step plateau age that includes 53.2% of the released ^{39}Ar. This plateau age corresponds to an age of 325.3 ± 1.2 Ma (Fig. 2.2c), which agrees within uncertainties with the 325.5 ± 2.9 Ma obtained for the isochron (MSWD = 1.66; Fig. 2.2d). Note, both amphibole samples yield initial ^{40}Ar/^{36}Ar values that are within uncertainties identical with the Ar composition of air, i.e., there seems to be no excess argon except for the low-temperature degassing steps.

The plateau ages of 325.3 ± 1.2 Ma and 335.4 ± 1.2 Ma for hornblende from the two spessartite samples are considered to date the time of lamprophyre emplacement. Our new ^{39}Ar–^{40}Ar ages are markedly older than the whole-rock K/Ar age of c. 230 Ma and supersede this age. The new ages show that the lamprophyres were emplaced during the late stage of the Variscan orogeny. The new age data imply that lamprophyric magmatism in Lusatia is coeval not only with lamprophyre emplacement in the adjacent areas of the Erzgebirge, the Sudetes, and the Moldanubian Zone of the Bohemian Massif (von Seckendorff et al., 2004; Awdankiewicz, 2007; Janoušek and Holub, 2007; Seifert, 2008), but also with lamprophyres from other parts of the Variscan orogen, such as the Black Forest, the Vosges, the French Massif Central, and the Balkan range (Turpin et al., 1988; Hegner et al., 1998; Buzzi et al., 2010).

Table 2.1.
$^{40}Ar/^{39}Ar$ step-heating data for amphiboles from calc-alkaline lamprophyre, Lusatia, Germany.

Laser output	$^{40}Ar/^{39}Ar$	$^{37}Ar/^{39}Ar$	$^{36}Ar/^{39}Ar$ (x10-3)	K/Ca	$^{40}Ar^*$ (%)	$^{39}Ar_K$ fraction (%)	$^{40}Ar^*/^{39}Ar_K$	Age(±1s) (Ma)
Sample 2680, Das Gericht, J= 0.00149								
0.018	923 ± 10	54.2 ± 128.7	682.3 ± 2.8	0.01	78.89	0.31	766 ± 96	1374 ± 120
0.02	239.2 ± 1.7	238 ± 174	191 ± 7	0.00	88.80	0.18	271 ± 61	612 ± 117
0.024	230.3 ± 0.9	99 ± 83	175 ± 3	0.01	82.90	0.45	210 ± 21	491 ± 42
0.028	140.4 ± 0.9	48 ± 36	54.1 ± 1.4	0.01	92.88	1.03	136 ± 7	334 ± 15
0.032	146.6 ± 0.4	1 ± 7	21.6 ± 0.4	1.02	95.69	5.10	140.3 ± 1.4	343 ± 3
0.034	133.8 ± 0.3	6 ± 3	10.30 ± 0.12	0.09	98.31	11.91	132.3 ± 0.6	324.9 ± 1.7
0.035	130.9 ± 0.3	33 ± 5	10.84 ± 0.20	0.02	99.48	19.08	134.1 ± 1.0	329 ± 2
0.036	128.5 ± 0.2	32 ± 5	8.3 ± 0.2	0.02	99.37	15.82	131.4 ± 0.9	323 ± 2
0.038	126.7 ± 0.8	14.6 ± 1.9	8.14 ± 0.09	0.04	99.53	46.13	127.8 ± 0.9	315 ± 2
Sample 2693, Julienstein, J= 0.00149,								
0.02	573.1 ± 2.9	131 ± 52	693 ± 9	0.00	67.10	0.70	436 ± 25	903 ± 40
0.025	198.2 ± 1.6	139 ± 44	308 ± 3	0.00	62.83	0.87	142 ± 9	347 ± 20
0.028	149.6 ± 0.5	73 ± 22	50.4 ± 1.0	0.01	96.08	1.76	154 ± 4	373 ± 10
0.03	135.5 ± 0.6	37 ± 10	23.0 ± 0.5	0.02	98.41	4.24	138.0 ± 2.0	338 ± 5
0.032	140.3 ± 0.3	1 ± 3	12.92 ± 0.12	0.75	97.35	12.92	136.7 ± 0.7	334.6 ± 1.9
0.034	136.0 ± 0.6	36 ± 6	9.49 ± 0.17	0.02	99.41	19.37	139.7 ± 1.3	341 ± 3
0.036	134.6 ± 0.5	15 ± 3	7.15 ± 0.13	0.04	99.79	50.89	136.1 ± 0.7	333 ± 2
0.037	128.97 ± 0.06	4 ± 5	5.2 ± 0.2	0.13	99.22	9.25	128.5 ± 0.9	316 ± 2

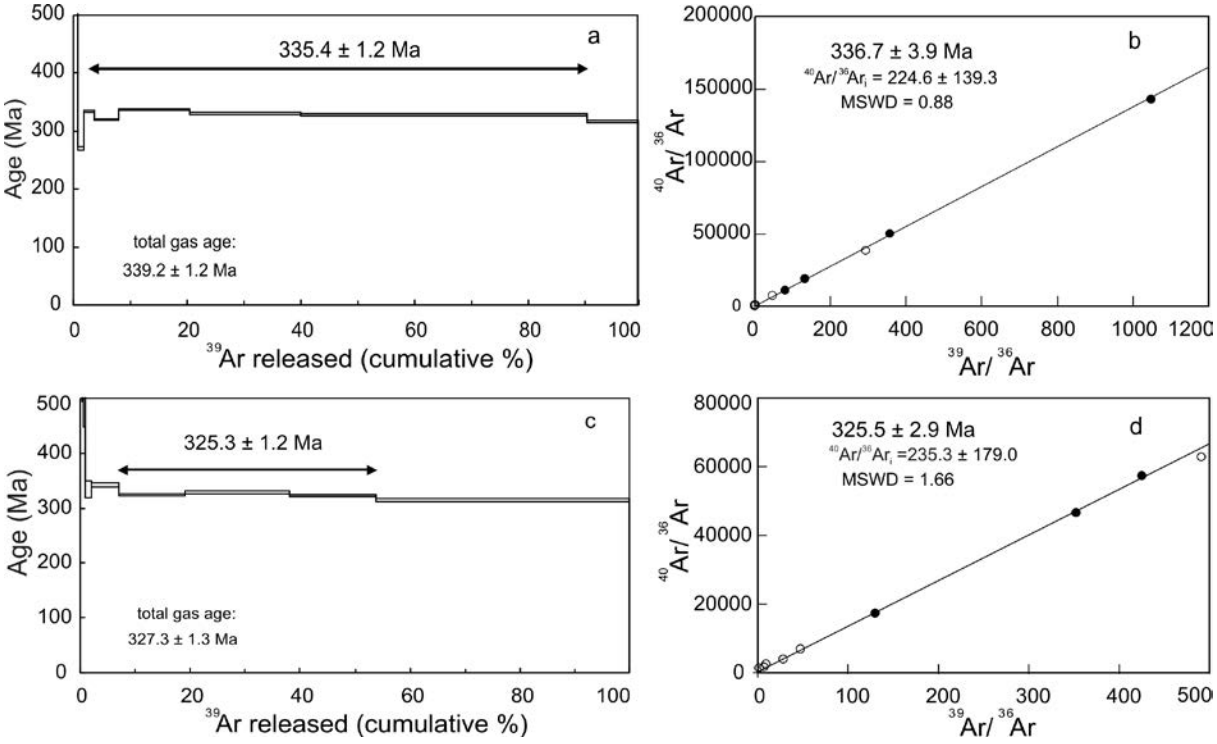

Fig. 2.2. $^{40}Ar/^{39}Ar$ age spectra (left) and isotope correlation diagrams (right) for the hornblende samples of two lamprophyre from Lusatia. MSWD- mean square of the weighted deviates. Filled symbols are the data of the "plateau steps" in the "age spectrum". Open symbols are the data of the other steps in the "age spectrum".

2.4.2. Petrographic description

Gabbros. Post-Cadomian and pre-Variscan intrusions in Lusatia form major bodies dominated by gabbro and olivine gabbro with local domains (at the decimeter to meter scale) of pegmatitic gabbro. The gabbro is mainly composed of clinopyroxene (c.40 vol.%), plagioclase (c.54 vol.%), and minor amounts of hornblende and biotite. Secondary minerals are actinolite, chlorite, epidote, zoisite, and sericite. Plagioclase forms subhedral labradorite to andesine crystals (Table 2.2). It is occasionally altered to sericite, epidote, and zoisite. Augite is partly replaced by chlorite. Ophitic and subophitic textures are common. The olivine gabbro, which is dominated by clinopyroxene (augite), plagioclase, and amphibole, in addition has pseudomorph serpentine after olivine. Pegmatitic gabbro is composed mainly of very coarse grained plagioclase and clinopyroxene with minor amounts of biotite. Chlorite is the main secondary mineral and apatite is the main accessory mineral. Quartz is interstitial. Some pyroxene is altered to iron oxide and chlorite. There are two generations of biotite, a primary yellow to dark brown pleochroic one and a secondary one after pyroxene. Locally, biotite is rimmed by chlorite and iron oxide.

Table 2.2.
Representative electron microprobe analyses of clinopyroxene, amphibole, and plagioclase from calc-alkaline lamprophyre and gabbros.

	Clinopyroxene								Amphibole								Feldspar				
	Spessartites				Gabbros				Spessartites			Gabbros					Spessartites		Gabbros		
									TMH	TMH	Ka	TPg	M Hb	TM Hb	FM Hb	M Hb	Kfs	Pl	Pl	Pl	Pl
Sample	S 16c	S 16r	S 17c	S 17r	S 23c	S 23r	S 9 c	S 9 r	101Dr	101Dc	S17c	S17r	S13c	S13	S13c	S13r	S12	S12c	S12r	S9p8c	S9p8r
SiO_2	50.43	50.76	51.78	51.62	52.52	52.49	51.48	52.24	41.74	41.71	41.64	42.09	48.92	47.65	48.73	48.24	63.92	66.34	66.11	55.64	56.74
TiO_2	0.77	0.71	0.60	0.55	0.66	0.58	0.79	0.69	4.50	4.44	4.49	4.40	1.27	2.48	1.24	1.29	na	na	na	na	na
Al_2O_3	3.21	3.26	2.20	2.32	2.66	2.19	2.73	2.58	11.47	11.36	11.36	11.37	5.43	3.95	5.37	5.74	18.22	20.67	21.01	27.26	26.84
Cr_2O_3	0.18	0.30	0.21	0.30	0.001	0.001	0.001	0.001	0.03	0.00	0.00	0.01	0.03	0.02	0.03	0.02	na	na	na	na	na
MgO	15.62	15.90	16.66	16.74	16.18	17.22	15.52	15.56	13.06	13.04	12.98	12.87	11.21	11.33	12.06	11.33	0.00	0.01	0.00	0.11	0.08
CaO	20.18	19.90	19.02	19.13	17.54	15.18	17.56	17.75	11.65	11.55	11.50	11.64	11.12	13.12	9.97	10.97	0.06	1.76	2.08	10.54	9.71
MnO	0.20	0.21	0.22	0.23	0.30	0.30	0.25	0.25	0.19	0.21	0.15	0.18	0.21	0.35	0.28	0.20	0.02	0.00	0.01	0.02	0.00
FeO	8.05	7.95	8.79	8.04	10.38	12.48	11.20	10.48	11.78	11.94	11.31	12.19	18.15	17.47	18.24	17.20	0.05	0.02	0.16	0.63	0.53
Na_2O	0.37	0.33	0.27	0.30	0.35	0.28	0.36	0.37	2.25	2.42	2.32	2.44	1.02	0.68	1.11	1.04	0.37	10.88	10.98	5.55	6.00
K_2O	0.01	0.00	0.00	0.00	0.01	0.00	0.01	0.00	1.07	1.11	1.09	1.06	0.45	0.55	0.50	0.52	15.31	0.08	0.06	0.28	0.35
Total	99.02	99.31	99.74	99.23	100.6	100.7	99.91	99.92	97.78	97.80	96.86	98.2	97.84	97.20	97.57	96.58	99.05	99.75	100.4	100	100.3
Si	1.89	1.89	1.92	1.92	1.93	1.94	1.92	1.94	6.16	6.16	6.198	6.195	7.20	7.167	7.08	7.174	2.995	2.920	2.899	2.515	2.551
Ti	0.02	0.02	0.02	0.02	0.02	0.02	0.02	0.02	0.50	0.49	0.503	0.487	0.14	0.281	0.14	0.144	na	na	na	na	na
Al	0.14	0.14	0.10	0.10	0.12	0.10	0.12	0.11									1.006	1.072	1.086	1.452	1.422
Mg	0.87	0.88	0.92	0.93	0.89	0.95	0.86	0.86	2.87	2.87	2.879	2.823	2.46	2.540	2.61	2.512	0.000	0.001	0.000	0.007	0.005
Ca	0.81	0.80	0.76	0.76	0.69	0.60	0.70	0.71	1.84	1.83	1.835	1.835	1.75	2.115	1.55	1.748	0.003	0.083	0.098	0.511	0.468
Mn	0.01	0.01	0.01	0.01	0.01	0.01	0.01	0.01	0.02	0.03	0.019	0.022	0.03	0.045	0.03	0.025	0.001	0.000	0.001	0.001	0.000
Fe^2	0.25	0.25	0.27	0.25	0.32	0.39	0.35	0.33	1.29	1.31	1.347	.401	1.73	2.197	1.08	1.675	0.002	0.001	0.006	0.024	0.020
Na	0.03	0.02	0.02	0.02	0.03	0.02	0.03	0.03	0.64	0.69	0.668	0.695	0.29	0.199	0.31	0.300	0.033	0.928	0.934	0.486	0.523
Al^{IV}	0.11	0.11	0.08	0.08	0.07	0.06	0.08	0.06	1.84	1.84	1.802	1.805	0.80	0.701	0.920	0.826					
Al^{VI}	0.03	0.04	0.02	0.02	0.05	0.03	0.04	0.05	0.15	0.14	0.190	0.167	0.14	0.000	0.00	0.180					
Wo	40.01	38.72	37.51	37.63	33.40	29.40	34.36	34.00													
En	46.55	47.85	48.22	49.13	48.98	50.19	46.73	47.90													
Fs	13.45	13.42	14.27	13.24	17.62	20.41	18.91	18.10													
Mg#	78	78	77	79	74	71	71	73	69	68	681	66	59	53	71	60					

*Cation calculated on the basis of 6 O for pyroxene, 23 for amphibole, and 8 for feldspar. Kfs: K. Feldspar, Pl: plagioclase, na: not analyzed. Mg#: 100*Mg/ (Mg+Fe^{+2}), Wo: Wollastonite: En: Enstatite, Fs: Ferrosilite. M Hb: Magnesio-hornblende; FM Hb: Ferri- magnesio-hornblende; TM Hb: Titanian magnesio- hornblende; TMH: Titanian magnesiohastingsite; ka: Kaersutite; TPg: Titanian pargasite.*

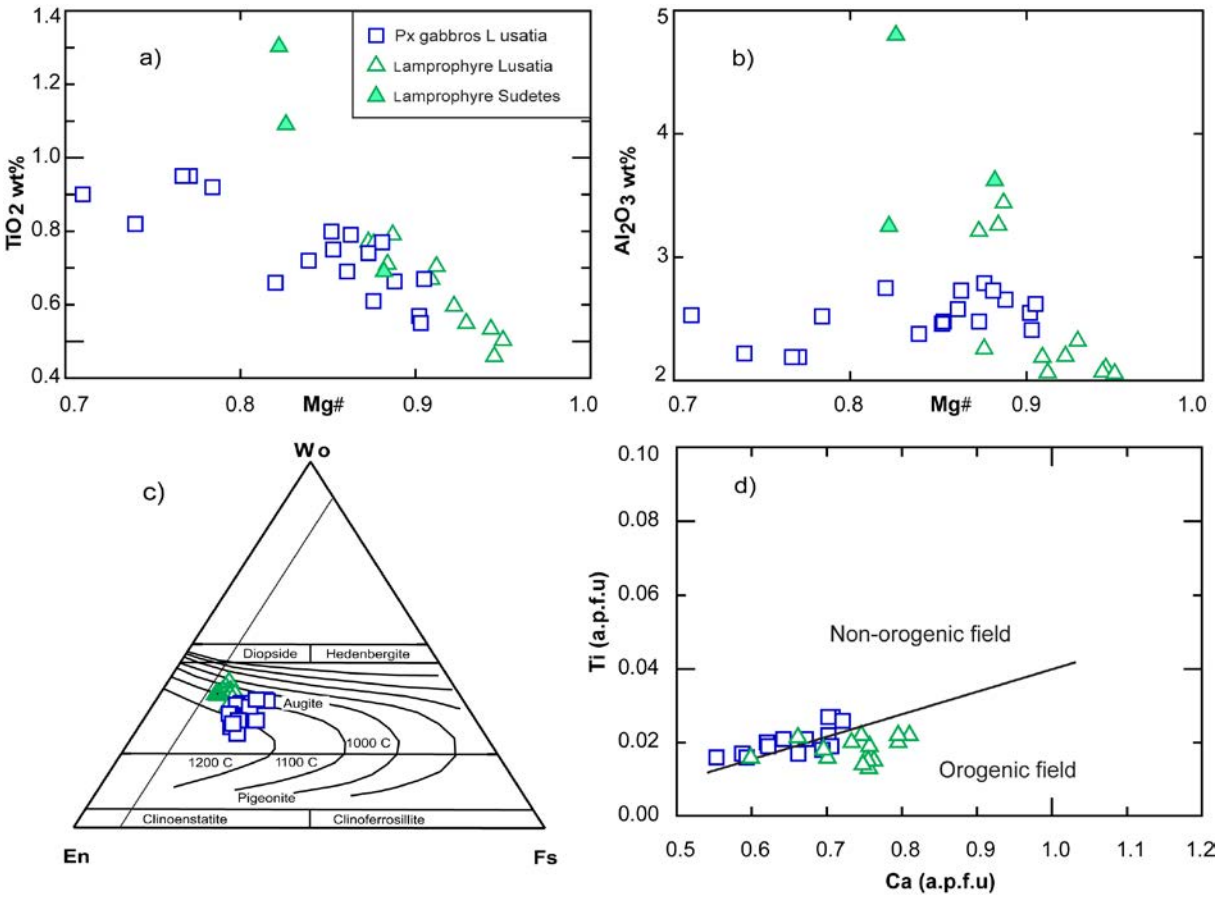

Fig. 2.3. a) Mg# vs. TiO_2; b) Mg# vs. Al_2O_3; c) Cpx triplot after Morimoto (1988), pyroxene thermometry after Lindsley (1983); d) Ca vs. Ti binary diagrams after Letterrier et al. (1982) modified by Sun and Bertrand (1991). a.p.f.u. – atoms per formula unit. Clinopyroxene composition from the Sudetes after Awdankiewicz (2007).

Amphibole is calcic (Table 2.2) and ranges according to the classification of Hawthorne and Oberti (2007) from titanian magnesio-hornblende, ferrian magnesio-hornblende, actinolitic hornblende to magnesio-hornblende. The end-member composition for clinopyroxene from the gabbros is $En_{39–52}Wo_{26–40}Fs_{17–24}$ (Table 2.2).

Calc-alkaline lamprophyres. Spessartite from Lusatia has a porphyritic to panidiomorphic texture, dominantly euhedral amphibole (c.38 vol.%) and more rarely clinopyroxene phenocrysts, and a groundmass of plagioclase (c.40 vol.%), minor amounts of intergrown K-feldspar and quartz, and accessory apatite and titanite. Amphibole is strongly pleochroic (brown to dark brown) and ranges from titanian magnesiohastingsite to pargasite and kaersutite (Table 2.2) (Kramer, 1976; Kramer, 1988; Kramer and Andrehs, 2011). Amphibole is zoned with Si and Fe increasing and Al, Cr, Na, and F decreasing from core to rim. Along the rims, amphibole may show overgrowth of actinolite with $X_{Mg} = 0.66$ (Table 2.2) and along cracks it may be replaced by chlorite and epidote. Plagioclase is a common groundmass

component, forms only rarely phenocrysts, and is typically strongly sericitized and albitized. It is albite and has the composition $Kfs_{0.8}Ab_{91}An_{8.2}$ (Table 2.2). The clinopyroxene composition in calc-alkaline lamprophyre from Lusatia is similar to the one of clinopyroxene in spessartite from the Sudetes (Fig. 2.3), but differs from the one of clinopyroxene from Lusatian gabbros, which have lower CaO, Cr_2O_3 and Mg# and higher MnO, Na_2O, SiO_2, TiO_2, and FeO (Table 2.2). It is Ca rich augite ($Wo_{36-40}En_{46-50.9}Fs_{12-16}$; Table 2.2; Fig. 2.3c) and rarely forms phenocrysts. According to Lindsley (1983), the clinopyroxene composition indicates crystallization temperatures that range from 900°C to ~1200°C for the calc-alkaline lamprophyre and from 1000°C to ~1200°C for the gabbros (Fig. 2.3c). Clinopyroxene from the gabbros and calc-alkaline lamprophyres have similar Ti/Al ratios (between 0.25 and 0.125). On the Ca–Ti discrimination diagram, clinopyroxene of the calc-alkaline lamprophyre mostly plot in the orogenic field consistent with formation in a subduction-related tectonic setting. The tholeiitic gabbro pyroxenes plot along the line separating the orogenic and non-orogenic fields (Fig. 2.3d).

2.4.3. Whole rock geochemistry of investigated rocks

Chemical analyses of 21 representative samples of the gabbros and spessartites are given in Table 2.3. Chemical variations among them are shown in Harker diagrams (Fig. 2.4). In the Alk–FeO*–MgO diagram of Irvine and Baragar (1971) (not shown), the gabbros are tholeiitic and the lamprophyres show a calc-alkaline trend. The lamprophyre samples fall within the range of calc-alkaline lamprophyres following the classification of Rock (1977 and 1991). In the total alkali silica (TAS) diagram (Fig. 2.5), they straddle the boundary between the alkaline and the sub-alkaline series similar to the lamprophyres from the adjacent areas and plot in the fields of trachybasalts, basaltic andesites, basaltic trachyandesites, and basalts. The Lusatian lamprophyres show lower alkali and silica contents relative to the lamprophyres from the adjacent areas (Fig. 2.5).

The gabbros generally have lower Mg# (38–57), MgO (4.4–6.2 wt %), Cr (40–167 ppm), and Ni (52–100 ppm) than the calc-alkaline lamprophyres (Mg# 52–61, MgO 5.1–8 wt%, Cr 85–321 ppm, Ni 22–187 ppm), except for two gabbroic samples that have high Mg# and high MgO, FeO, Cr, and Ni contents as the result of olivine accumulation. The gabbros have high contents of CaO (9.3–11.2 wt %). The calk-alkaline lamprophyres are characterized by moderate contents of Al_2O_3 (14.3–16.9 wt %), TiO_2 (1–2.46 wt %), and CaO (5.7–9.1) and high contents of K_2O (0.88–3.20 wt %). Furthermore, the calc-alkaline lamprophyres have greater abundances of Rb (24–111 ppm), Zr (105–360 ppm), Nb (11–20.8 ppm), Ba (173–

1662 ppm), Pb (3.1–14.7 ppm), Th (2–15.2 ppm), and Sr (273–625 ppm) than the gabbros (Rb 2–44 ppm, Zr 64–115 ppm, Nb 6.1–8.1 ppm, Ba 106–170 ppm, Pb 1.8–3.9 ppm, Th 1.2–2.9 ppm, and Sr 198–337 ppm).

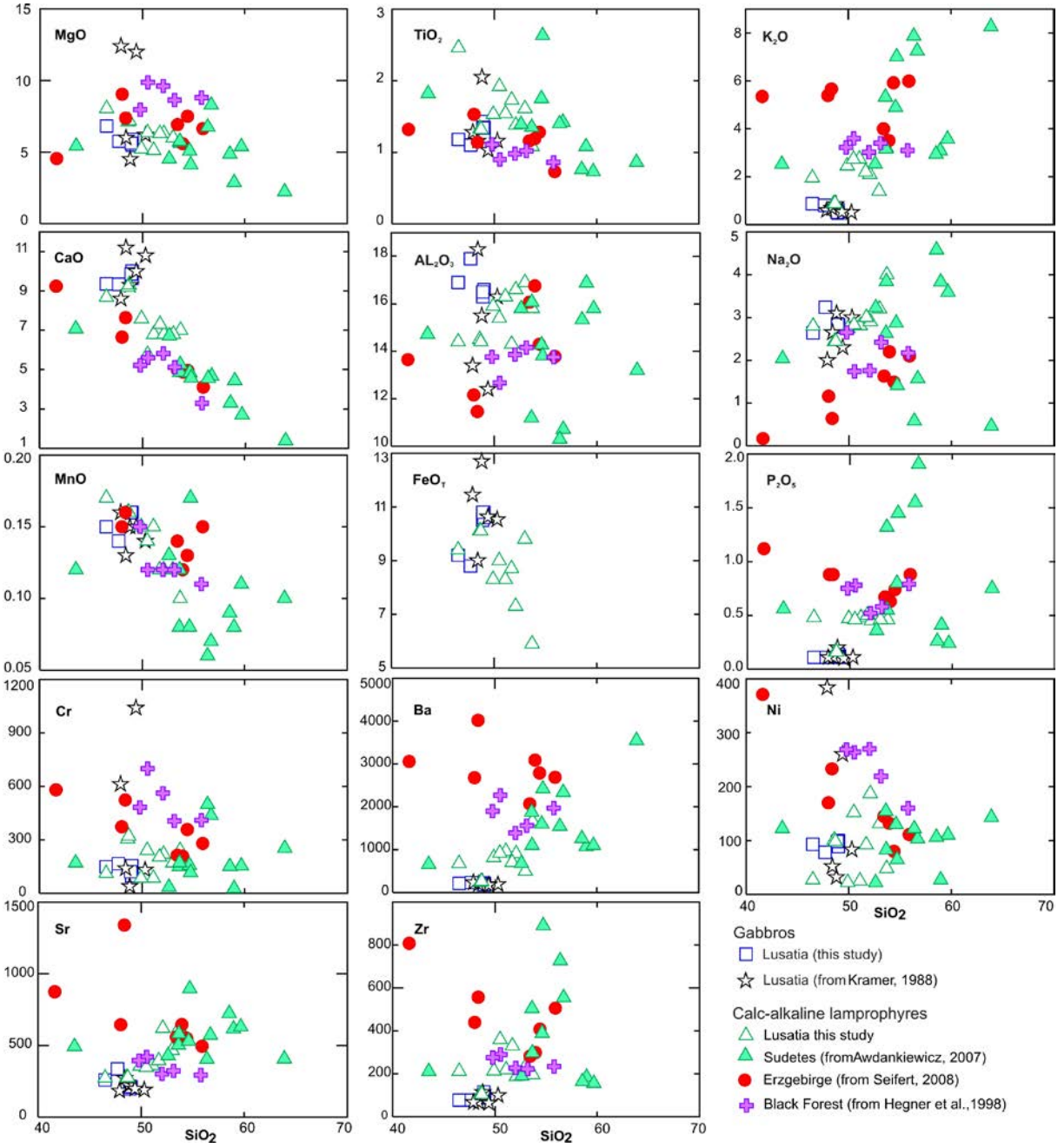

Fig.2.4. Major (wt%) and trace elements (ppm) composition of Lusatian gabbros and lamprophyres compared with those from other regions. Data sources: gabbros (Kramer, 1988), lamprophyres from the Sudetes (Awdankiewicz, 2007); lamprophyres from the Erzgebirge (Seifert, 2008); and lamprophyres from the Black Forest (Hegner et al., 1998).

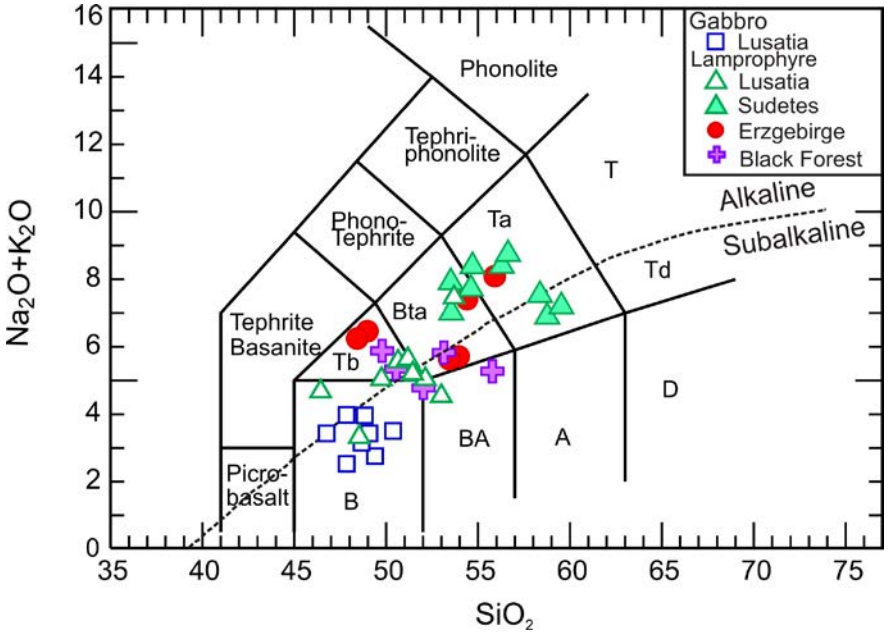

Fig. 2.5. The total alkali versus silica (TAS) diagram (Le Maitre et al., 2002), with selected fields annotated: A (andesites), B (Basalts), BA (basaltic andesites), BTa (basaltic trachyandesites), D (dacites), R (rhyolites), T (trachytes), Ta (trachyandesites), Tb (trachybasalts). The boundary between the alkaline and subalkaline series is after Irvine and Baragar (1971). Data sources of the lamprophyres from the adjacent areas are as in Fig.2.4.

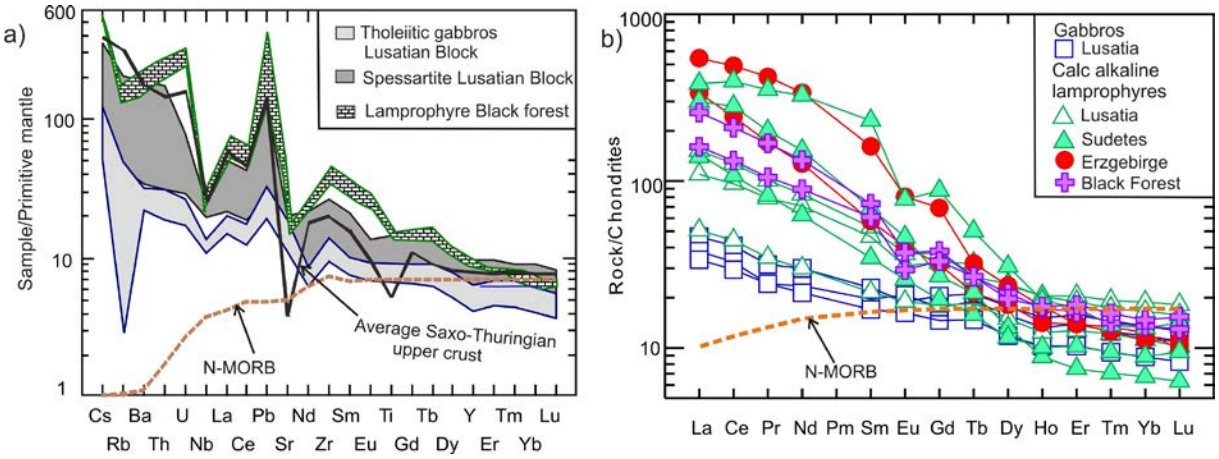

Fig. 2.6. a) Primitive-mantle-normalized pattern (Sun and McDonough, 1989); b) Chondrite-normalized patterns (Sun and McDonough, 1989) of Lusatian gabbros and calc-alkaline lamprophyres from Variscan Massifs. Data sources: N-MORB (Sun and McDonough, 1989); lamprophyres from the Sudetes (Awdankiewicz, 2007); lamprophyres from the Erzgebirge (Seifert, 2008); lamprophyres from the Black Forest (Hegner et al., 1998). Saxo-Thuringian upper crust from Romer and Hahne (2010) is shown for reference. Some calc-alkaline lamprophyres from Sudetes with the most extreme pattern are described as lamproites (Krmíček, 2010).

Table 2.3.

Geochemical data of gabbros and calc-alkaline lamprophyres from Lusatia.

	Gabbro											Calc-alkaline lamprophyre									
Rock	gb	gb	pg-gb	pg-gb	ol-gb	ol-gb	dt	ol-gb	gb	gb	gb-nt	sp	sp	sp	sp	sp	sp	sp	sp	sp	sp
No	VG1	VG2	VG3	VG4	KE5	KE6	BS7	VG8	SH9	FB10	SH11	DG12	DG13	JS14	JS15	JS16	DG17	JS18	SW19	HB20	IS21
SiO_2	48.9	49.0	49.0	48.9	46.5	47.7	48.8	50.3	48.4	49.4	47.9	51.1	49.9	48.6	48.7	46.5	50.5	52.1	51.7	53.7	53.0
TiO_2	1.43	1.35	1.22	1.34	1.18	1.10	2.05	1.16	1.16	1.03	1.28	1.54	1.53	1.33	1.32	2.46	1.92	1.38	1.73	1.08	1.61
Al_2O_3	16.3	16.6	16.6	16.5	16.9	17.9	15.5	16.3	18.3	12.4	13.4	16.3	15.9	14.5	14.4	14.4	15.4	16.6	14.3	15.8	16.9
FeOt	10.5	10.8	10.6	10.8	9.2	8.8	13	10.5	9	10.6	11.5	8.3	8.3	10.1	10.1	9.4	9	7.3	8.7	5.9	9.8
MnO	0.16	0.16	0.16	0.16	0.15	0.14	0.15	0.14	0.13	0.15	0.16	0.15	0.15	0.16	0.16	0.17	0.14	0.12	0.12	0.10	0.12
MgO	5.90	5.5	5.9	5.6	6.8	5.8	4.5	6.2	6.0	12.0	12.4	5.1	5.2	7.1	7.2	8.0	6.4	6.3	6.3	5.6	6.0
CaO	9.7	9.6	10.0	9.9	9.4	9.3	9.3	10.8	11.2	10.0	8.6	6.8	7.6	9.2	9.3	8.7	5.8	6.8	7.3	7.0	6.8
Na_2O	2.85	2.83	2.78	2.84	2.64	3.24	3.10	3.00	2.65	2.30	2.00	2.81	2.74	2.44	2.44	2.80	2.83	2.90	3.00	4.00	3.20
K_2O	0.57	0.62	0.48	0.51	0.87	0.80	0.85	0.51	0.68	0.53	0.60	2.74	2.45	0.88	0.88	1.95	2.73	2.10	2.20	3.20	1.40
P_2O_5	0.14	0.12	0.11	0.12	0.11	0.11	0.20	0.11	0.11	0.10	0.11	0.48	0.47	0.16	0.16	0.48	0.46	0.45	0.50	0.46	0.46
H_2O	1.51	1.41	1.28	1.36	3.86	3.26	2.10	0.40	1.58	1.03	1.88	3.06	3.33	3.29	3.11	2.08	3.16	2.42	2.40	1.50	2.14
CO_2	0.58	0.46	0.40	0.41	1.03	0.32	0.43	0.56	0.30	0.71	0.36	0.38	1.01	0.67	0.70	1.26	0.14	0.22	0.51	0.14	0.40
Total	99.6	99.6	99.6	99.6	99.6	99.5	100.3	100.3	99.6	100.6	100.4	99.6	99.5	99.5	99.6	99.2	99.0	99.4	98.9	99.3	100.3
Ba	155	138	113	115	143	163	170	122	128	106	165	960	815	173	189	676	918	907	701	1662	500
Cr	134	98	155	121	149	167	40	132	140	1041	613	85	85	305	321	112	241	220	204	241	171
Ni	97	89	100	98	93	78	32	83	52	260	384	25	22	101	98	27	152	187	92	48	131
Rb	7	8	2	4	20	27	44	13	22	17	22	111	96	27	24	72	66	35	65	64	54
Sr	198	209	212	213	259	337	222	190	272	198	184	360	356	277	276	273	348	620	394	625	466
V	226	230	205	213	222	212	260	199	232	175	214.0	214	216	216	222	321	174	178	170	184	130
Zn	93	95	91	96	81	72	119	91	68	82.0	89.0	79	81	92	89	77	103	94	100	61	62
Zr	115	96	88	93	78	78	115	100	68.0	64.0	68.0	219	214	105	105	212	360	188	330	196	236
Y	22	19	19	20	14	14	25	18	14	14	16	31	29	17	18	56	35	24	28	29	26
Li	8	8	7	7	30	20	15	7	9	8	10	12	12.9	17	16	11.5	7.9	15.9	16.2	8.4	15.3
Nb	7.7	7	6.1	6.5	7.7	7.6	13	6.4	8.1	6.3	7.6	14	13	12	11	19	24	14.1	20.8	14	14.9
Mo	0.61	0.5	0.43	0.12	0.45	0.4	1.5	0.69	0.58	0.97	0.63	0.57	0.45	0.72	0.86	0.492	1.14	0.67	2.76	0.24	0.94
Cd	0.11	0.11	0.12	0.12	0.12	0.15	0.16	0.12	0.12	0.12	0.12	0.11	0.11	0.11	0.12	0.098	0.19	0.2	0.16	0.29	0.17
Cs	1.09	1.23	0.92	0.96	25	1.9	14	0.66	3.0	2.1	2.7	1.04	1.12	6.32	6.01	1.48	0.66	6.7	1.5	0.38	1.19
Pb	2.6	3.1	2.39	2.72	3.88	2.34	3.7	2.3	2.8	1.8	2.2	14.74	10.49	3.1	3.08	6.45	9.48	11.65	6.34	7.56	8.52

Th	2.04	1.84	1.57	1.59	1.19	1.17	2.9	1.8	1.9	1.7	1.9	11.11	10.46	2.03	2.17	9.15	10.16	11.95	8.41	15.15	7.04
U	0.47	0.48	0.38	0.39	0.32	0.31	0.69	0.40	0.51	0.34	0.43	1.35	1.34	0.53	0.54	1.77	1.77	1.9	1.9	2.21	1.09
Sc	23	23	23	23	25	24	22	23	24	24	24	30	29	26	25	89	27	22	23	24	20
Co	40	40	39	39	39	34	52	54	56	70	35	26	26	40	38	30	30	27	46	22	28
Cu	47	46	49	54	53	39	48	52	76	67	44	16	13	39	38	28	29	66	37	248	36
Ga	20	20	19	20	18	18	22	19	15	14	18	19	18	18	18	19	19	18	19	16	17
Sb	0.08	0.12	0.11	0.11	0.47	0.81	0.09	0.06	0.08	0.03	0.08	0.12	0.11	0.17	0.15	0.3	0.14	0.33	0.24	0.21	0.15
Sn	0.97	1.01	0.82	0.86	0.68	0.72	1.5	0.82	0.82	0.67	0.76	2.21	2.18	0.88	0.8	1.82	2.51	4.37	2.04	19.1	1.25
La	11	10	9	10	8	8	14	8.2	8.3	8	8.8	28	26	12	12	27	38	40	36	40	30
Ce	25	22	20	22	18	18	32	19	18	17	20	62	59	27	27	72	78	82	78	77	66
Pr	3	2.5	2.3	2.4	2.3	2.3	3.9	2.2	2.2	2.1	2.6	8.2	7.5	3.2	3.3	11	9.9	9.7	9.6	9.2	7.9
Nd	14	12	11	12	10	10	18	10	9.7	9.7	11	35	33	14	14	52	39	37	39	40	32
Sm	3.5	3.1	3	3.1	2.6	2.6	4.5	2.8	2.4	2.6	2.8	7.4	7.1	3.2	3.3	14	8	6.9	8.1	7.5	6.4
Eu	1.1	1.1	1.2	1.2	0.94	0.91	1.5	0.98	0.89	0.88	0.92	1.8	1.8	1	1.1	3.1	2	1.71	2.12	2.2	1.73
Gd	4.2	3.7	3.6	3.8	3	3	5.3	3.5	2.8	3.1	3.2	7	6.7	3.7	3.7	14	7.3	6.1	7.6	7	6.1
Tb	0.79	0.72	0.71	0.72	0.55	0.56	0.86	0.60	0.49	0.52	0.59	1.2	1.2	0.66	0.69	2.3	1.2	0.81	0.99	0.78	0.82
Dy	4.5	4	4	4.1	3	3	5.3	3.7	2.9	3.1	3.3	6.3	6	3.7	3.8	13	6.1	5.02	6.17	6	5.31
Ho	0.86	0.74	0.75	0.78	0.58	0.57	0.98	0.70	0.55	0.57	0.61	1.2	1.16	0.7	0.7	2.3	1.1	0.95	1.15	1.02	1
Er	2.6	2.3	2.3	2.3	1.7	1.7	2.9	2.1	1.6	1.7	1.8	3.6	3.4	2.1	2.1	6.6	3.2	2.67	3.14	3.02	2.86
Tm	0.37	0.32	0.32	0.33	0.24	0.25	0.38	0.31	0.24	0.23	0.24	0.49	0.49	0.29	0.31	0.91	0.43	0.36	0.44	0.41	0.4
Yb	2.3	2	2	2.1	1.5	1.6	2.5	1.9	1.5	1.4	1.6	3.4	3.2	1.9	1.9	5.5	2.9	2.45	2.81	2.4	2.69
Lu	0.32	0.28	0.28	0.29	0.21	0.21	0.35	0.27	0.21	0.20	0.23	0.47	0.46	0.25	0.26	0.79	0.42	0.35	0.4	0.43	0.39
Mg#	49.9	47.6	49.8	48.18	56.97	53.83	38.25	51.2	54.3	66.85	65.94	52.4	52.8	55.6	55.9	60.5	55.7	59.2	56.7	60.5	56.68

Samples 7 to 10 major elements after Kramer (1988). gb: gabbros; peg-gb: pegmatitic gabbro; ol-gb: olivine gabbros; dt: diorite; sp: spessartites, Locations: samples VG1, VG2, VG3, VG4 and VG8 from Valtengrund; KE5 and KE6 from Klunst Ebersbach; BS7 from Bautzen-Stiebitz; SH9 and SH11 from Soraer Höhe; FB10 from Fichtenberg; DG12, DG13 and DG17 from Das Gericht; JS14, JS15, JS16 and JS18 from Julienstein; SW19 from Strahwalde; HB20 from Hutzelberg; IS21 from Israel.

Table 2.4
Whole-rock Sr, Nd, and Pb isotope data of gabbros and calc-alkaline lamprophyres from Lusatia, Germany.

Sample[a]		Age (Ma)	$^{87}Sr/^{86}Sr$ [b]	$^{87}Sr_{(T)}/^{86}Sr$ [c]	$^{143}Nd/^{144}Nd$ [b]	$\varepsilon Nd_{(T)}$ [c]	$^{206}Pb/^{204}Pb$ [d]	$^{207}Pb/^{204}Pb$ [d]	$^{208}Pb/^{204}Pb$ [d]	$^{206}Pb/^{204}Pb$ [e]	$^{207}Pb/^{204}Pb$ [e]	$^{208}Pb/^{204}Pb$ [e]
1	VG1	330	0.705136±5	0.70466	0.512593±7	1.0	18.475	15.611	39.221	17.86	15.58	38.36
		400		0.70455		1.4				17.73	15.57	38.18
2	VG2	330	0.705217±4	0.70470	0.512568±4	0.3	18.272	15.566	38.455	17.76	15.54	37.82
		400		0.70459		0.7				17.65	15.53	37.68
3	VG3	330	0.704793±4	0.70466	0.512573±3	0.1	18.411	15.576	38.695	17.87	15.55	37.98
		400		0.70464		0.4				17.76	15.54	37.83
4	VG4	330	0.704955±3	0.70470	0.512670±4	2.3	18.241	15.553	38.427	17.77	15.53	37.80
		400		0.70465		2.7				17.66	15.52	37.66
5	KE5	330	0.707064±6	0.70601	0.512680±4	2.5	18.157	15.588	38.348	17.88	15.57	38.02
		400		0.70579		2.8				17.82	15.57	37.95
6	KE6	330	0.707441±4	0.70635	0.512642±4	1.7	18.25	15.566	38.353	17.82	15.54	37.82
		400		0.70612		2.1				17.72	15.54	37.70
7	SH9	330	0.704856±4	0.70448	0.512658±6	2.4	18.331	15.559	38.517	17.72	15.53	37.79
		400		0.70438		2.8				17.59	15.52	37.63
8	BS7	330	0.706281±5	0.70359	0.512646±5	2.1	18.395	15.558	38.570	17.77	15.53	37.72
		400		0.70301		2.5				17.64	15.52	37.54
9	VG8	330	0.704869±4	0.70394	0.512613±5	0.7	18.338	15.553	38.529	17.76	15.52	37.68
		400		0.70374		0.9				17.63	15.51	37.50
10	DG12	330	0.711938±2	0.70775	0.512256±5	-4.6	18.334	15.591	38.991	18.03	15.58	38.17
11	DG13	330	0.711637±4	0.70797	0.512259±5	-4.6	18.47	15.602	39.218	18.04	15.58	38.13
12	JS14	330	0.706119±5	0.70479	0.512608±4	1.9	18.368	15.568	38.541	17.80	15.54	37.83
13	JS15	330	0.706116±6	0.70493	0.512651±3	2.5	18.379	15.566	38.548	17.80	15.54	37.79
14	JS18	330	0.708408±5	0.70764	0.512356±6	-2	18.635	15.603	39.008	18.09	15.57	37.89
15	SW19	330	0.707204±4	0.70496	0.512476±7	-0.1	18.86	15.594	39.160	17.85	15.54	37.71
16	DG17	330	0.707592±5	0.70501	0.512472±4	-0.2	18.888	15.62	39.236	18.25	15.59	38.06
17	HB20	330	0.708766±4	0.70737	0.512299±6	-3.1	18.97	15.64	39.928	17.97	15.59	37.70
18	IS21	330	0.706213±5	0.70463	0.512514±5	0.7	18.534	15.606	38.904	18.10	15.58	38.01

a Sr, Nd and Pb isotopic compositions were analyzed at Deutsches GeoForschungsZentrum GFZ (Potsdam). The samples were dissolved with concentrated HF for four days at 160°C on the hot plate. The digested samples were dried, taken up in 2N HNO_3 and slowly dried then the samples were taken up in 6N HCl.

b $^{87}Sr/^{86}Sr$ and $^{143}Nd/^{144}Nd$, normalized to $^{86}Sr/^{88}Sr = 0.1194$ and $^{146}Nd/^{144}Nd = 0.7219$, respectively, were obtained on a Thermo Triton and a Finnigan MAT262 multi-collector mass-spectrometer, respectively, using dynamic multi,collection. Analytical uncertainties are given at $2\sigma_m$ level.

c $^{87}Sr/^{86}Sr_{(T)}$ and $\varepsilon Nd_{(T)}$ were calculated for the emplacement age using $\lambda^{87}Rb = 1.42E\text{-}11\ y^{-1}$ and $\lambda^{147}Sm = 6.54E\text{-}12\ y^{-1}$, $(^{147}Sm/^{144}Nd)^0_{CHUR} = 0.1967$, and $(^{143}Nd/^{144}Nd)^0_{CHUR} = 0.512638$, respectively, and the concentration data given in Table 2.3.

d Pb was separated and purified using ion-exchange chromatography as described in Romer et al. (2005). The Pb isotopic composition was determined on a Finnigan MAT262 multi-collector mass-spectrometer using static multicollection. Lead isotope data corrected for mass discrimination with 0.1% / A.M.U. as estimated from the repeated measurement of lead reference material NBS 981. Reproducibility at 2σ level is better than 0.1%.

e Lead isotope data recalculated to the emplacement age using the contents of Pb, Th, and U (Table 2.3) and the constants recommended by IUGS ($\lambda^{232}Th = 4.9475E\text{-}11\ y^{-1}$, $\lambda^{235}U = 9.8485E\text{-}10\ y^{-1}$, and $\lambda^{238}U = 1.55125E\text{-}10\ y^{-1}$).

Trace element variation diagrams show no systematic variations of Zr, Rb, Sr, and Nb with SiO_2 for gabbros and calc-alkaline lamprophyres (Fig. 2.4). The gabbros cluster in a relatively narrow field, whereas the calc-alkaline lamprophyres typically have higher trace

element and SiO_2 contents (Fig. 2.4). Only two spessartite samples overlap with the gabbro composition.

In multi-element variation diagrams, gabbros and calc-alkaline lamprophyres from Lusatia show a strong enrichment relative to primitive mantle (Fig. 2.6a). Both groups show similar pattern with a significant Nb trough, although the calc-alkaline lamprophyres have distinctly higher trace element contents (i.e., U, Pb, Th, Ti, Ba, Rb, Cs, Zr, and Nb). The rare earth element pattern of the gabbros is steeper compared to the average N-MORB, showing slight relative light rare earth elements (LREE) enrichment and heavy rare earth elements (HREE) depletion (Fig. 2.6b). The gabbros are strongly enriched in large-ion lithophile elements (i.e., the LILE- Cs, Pb, Rb, Ba, Sr) relative to N-MORB (Fig. 2.6a). The gabbros show slightly less enriched Nb contents than those of U and La (Fig. 2.6a). The calc-alkaline lamprophyres show a stronger enrichment in Rb/Nb and Ba/Nb than the gabbros. Furthermore, the calc-alkaline lamprophyres exhibit a strong Pb peak, and a slight trough in Sr relative to Pb and Nd concentrations. A similar geochemical fingerprint has been documented for late-Variscan lamprophyres of the Black Forest (Hegner et al., 1998; Fig. 2.6a), the Sudetes (Awdankiewicz, 2007), and the Erzgebirge (Seifert, 2008) and alkaline basalts and Cretaceous ultramafic lamprophyres of Lusatia (Renno et al., 2003a, 2003b; Abdelfadil et al., 2010) and Saxo-Thuringian upper crust (Romer and Hahne, 2010).

Chondrite normalized REE pattern for gabbros and calc-alkaline lamprophyres (Fig. 2.6b) exhibit strong enrichment in LREE with La abundances up to 200 times chondritic values (Sun and McDonough, 1989). REE pattern for the gabbros are moderately fractionated with $(La/Yb)_N$ = 3–3.8, whereas those for the calc-alkaline lamprophyres are strongly fractionated with $(La/Yb)_N$= 3.3–11. The HREE in the gabbro samples are less enriched than those in the calc-alkaline lamprophyres. There is no Eu anomaly in gabbro and calc-alkaline lamprophyre samples, except for one lamprophyre sample that has a slightly negative Eu anomaly. The calc-alkaline lamprophyres of Lusatia have similar REE pattern as lamprophyres from the Black Forest (Hegner et al., 1998), but flatter REE pattern (i.e., lower LREE) than lamprophyres from the Erzgebirge (Seifert, 2008) and the Sudetes (Awdankiewicz, 2007; Fig. 2.6b).

The Nd, Sr, and Pb isotopic compositions of gabbros and calc-alkaline lamprophyres are presented in Table 2.4. Gabbros and calc-alkaline lamprophyres encompass a relatively wide range of measured Sr isotopic compositions from 0.7048 to 0.7074 and 0.7061 to 0.7119, respectively. The gabbros show a narrow range of measured Nd isotope compositions from 0.51256 to 0.51268, whereas the calc-alkaline lamprophyres show a broader variation

from 0.51225 to 0.51265. The Nd isotopic composition of the gabbros falls in the compositional range of the depleted mantle, although the trace-element signatures and to a lesser extent from the Sr isotopic compositions indicate that this mantle had been affected by metasomatic additions of evolved material. The calc-alkaline lamprophyres fall between the compositions of depleted mantle and the Saxo-Thuringian upper crust (Linnemann and Romer, 2002; Romer and Hahne, 2010) in the εNd_{init} vs. $^{87}Sr/^{86}Sr_{init}$ diagram (Fig. 2.7a). The measured Pb isotope composition of the gabbros and calc-alkaline lamprophyres exhibit relatively wide compositional variations with $^{206}Pb/^{204}Pb$= 18.16–18.97, $^{207}Pb/^{204}Pb$ = 15.55–15.64, and $^{208}Pb/^{204}Pb$ = 38.35–39.93 (Table 2.4). The Pb from both gabbros and lamprophyres have at a given $^{206}Pb/^{204}Pb_{init}$ far higher $^{207}Pb/^{204}Pb_{init}$ than the mantle, i.e., their Pb is dominated by crustal Pb (Fig. 2.7b). The calc-alkaline lamprophyres, however, have higher $^{207}Pb/^{204}Pb_{init}$ ratios than the gabbros for corresponding $^{206}Pb/^{204}Pb_{init}$, indicating that crustal contributions to the lamprophyres (and their source) are much more prominent than to the gabbros.

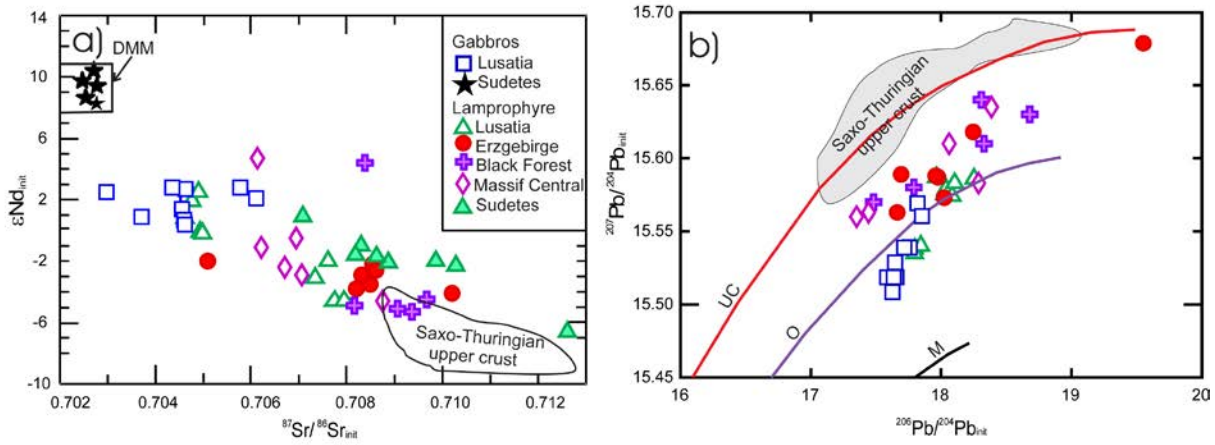

Fig. 2.7. a) The εNd_{init} versus $^{87}Sr/^{86}Sr_{init}$ and b) initial Pb isotopic composition of Lusatian lamprophyres and gabbros compared with late and post-Variscan lamprophyres from the Sudetes (Awdankiewicz, 2007), the Erzgebirge (Seifert, 2008), the Black Forest (Hegner et al., 1998), the French Massif Central (Turpin et al., 1988), gabbros from the Sudetes (Pin et al., 1988), and Saxo-Thuringian upper crust (Romer and Hahne, 2010). Depleted MORB mantle (DMM) from Zindler and Hart (1986). Mantle (M), orogene (O) and upper crust (UC) Pb evolution curves are after Zartman and Doe (1981). Note the gabbros are recalculated to 400 Ma, whereas the lamprophyres are calculated to 330 Ma.

2.5. Discussion

2.5.1. Alteration and assimilation processes

Alteration of minerals is typical in lamprophyres and could affect also the element and isotope geochemistry of the whole-rock samples (Rock, 1977; Turpin et al., 1988). The samples used for geochemical analysis are fresh and show no systematic correlation between LOI and Sr isotopic composition (not shown), except for sample DG12, which has the highest $^{87}Sr/^{86}Sr$ value (0.71194), a high LOI of 3.44 wt%, and Rb contents of 111 ppm. These features may be ascribed to alteration. Similarly, the two olivine gabbro samples (KE5, KE6) with the highest LOI (3.58 wt% and 4.89 wt%, respectively) show the most radiogenic Sr isotopic compositions for gabbro (0.70601 and 0.70635, respectively). The association of high volatile content and radiogenic Sr isotopic composition indicates that fluids released from the wall-rocks during emplacement of the gabbros and the lamprophyres have transported radiogenic Sr – also derived from the wall-rocks – into the magmatic rocks. In addition, the highest LOI, Sr, and Rb samples show similar range of Nd isotopic ratios as samples with lower contents of LOI. To avoid effects of fluid-rock interaction during emplacement, only immobile elements were used for petrogenetic interpretations.

The crustal geochemical fingerprints in the gabbros and the calc-alkaline lamprophyres may be the result of two types of processes (and their combination). The first type of process is related to the ascent and emplacement of the magma, i.e., differentiation of basic magma by fractional crystallization (FC; e.g., Kramer, 1976; Currie and Williams, 1993) and assimilation of country rocks with fractional crystallization (AFC; e.g., DePaolo, 1981). The second type of processes involves the modification of the mantle source by subduction-related fluids/melt (Condie, 1990; Feng et al., 2004; Prelević et al., 2005; Awdankiewicz, 2007; Nédli and Tóth, 2007).

Using incompatible trace elements to distinguish between fractional crystallization, assimilation with fractional crystallization, and mixing processes (e.g., DePaolo, 1981; Cribb and Barton, 1996), we modeled FC and AFC processes (Fig. 2.8). This modeling demonstrates that fractional crystallization and assimilation with fractional crystallization cannot account for the observed variation within the data and indicates that two source components are better suited to explain the geochemical and isotopic variability among the samples. The key results of the modeling are:

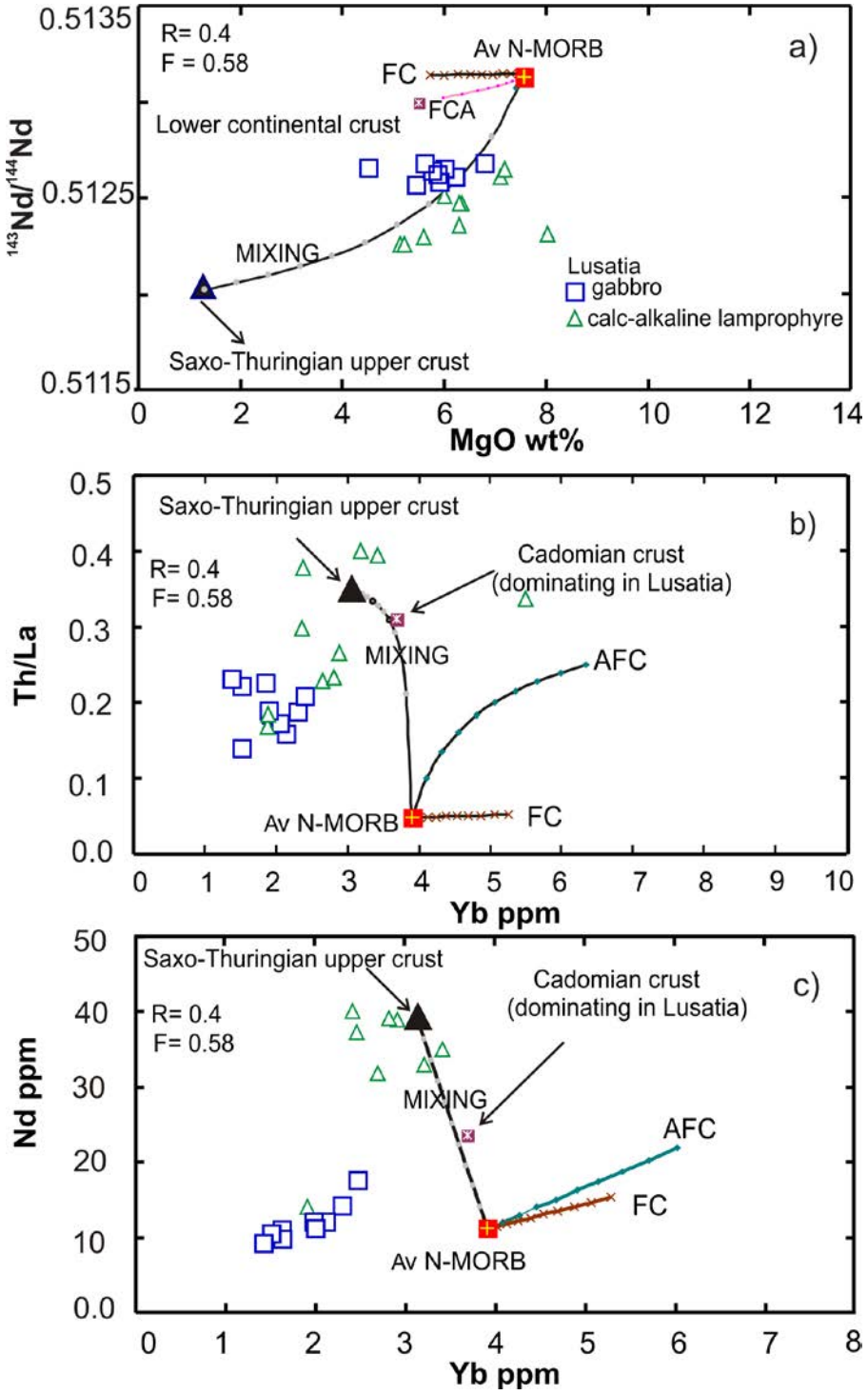

Fig. 2.8. (a) $^{143}Nd/^{144}Nd$ versus MgO (b) plots showing the results of FC, AFC, FCA, and mixing modeling results. C_0= N-MORB average is from Hofmann (1988), Ito et al. (1987), and Hauri and Hart (1997); MgO=7.57, Th=0.187, La=3.89, Nd=11.18, Yb=3.9 and $^{143}Nd/^{144}Nd$=0.5131. Saxo-Thuringian upper crust from Romer and Hahne (2010). Two assimilants have been used; average lower continental crust from Taylor and McLennan (1995) and Cadomian crust from Linnemann and Romer (2002). Bulk partition coefficient; Kd_{La}=0.182, Kd_{Th}=0.028, Kd_{Nd}=0.300, Kd_{Yb}=0.323 and Kd_{MgO}=0.249, which are calculated

for the fractionating mineral assemblage of plagioclase$_{(0.6)}$, clinopyroxene$_{(0.2)}$, and olivine$_{(0.2)}$ in a basic magma. Fractional crystallization assimilation (FCA).

(i) The scattered variation of initial $^{87}Sr/^{86}Sr$ with MgO concentration (Fig. 2.9a) can not be obtained by AFC. Assimilation of crustal rocks will decrease MgO and increase $^{87}Sr/^{86}Sr$. Similarly, FC would result in lower MgO at constant Sr isotopic composition.

(ii) The strong enrichment in LREE and LILE (Fig. 2.6a, b) in combination with low Ce/Pb and high Mg# and compatible element (e.g., Cr, Ni, MgO; Fig. 2.4) contents can not be obtained by AFC processes.

(iii) The absence of regular trends in binary diagrams of gabbros and spessartites (Fig. 2.4) and the more radiogenic Sr and Pb isotopic composition and the lower $^{143}Nd/^{144}Nd$ ratios (Fig. 2.7) of the lamprophyres in comparison to the gabbros do not support a derivation of spessartite by fractionation from the gabbro source as suggested by Kramer (1976) and Currie and Williams (1993). In particular, continued development of the Sr, Nd, and Pb isotopic composition in the gabbro source from the time of gabbro extraction to the time of lamprophyre emplacement can not account for the contrasting isotopic compositions of gabbros and lamprophyres.

2.5.2. Pre/late Variscan geochemical fingerprints of the mantle beneath Lusatia

The pre-Variscan gabbros have Nb/U, Ce/Pb, Th/La, Sm/La and Ba/Nb ratios that resemble crust rather than mantle and that demonstrate the involvement of crustal material in the mantle source of the gabbros (Fig. 2.9). The transfer of crustal signatures from subducted rocks to the mantle is a selective process that depends on the devolatization and melting history of the subducted material. Thus it does not impose crustal trace-element signatures completely unchanged to the metasomatized mantle. The striking similarity of the trace element patterns of Saxo-Thuringian upper crust and lamprophyres with Nb, Sr, Pb, and Zr anomalies (Fig. 2.6a) reflects that rocks with this regionally occurring geochemical signature have modified the lamprophyre source. The contrasting enrichment or depletion of trace element abundance in mantle normalized pattern in Variscan lamprophyres from Lusatia and from other areas (e.g., Sudetes, Black Forest, French Massif Central) indicates both the heterogeneity of the mantle source and regionally variable contribution of the subducted crustal material. Crustal contributions to the gabbro source are also evident in trace element pattern normalized to continental crust (Fig. 2.10a), as the gabbros have flat pattern with marked depletions in Pb and Rb and slight enrichments in Cs, and Sr. The crustal Pb isotopic

compositions and the high initial $^{87}Sr/^{86}Sr$ values of the gabbros at essentially constant initial $^{143}Nd/^{144}Nd$ values indicate fluid-mediated uncoupling of Pb and Sr from Nd (Fig. 2.7a, b). The tholeiitic gabbros in the Lusatian Block show a marked geochemical contrast to the c. 400 Ma old gabbros of the adjacent Sudetes that show N-MORB affinity, εNd_{400} (8.1 to 8.5) and Sr isotopes (0.7021 to 0.7028; Fig. 2.7a) and are considered to be a part of an ophiolite complex (Kryza and Pin, 2010). Thus, the geochemical signature of the Lusatian gabbros reflects a mantle source that has been metasomatized during subduction related to the Cadomian orogeny.

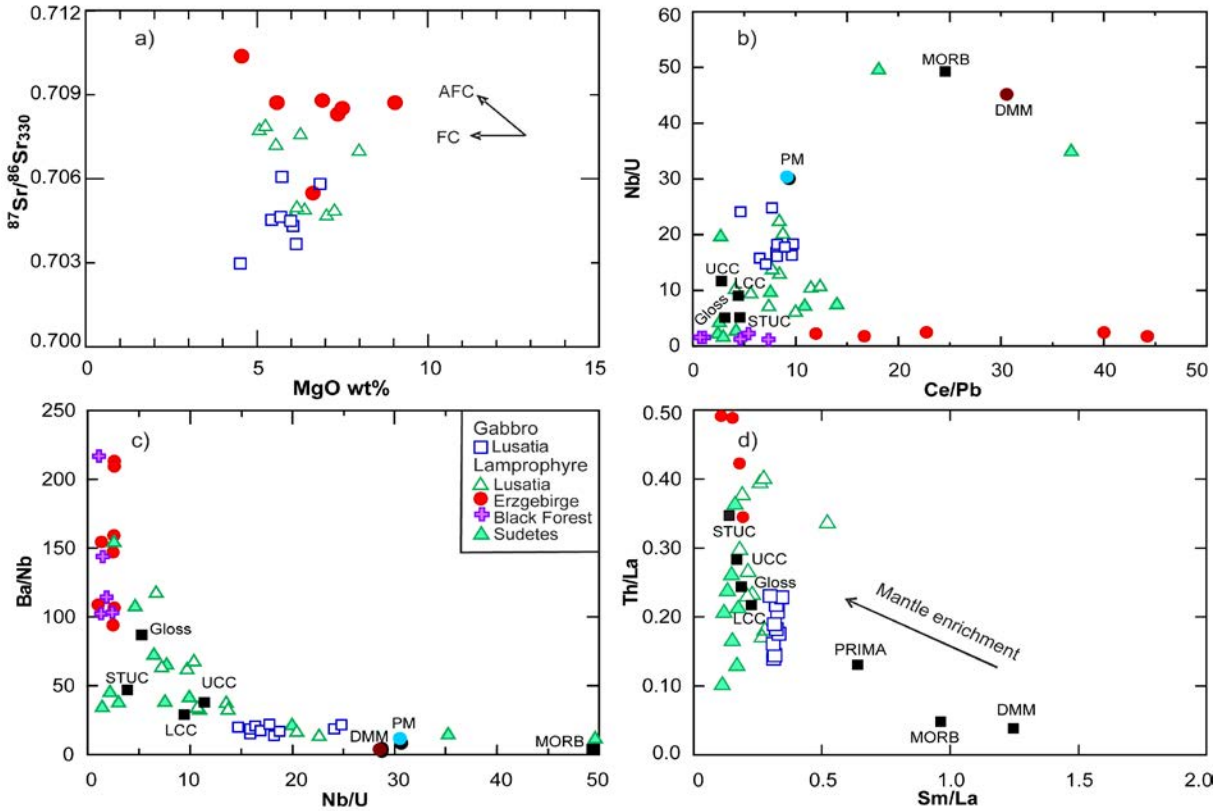

Fig. 2.9. (a) $^{87}Sr/^{86}Sr_{330}$ vs. MgO showing the effect of the FC and AFC; (b) Nb/U vs. Ce/Pb, (c) Ba/Nb vs. Nb/U, and (d) Th/La vs. Sm/La of the gabbros and the calc-alkaline lamprophyres. Average continental crustal compositions of lower (LCC) and upper crust (UCC) are from Rudnick and Fountain (1995); primitive mantle (PM) from Hofmann (1988); global subducting sediment (GLOSS) from Plank and Langmuir (1998), Saxo-Thuringian upper crust (STUC) from Romer and Hahne (2010), mid-ocean ridge basalts (MORB) and primitive mantle from Hofmann (1988) and average depleted MORB mantle (DMM) from Workman and Hart (2005). Data sources are as in Figure 2.6.

The late-Variscan calc-alkaline lamprophyres show trace element pattern characteristic for the involvement of crustal material in their source, with their high Rb, Ba, Pb, Sr, U, Th, and Cs contents, high Th/La, and low Sm/La (Fig. 2.9d). Furthermore, their Ba/Nb (14.4–118), Nb/U (6.35–22.6), Th/U (3.8–8.2), Th/Nb (0.17–1.08), and Ce/Pb (4–12) ratios are typical for continental crust (e.g., Taylor and McLennan, 1995) and their trace element pattern resembles Saxo-Thuringian upper crust (Fig. 2.6a), i.e., the rocks that are supposed to have been subducted during the Variscan orogeny (e.g., Mingram, 1998; Rötzler and Plessen, 2010; Kroner and Romer, 2010).

2.5.3. Repeated mantle-metasomatism beneath Lusatia

Even, the crustal signature of late-Variscan calc-alkaline lamprophyres of Lusatia is distinct from the pre-Variscan gabbros by high initial $^{87}Sr/^{86}Sr$, $^{207}Pb/^{204}Pb$, and $^{206}Pb/^{204}Pb$ ratios and low $^{143}Nd/^{144}Nd$ ratios (εNd_{330} range from +2.5 to -4.9) (Fig. 2.7a), they both have crustally influenced Pb (Fig. 2.7b). The higher $^{207}Pb/^{204}Pb$ values at similar $^{206}Pb/^{204}Pb$ values in most spessartite samples than for the majority of the gabbro samples indicates that the spessartites generally have higher input of crustal Pb. The shift of the initial Pb of the spessartites of Lusatia to higher $^{206}Pb/^{204}Pb$ values is due to the younger age of the spessartites and reflects Pb growth in the spessartite source from the time of gabbro formation to the time of spessartite formation. The higher $^{207}Pb/^{204}Pb$ values in lamprophyres from the Erzgebirge, the Black Forest, and the French Massif Central reflects the larger contribution of crustal Pb in the source of these rocks than in the source of the Lusatian spessartites.

The $^{143}Nd/^{144}Nd$ and $^{87}Sr/^{86}Sr$ ratios of the gabbros (and more importantly their source) range at 330 Ma from 0.51222 to 0.51234 and from 0.7036 to 0.7064, respectively, which is generally lower from the one of the lamprophyres at 330 Ma (0.51198–0.51234 and 0.7046–0.7080, respectively). The lamprophyres cannot be extracted from the same source as the gabbros, as the 330 Ma old spessartites with the least radiogenic initial Nd have lower $^{143}Nd/^{144}Nd$ values than the 400 Ma old gabbros at the time of their extraction from the mantle. Thus to serve also as source for the spessartites, the gabbro source had to experience Variscan metasomatism accounting for the less radiogenic Nd isotopic compositions.

The similarity of high Cr, MgO, Mg#, the trace-element pattern (Fig. 2.4, 2.6a) and Th/La, Sm/La, and Ce/Pb ratios (Fig. 2.9) indicates that gabbros and calc-alkaline lamprophyres have been extracted from a similar mantle source, whereas the contrasting isotopic compositions of Sr and Nd indicates that this source either was heterogeneous or that there was a second, i.e., Variscan, event of mantle enrichment.

Melting of heterogeneous (veined) mantle with depleted and metasomatically enriched domains will result in the preferential melting of the metasomatized domains. These melts will react with the depleted mantle and induce melting of the depleted mantle and lead to rocks with a depleted geochemical signature for the compatible elements (high Cr, Ni, Mg, Mg#) and enriched trace element signatures for incompatible elements (e.g., Foley, 1992; Tappe, et al. 2008). For a small degree of melting, the metasomatic component will be more prominent than for a large degree of melting. Thus, the isotopic and geochemical fingerprints of incompatible elements are less prominent in melts reflecting a high degree of melting. Thus, the contrasting degree of melting could account for some differences between the isotopic composition and geochemical signatures of gabbros and calc-alkaline lamprophyres.

Melting of the mantle to produce the gabbros, however, would result in the preferential melting of the metasomatized domains and leaving behind a mantle that is depleted in incompatible elements. Renewed small-scale melting of this mantle would not produce a melt that is highly enriched in incompatible elements, as the metasomatized parts of the mantle that could provide these elements have been consumed during the melting of the gabbro source. Thus, the late-Variscan lamprophyres require a refertilization of the mantle after the extraction of gabbro melts. The two events possibly account for the contrasting positions occupied by the gabbros and the calc-alkaline lamprophyres in the Th-Zr-Nb discrimination diagram (Fig. 2.10b) with the systematically stronger Th enrichment and Nb depletion in the calc-alkaline lamprophyre than in the gabbros.

Variscan mantle enrichment has also been inferred for the source of other lamprophyre occurrences throughout the Variscan orogen, typically stressing the predominance of geochemical fingerprints inherited from melted sedimentary rocks (Turpin et al., 1988; Awdankiewicz, 2007). In addition, the lamprophyres of Lusatia show similar $^{87}Sr/^{86}Sr$ and εNd_{330} values as the calc-alkaline lamprophyres from the Sudetes (Awdankiewicz, 2007) and the French Massif Central (Turpin et al., 1988), but have lower $^{87}Sr/^{86}Sr$, $^{207}Pb/^{204}Pb$, and $^{206}Pb/^{204}Pb$ and higher εNd_{330} values than calc-alkaline lamprophyres from the Black Forest (Hegner et al., 1998) and adjacent Erzgebirge (Fig. 2.7a, b), which may reflect more extensive metasomatism in the lamprophyre source of the Erzgebirge. Minettes are also derived from a Variscan metasomatized mantle source, although the metasomatic fluids have been interpreted to be derived from recycled continental crust (Hoch et al., 2001). Thus, the key message is not that there is a Variscan metasomatism of the mantle, but that there was already an earlier metasomatic event and that mantle can be repeatedly refertilized: in the special case of

Lusatia, by a Cadomian metasomatism recorded by the post-Cadomian/pre-Variscan tholeiitic gabbros and by Variscan metasomatism recorded by the late-Variscan lamprophyres.

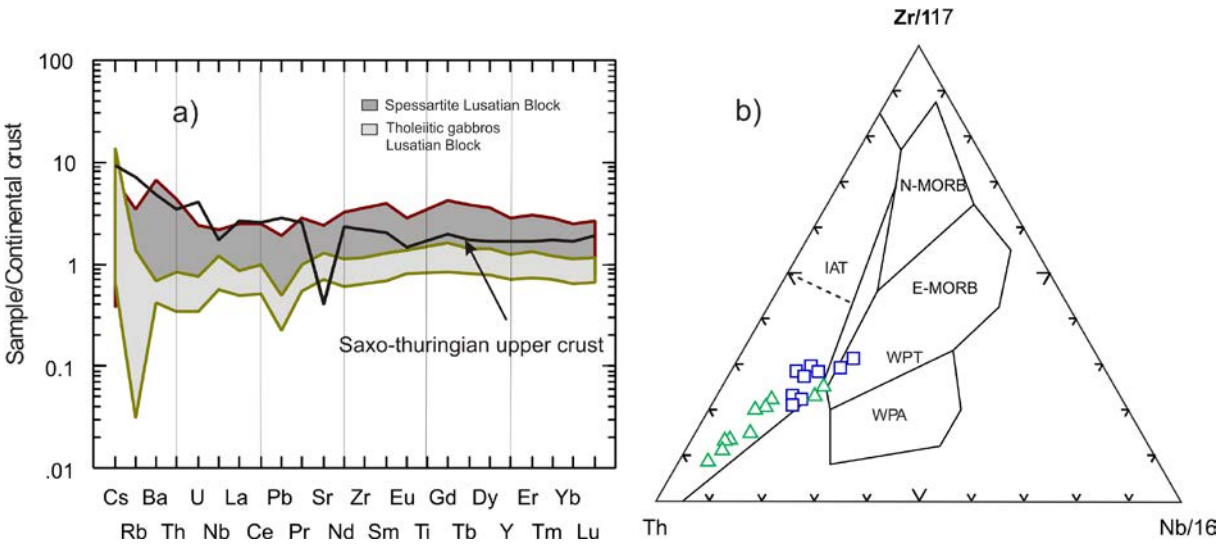

Fig. 2.10. (a) Continental crust-normalized patterns (Taylor and McLennan, 1985), and (b) Th-Zr-Nb discrimination diagram; N-MORB: normal-type mid-oceanic ridge basalt; E-MORB (WPT): enriched mid-oceanic ridge basalt (within-plate tholeiite); WPA: within-plate alkali; and IAT; island-arc tholeiite (Wood, 1980). Data sources are as in figures 2.6, and 2.9. The two samples in WPT are olivine gabbros.

2.6. Conclusions

The mantle beneath Lusatia was modified by Cadomian (c. 600-570 Ma) and Variscan (c. 380-340 Ma) subduction. The metasomatic signature of this mantle was inherited by intra-plate magmatism at c. 400 Ma (gabbros) and c. 330 Ma (calc-alkaline lamprophyres). The effect of assimilation, alteration, and fractional crystallization as a source for the enrichment may be limited and the geochemical and isotopic signatures of these rocks were mainly inherited from an earlier subduction event by transferring the subducted materials as partial melts, which will not have the same compositions as the bulk subducted materials, but it will metasomatize the mantle. The pre-Variscan gabbros and the late-Variscan calc-alkaline lamprophyres in Lusatia were derived from the same mantle source. The calc-alkaline lamprophyres of Lusatia show the mantle enrichment much more distinctly than the gabbro, which indicates an enrichment of the mantle source after gabbro extraction during the Variscan orogeny and implies a repeatedly enriched mantle source. This is also supported by the similar age of the Lusatian calc-alkaline lamprophyres with the lamprophyres from the

Central Europe (300-330 Ma) (e.g., Erzgebirge, Sudetes, and Black Forest). The lamprophyres have high large ion lithophile element contents (up to 350 times primitive mantle), high LREE/HREE, and elevated high-field-strength element contents, and crust-like Nd and Sr isotopic signatures. Their trace element pattern is similar to Saxo-Thuringian upper crust. Similar pattern also is observed for lamprophyres from the adjacent Sudetes, Black Forest, French Massif Central, and Erzgebirge regions. The different enrichments extent between late-Variscan lamprophyres in different domains in Central Europe reflects the regional heterogeneous effect of the Variscan orogeny.

Acknowledgments

We thank the academic and technical staff at Deutsches GeoForschungsZentrum for help with the analytical work, especially, R. Naumann for the XRF analysis, K. Hahne for trace element analysis, S. Tonn for REE data, and O. Appelt for support with the microprobe work. We thank M. Sudo for help with the Ar-dating of the two amphibole samples. K.M.A. gratefully thanks W. Kramer for guidance in the field. We gratefully acknowledge detailed and constructive reviews by L. Krmíček and two anonymous reviewers and thoughtful editorial comments by D. Prelević.

3. Enriched mantle beneath Lusatia, Germany: Evidence from alkaline basalt and ultramafic lamprophyre

Abstract

Strontium, neodymium, and lead isotopic compositions as well as major and trace element compositions have been determined on a suite of post-Variscan alkaline basalt and ultramafic lamprophyre dikes from Lusatia, Germany. These rocks seem to be derived from a variably depleted mantle source with high Mg#, MgO, FeO as well as high Cr and Ni contents, whereas their incompatible trace elements and isotope composition demonstrate a later enrichment of this depleted mantle and show crustal signatures. The ultramafic lamprophyre dikes are characterized by high Th, Cr, Ni, Ba, La, and Sr contents and a strong enrichment of LREE over HREE. The alkaline basalt dikes show similar trace and REE patterns, slight Nb depletion in mantle-normalized trace elements plots, and a less pronounced crustal signature than the ultramafic lamprophyres. The initial $^{87}Sr/^{86}Sr$ and $^{143}Nd/^{144}Nd$ ratios of the various rocks reflect Sr and Nd contributions from both mantle and crust. The ultramafic lamprophyres and the alkaline basalts have the same trace-element signatures as the much older late-Variscan calc-alkaline lamprophyres, indicating that melts have been repeatedly extracted from the same metasomatic mantle source. As melt extraction in Lusatia is coeval with geochemically corresponding magmatism in other parts of Europe, melting of metasomatized mantle may be directly related to large-scale reorganization of the stress field and the partial melting of the metasomatized mantle source due to crustal thinning and mantle upwelling.

3.1. Introduction

The Saxo-Thuringian Zone has been variably affected during the Variscan orogeny. Some blocks were strongly reworked (e.g., Erzgebirge) whereas others (e.g., Lusatia) escaped significant Variscan deformation and metamorphism (Kroner et al., 2010). Crust subducted during the Variscan orogeny is thought to have provided the agents to metasomatize the mantle beneath large parts of Variscan Europe (Turpin et al., 1988; Hegner et al., 1998). The subducted material was highly variable on the regional scale and during the development of the Variscan orogeny and included oceanic crust, thinned continental crust, and its sedimentary cover (Kroner and Romer, 2010, 2013). Accordingly, the mantle beneath the

Variscan orogen in general and the Saxo-Thuringian Zone in particular was heterogeneous, which is reflected in the regionally contrasting composition of the metasomatic component in post-Variscan mantle-derived magmas (e.g., Hegner et al., 1998: von Seckendorff et al., 2004, Abdelfadil et al., 2012). In Lusatia, there occur c. 330–330 Ma late-Variation calc-alkaline lamprophyres and c. 120–130 Ma ultramafic lamprophyres. The comparison of the metasomatic component of these mantle-derived rocks allows to constrain the persistence of metasomatic signatures in the mantle over extended periods of time. Such situations of multiple melt-extraction from a metasomatized mantle during later extensional events are also known from, e.g., Labrodor (Tappe et al., 2007) and New England-Quebec (McHone and Butler, 1984). The geological situation of Lusatia is unusual as adjacent areas of the Variscan orogen have a contrasting geochemical signature of enrichment (Abdelfadil et al., 2012).

Should the calc-alkaline and ultramafic lamprophyres have the same crustal signature for the metasomatic component, this would imply (i) that the metasomatic signature acquired by subduction of crustal material persists in the mantle beneath continental crust as long as this mantle is not affected by another metasomatic event. Consequently, lamprophyres of contrasting age may be used to constrain regional variations in mantle metasomatism. Furthermore, (ii) the extraction of mantle melts carrying a metasomatic signature may be entirely unrelated to the event causing the metasomatism. Crustal thinning resulting in mantle upwelling will cause preferential melting of metasomatic domains in the previously enriched mantle. Lamprophyres and related alkaline rocks would provide samples from such a modified mantle.

Different subduction regimes and the related contrasting nature of subducted material, as well as post collisional reorganization and change in the field stress in an orogenic belt, may result in distinctive suites of post-collisional lamprophyres and associated volcanic rocks that record the history of collisional system. Using the geochemical signature of subducted continental material as a tracer, these rocks can provide insights into post-collision mantle dynamics (Tappe et al., 2007; Scarrow et al., 2011; Prelević et al., 2012; Abdelfadil et al., 2012). The late/post-Variscan mantle-derived magmatic rocks of Saxo-Thuringian Zone are particularly well-suited for this approach, as (i) melts have been extracted repeatedly from the Variscan metasomatic mantle and (ii) areas bordering to Lusatia have a different geochemical signature for Variscan mantle metasomatism (Abdelfadil et al., 2012).

In this paper we present the first chemical and Nd, Sr, and Pb isotope data for the post-Variscan alkaline basalts and ultramafic lamprophyres from Lusatia to characterize the

underlying mantle and to compare this mantle source with the one of the late-Variscan calc-alkaline lamprophyres.

3.2. Geological setting

The late Palaeozoic Varican orogen formed by the collision of Gondwana with Laurussia (Matte, 1986; Franke, 2000; Kroner et al., 2007, 2010). The irregular shape of the Variscan orogen largely reflects the complex arrangement of crustal blocks with thick continental crust that are separated by segments of predominantly thin continental crust with overlaying volcanosedimentary sequences. The blocks of thick continental crust, such as Armorica, Iberia, and Lusatia, were not subducted during the orogeny and their arrival in the Rheic suture zone forced a reorganization of the subduction zones within the Variscan plate boundary zone (see Kroner et al., 2007; Kroner and Romer, 2010, 2013). In contrast, segments of thin continental crust were subducted. When a non-subductibel block chocked the subduction zone and a new subduction zone was established behind this block, some of the subducted rocks exhumed from beneath the thick continental crust and are now exposed in belts of high-grade metamorphic rocks bordering the blocks of thick continental crust (Kroner and Romer, 2010, 2013).

The Mid-German Crystalline-Zone (MGCZ) represents the trace of a magmatic arc that formed by subduction of the oceanic crust of the Rheic Ocean during the convergence of Gondwana and Laurussia. Once the oceanic crust was consumed beneath the MGCZ, the crustal blocks of the Armorican Spur as leading segment of Gondwana started to collide with Laurussia (Kroner and Romer, 2010, 2013). The Bohemian Massif was one of the first blocks that collided with Laurussia. After this collision, a new subduction zone established itself in the thinned continental crust behind the Bohemian Massif. The Saxo-Thuringian zone is an important part of the Variscan orogen. It contains low-strain segments that were not subducted along with high-strain segments that were subducted during the Variscan orogeny. Lusatia was such a low-strain block that was separated from Bohemia by a strike slip zone and was not subducted. It was marginally overthrust by allochthonous units (Kroner and Goerz, 2010). The Sudetes and the Erzgebirge, which constitute the northern and northeastern part of the Bohemian Massif (Fig. 3.1), are part of the high-strain domain and underwent Variscan high-grade metamorphism and deformation (Kryza, 2008; Kroner et al., 2010). These rocks are distinct by the nappes of HP-HT granulites and HP eclogites that are intruded by huge masses of Variscan granites (Kryza, 2008; Kroner and Romer, 2010).

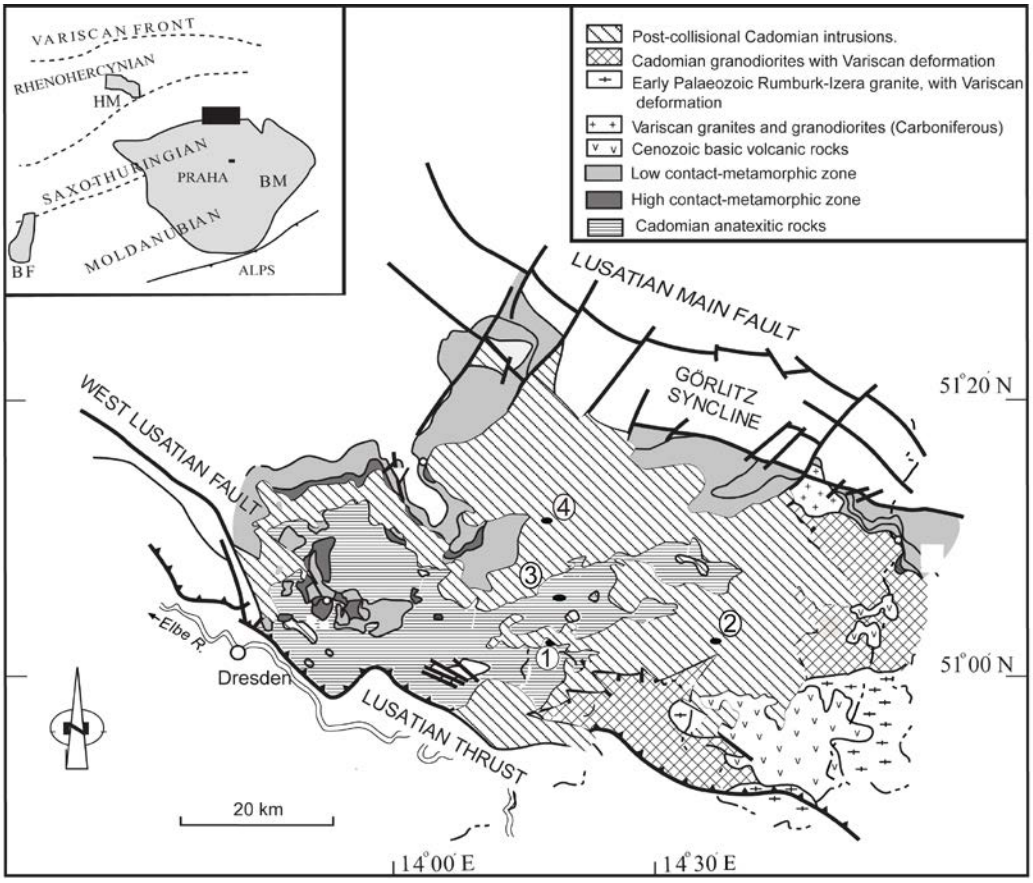

Fig. 3.1. Geological map of the Lusatian Block in the Saxo-Thuringian Zone (after Kemnitz, 2007). Sampling locations: 1- Valtengrund, 2- Klunst Ebersbach, 3- Picho, 4- Nucknitz. BM: Bohemian Massif; BF: Black Forest; HM; Harz Mountains. Ultramafic lamprophyres are known only from the Klunst quarry.

Variscan granitic magmatism in the Saxo-Thuringian zone includes (i) 335-326 Ma old granites in the Elbe Zone and the roof zone of the Saxon Granulite Massif, (ii) 318-327 Ma old I-, S-, and A-type late-Variscan granites of the Erzgebirge, and (iii) 300 and 280 Ma Permian volcanic rocks related to the post-Variscan reorganization of the stress-field in Europe. The terms syn-, late-, and post-Variscan are used relative to nappe emplacement and deformation of the sedimentary foreland basin. Spatially and/or temporally associated with the various groups of granitic magmatism in the Saxo-Thuringian Zone are mantle-derived potassic rocks, such as ca. 335-326 Ma diorites, monzodiorites, monzonite, and granites of the Meissen Massif (Wenzel et al., 1997) and ca. 335-320 Ma and c. 290-305 Ma lamprophyric dikes of the Erzgebirge and Sudetes (Awdankiewicz, 2007). Younger mantle-derived magmatism is subordinate (e.g., Renno et al., 2003b; Kramer and Andrehs, 2011) and possibly follow the same temporal distribution as hydrothermal vein deposits in the

Erzgebirge (e.g., Romer et al., 2010), which are related to large-scale reorganization of the stress field during different stages of the opening of the Tethys and the North Atlantic, as well as different stages of the Alpine orogeny.

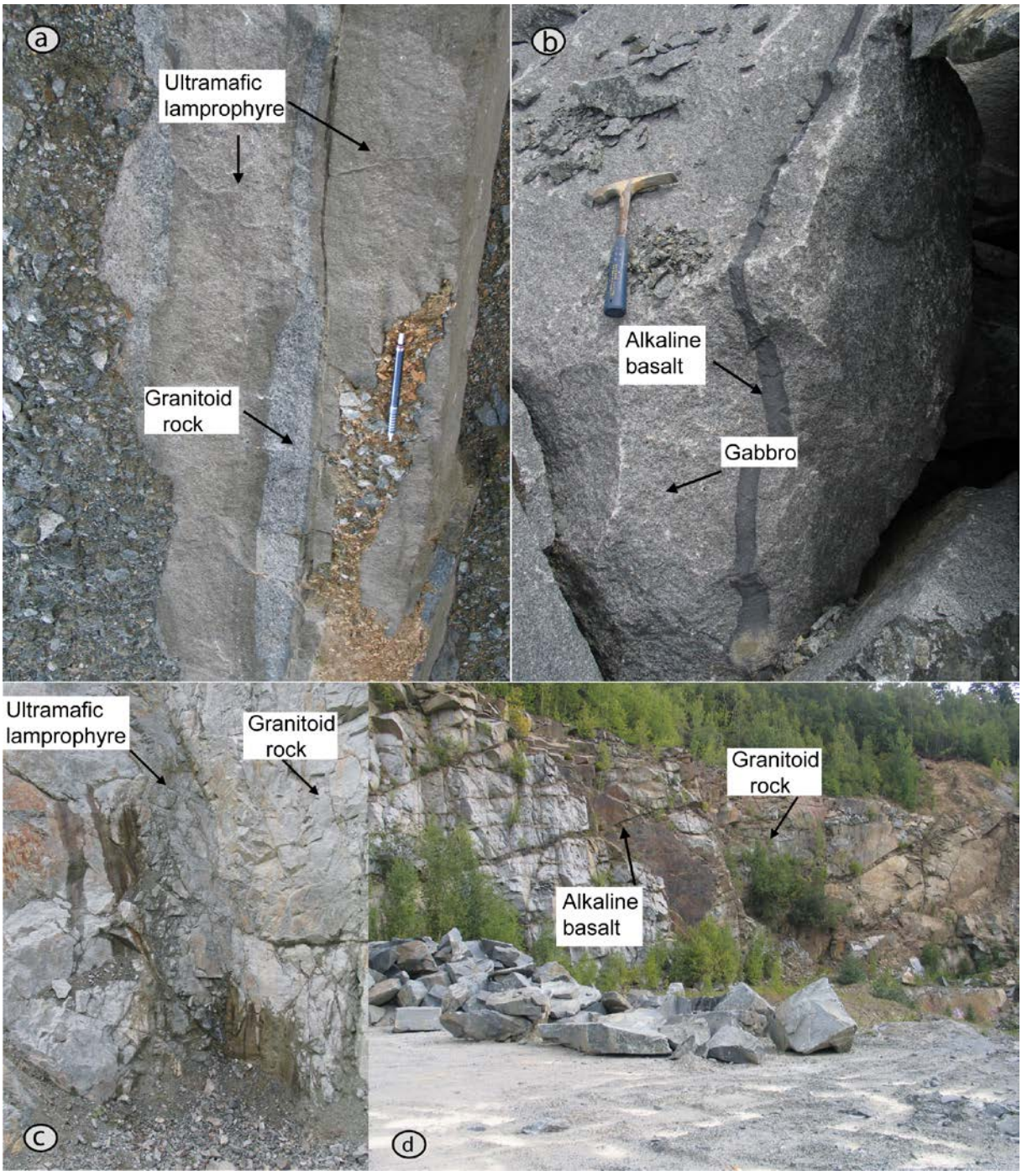

Fig. 3.2. Field photograph showing the contact between alkaline basalt, ultramafic, lamprophyre, granitoid, and gabbroic rocks. a) Ultramafic lamprophyre dike in granitoid host rock; b) Alkaline basalt vein in gabbro host rock. c) Ultramafic lamprophyre dike in granitoid host rock. d) Alkaline basalt in granitoid host rock.

Late-Variscan lamprophyres fall in the age range 290–335 Ma and are relatively common in Variscan high-strain domains, such as the Erzgebirge – and on a broader scale the Sudetes, the Bohemian Massif, the Black Forest, and the French Massif Central (Turpin et al., 1988; Hegner et al., 1998; von Seckendorff et al., 2004; Awdankiewicz, 2007; Seifert, 2008) – and are relatively rare in low-strain blocks, such as Lusatia. In addition to the late-orogenic calc-alkaline lamprophyres, there are also subordinate dikes related to a younger, i.e., post-Variscan magmatism. In Lusatia, there occur in the same general area as the calc-alkaline lamprophyres also c. 120 Ma ultramafic lamprophyres and alkaline basalts (e.g., Renno et al., 2003b). The ultramafic lamprophyre, which form several meters thick NW trending dikes, cross-cut the gabbro and granodiorite (Fig. 3.2a), and recorded only Klunst Ebersbach (Fig. 3.1). Alkaline basalt is intruded into gabbro and granitoid (Fig. 3.2) rocks and in some localities, occurs as vein-like in the previous older rocks (Fig. 3.2b). The alkaline basalt dikes are common in Lusatia compared to the ultramafic lamprophyres. No xenoliths have been recorded in any of these rocks.

The Lusatian block contains a wide range of mantle-derived late-Variscan and post-Variscan mafic intrusions, i.e., (i) dikes of sub-alkaline basalt, (ii) dikes of spessartite, and (iii) dikes of ultramafic alkaline lamprophyre, (cf., Kramer et al., 1977; Heinrich, 1993; Kramer, 1988; Renno et al., 2003a, 2003b, 2003c; Haase and Renno, 2008; Kramer and Andrehs, 2011; Abdelfadil et al., 2012). The emplacement of these mineralogically and geochemcially distinct rocks seems to have been controlled by the reactivation of older faults and deformation zones. As dikes of coherent orientation are geochemically similar, they are thought to have been derived from a single source and to reflect distinct magmatic events (e.g., Kramer et al., 1977; Kramer, 1988). The relative ages of the various groups of mantle-derived magmatism is mainly known from field relations.

The spessartite dikes yield Ar-Ar amphibole ages of c. 330–335 Ma (Abdelfadil et al., 2012) and fall in the same age range as calc-alkaline lamprophyres from the adjacent areas (Turpin et al., 1988; Hegner et al., 1998: von Seckendorff et al., 2004). The ultramafic lamprophyres have a $^{39}Ar/^{40}Ar$ phlogopite age of 126.64±0.27 Ma (Renno et al., 2003b). This age agrees with the alkaline lamprophyres from the Silesian Nappe in the western Carpathians that have Ar-Ar ages ranging from 120.4±1.4 Ma to 122.3±1.6 Ma (Lucinska-Anczkiewicz et al., 2002) and alkaline magmatism of Moravia and the North Pyrenean Rift Zone (e.g., Rossy et al., 1992; Dostal and Owen, 1998).

3.3. Analytical methods

All analytical work was performed at Deutsches GeoForschungZentrum (GFZ). The chemical composition of minerals was determined using a CAMECA SX100 electron microprobe operated at 15 kV acceleration voltage and a beam current of 20 nA with peak counting times of 20-30 s for major and 30 s for minor elements. The backgrounds were counted for 5-15 s. Data reduction used the PAP correction procedure applied in the CAMECA software

Whole-rock major element composition and selected trace elements (Zn, Zr, Ba, Cr, Nb, Ni, Sr and V) were measured with X-ray fluorescence spectrometry. H_2O and CO_2 were determined by high-temperature catalytic combustion with vario EL III instrument. Additional trace elements (Nb, Mo, Cd, Cs, Ti, Pb, Th, U, Sc, Co, Cu, Ga, Sb, and Sn) were analyzed using ELEMENT 2XR ICP-MS. Sample powders were decomposed using HF, aqua regia, and $HClO_4$. The dissolved samples were dried and redissolved in HNO_3 and then diluted with H_2O for analysis. Rare earth elements (REE) and Y were analyzed with inductively coupled plasma-atomic emission spectroscopy (ICP-AES) following the procedure of Zuleger and Erzinger (1988). These samples were decomposed using Na_2O_2 fusion and the REE were separated and concentrated chromatographically using ion-exchange methods.

For Sr, Nd, and Pb isotope analysis, whole-rock sample powders were dissolved with concentrated HF for four days at 160° C on a hot plate. The digested samples were dried and taken up in HNO_3 to transfer fluorides into nitrates. The dried samples re-dissolved in 6N HCl overnight and split with one half for Pb and the other half for Sr and Nd ion-chromatographic separation. The HCl-HBr ion exchange technique for Pb separation was described by Romer et al. (2005). Lead was loaded with H_3PO_4 and silica-gel on single Re-filaments (Gerstenberger and Haase, 1997) and the isotopic ratios were analyzed using a Finnigan Mat262 TIMS multi-collector mass spectrometer using static multicollection. Instrumental mass-fractionation of 0.1% per a.m.u. was corrected as determined from repeated measured of lead standard material NBS 981. The accuracy and the precision of the Pb isotopic ratios are better than 0.1% at the 2σ level. Strontium and neodymium separates were produced using standard cation exchange techniques. $^{87}Sr/^{86}Sr$ and $^{143}Nd/^{144}Nd$ were analyzed on a Triton and Finnigan Mat262 multi-collector mass-spectrometer, respectively, operated in dynamic multicollection mode. The isotopic ratios of Sr and Nd were normalized to $^{86}Sr/^{88}Sr=0.1194$ and $^{146}Nd/^{144}Nd=0.7219$, respectively. Analytical uncertainties are given as $2\sigma_m$. Repeated measurements of NBS987 Sr reference material gave $^{87}Sr/^{86}Sr$ of 0.710249 ± 0.000005 (n = 20; 2σ) and of the La Jolla Nd standard yielded $^{143}Nd/^{144}Nd$ = 0.511855 ± 0.000006 (n = 14; 2σ).

3.4. Results

3.4.1. Mineral chemistry and petrography

3.4.1.1. Late Variscan calc-alkaline lamprophyres

Calc-alkaline lamprophyres from Lusatia contain phenocrysts of dominantly euhedral amphibole, which range from titanian magnesiohastingsite to pargasite and kaersutite, and more rarely clinopyroxene phenocrysts. The groundmass is dominated by plagioclase. The amphibole crystals are zoned with Si and Fe increasing and Al, Cr, Na, and F decreasing from core to rim. Clinopyroxene is Ca rich augite ($Wo_{36-40}En_{46-50.9}Fs_{12-16}$) and rarely forms phenocrysts. Its composition indicates crystallization temperatures that range from 900°C to ~1200°C for the calc-alkaline lamprophyre and mostly plot in the orogenic field, consistent with the formation in a subduction-related tectonic setting. For details see Abdelfadil et al. (2012).

3.4.1.2. Ultramafic lamprophyre dikes

The ultramafic lamprophyres contain phenocrysts of phlogopite, pseudomorphosed olivine, and clinopyroxene in a groundmass of carbonates, phlogopite, magnetite, pyrite, and clinopyroxene (Renno et al., 2003a). Phlogopite shows strong pleochroism and minor zonation, is partly rounded, and its cleavage cracks are filled with carbonate (Fig. 3.3a). Clinopyroxene occurs mainly as zoned euhedral crystals; fragmented or rounded crystals are rare. Locally, pyroxene is uralitized. Olivine phenocrysts typically are pseudomorphosed by secondary carbonate, chlorite, and serpentine (Fig. 3.3a and 3.3b). Pyrite, ilmenite, and magnetite are common. Carbonates occur both as primary ocelli and as secondary minerals in olivine (e.g., Renno et al., 2003a).

The chemical composition of phlogopite and pyroxene, in particular their high contents of Al_2O_3 and TiO_2, falls in discrimination diagrams (Fig. 3.4) into the field for ultramafic lamprophyre (e.g., Rock, 1987; Mitchell, 1995; Mitchell et al., 1999). The low SiO_2 (35.7 to 37.7 wt %) and the high Al_2O_3 contents of phlogopite suggests relatively low-pressure (and possibly low-temperature) conditions of formation (Arai, 1984). Phlogopite shows a small variation range in K/(K+Na) ratios (Table 3.1), range from 0.94 to 0.96 indicating absence of in situ fractional crystallization. Furthermore, the very low Na/(Na+K) ratios 0.03 to 0.04 is typical for a garnet peridotite origin (Arai, 1986). The clinopyroxene

composition indicates crystallization temperatures that range from 600°C to ~800°C (Fig. 3.5a).

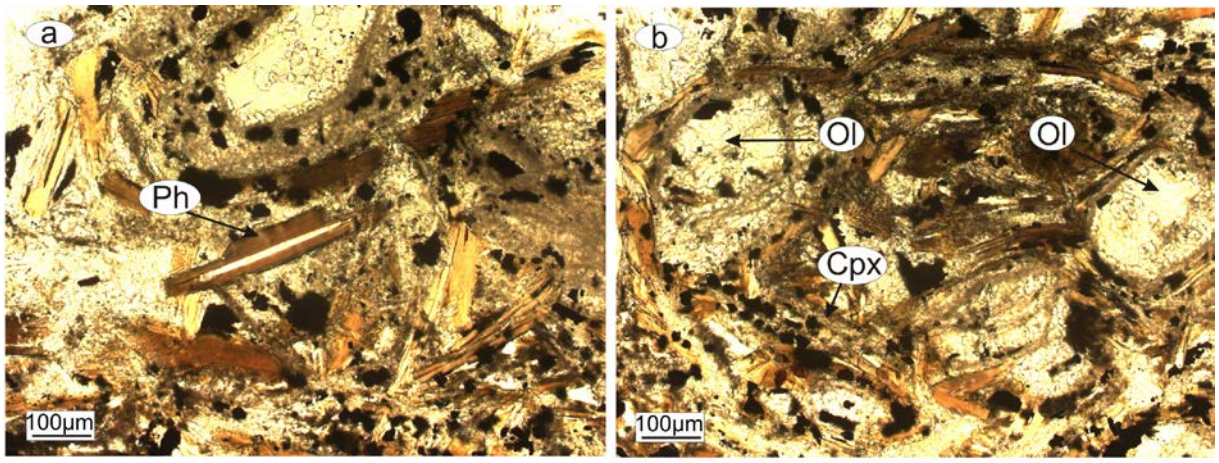

Fig. 3.3 Photomicrographs showing characteristic textures of the ultramafic lamprophyre; a) Olivine phenocrysts completely pseudomorphed by serpentinite, carbonate, and iron oxides. b) Euhedral phlogopite phenocrysts in fine-grained groundmass of carbonate minerals. Ol-Olivine; Cpx-Clinopyroxene; Ph-Phlogopite.

3.4.1.3. Alkaline basalt

Alkaline basalt dikes occur at Valten Grund, Klunst Ebersbach, Pischow, and Nucknitz (Fig. 3.1). The dikes show a broad range of phenocryst assemblages and textures that range from porphyritic to ophitic and subophitic. For example, at Klunst Ebersbach, plagioclase and clinopyroxene are the major phenocrysts phases, whereas at Valtengrund, additional phenocrysts of late, up to 3 mm long, platy to needle-like ilmenite are present. The matrix in all alkaline basalt dikes consists of small plagioclase laths together with pyroxene, phlogopite, magnetite, and amphibole, which in part also forms rims around pyroxene phenocrysts, serpentine, ilmenite, and pyrite.

Some clinopyroxene crystals are rimed by actinolite. Clinopyroxene plots in the augite field in the En-Wo-Fs diagram (Wo $_{35-39}$, En $_{41-50}$ and Fs $_{14-22}$; Table 3.2, Fig. 3.5a). In terms of provenance diagrams, it plots predominantly in the field of alkaline magma and straddles the non-orogenic and orogenic fields (Le Bas, 1962; Letterrier et al., 1982, Fig. 3.5b, c). Clinopyroxene from the alkaline basalts has lower Mg-numbers (79 to 67), CaO (17.5 to 20.1 wt %), TiO_2 (1.07 to 2.82 wt %), and Al_2O_3 (1.9 to 5.1 wt %) content than clinopyroxene of

the ultramafic lamprophyre (Fig. 3.5d). The clinopyroxene composition indicates crystallization temperatures that range from 700°C to ~1100°C (Fig. 3.5a).

The Ti/A1 ratio of pyroxene can be used as a qualitative indicator of the pressure prevailing during crystallization (Yagi and Onuma, 1967). For pyroxene that crystallized at elevated pressure, the Ti/Al ratios are low (0.1-0.2 or less), whereas low-pressure pyroxene (phenocryst rims, microphenocrysts and groundmass pyroxene) typically have a higher Ti/A1 ratio close to 0.5 (Yagi and Onuma, 1967; Dobosi et al, 1991). The clinopyroxene from alkaline basalt have lower Ti/Al ratios (between 0.125 and 0.25) than the ultramafic lamprophyre (between 0.25 and ~ 0.4), indicating that the alkaline basalt may have crystallized at higher pressure relative to the ultramafic lamprophyre (Fig. 3.5e, 5f).

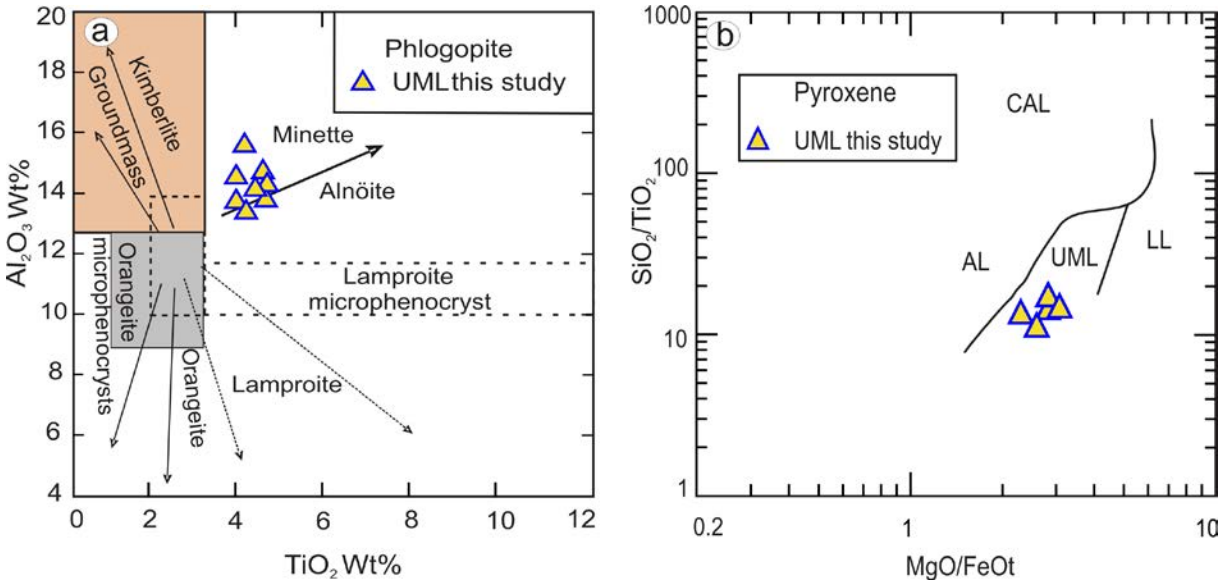

Fig. 3.4. Major-element composition of mineral phases from the alkaline basalt and ultramafic lamprophyre: a) Al_2O_3 versus TiO_2 for phlogopite; compositional trend lines and field from Michell (1995); b) MgO/FeOt vs. SiO_2/TiO_2 discrimination diagram for pyroxene composition in lamprophyres (Rock 1987). CAL: calc-alkaline lamprophyres, AL: alkaline lamprophyres, UML: ultramafic lamprophyres and LL: lamproites

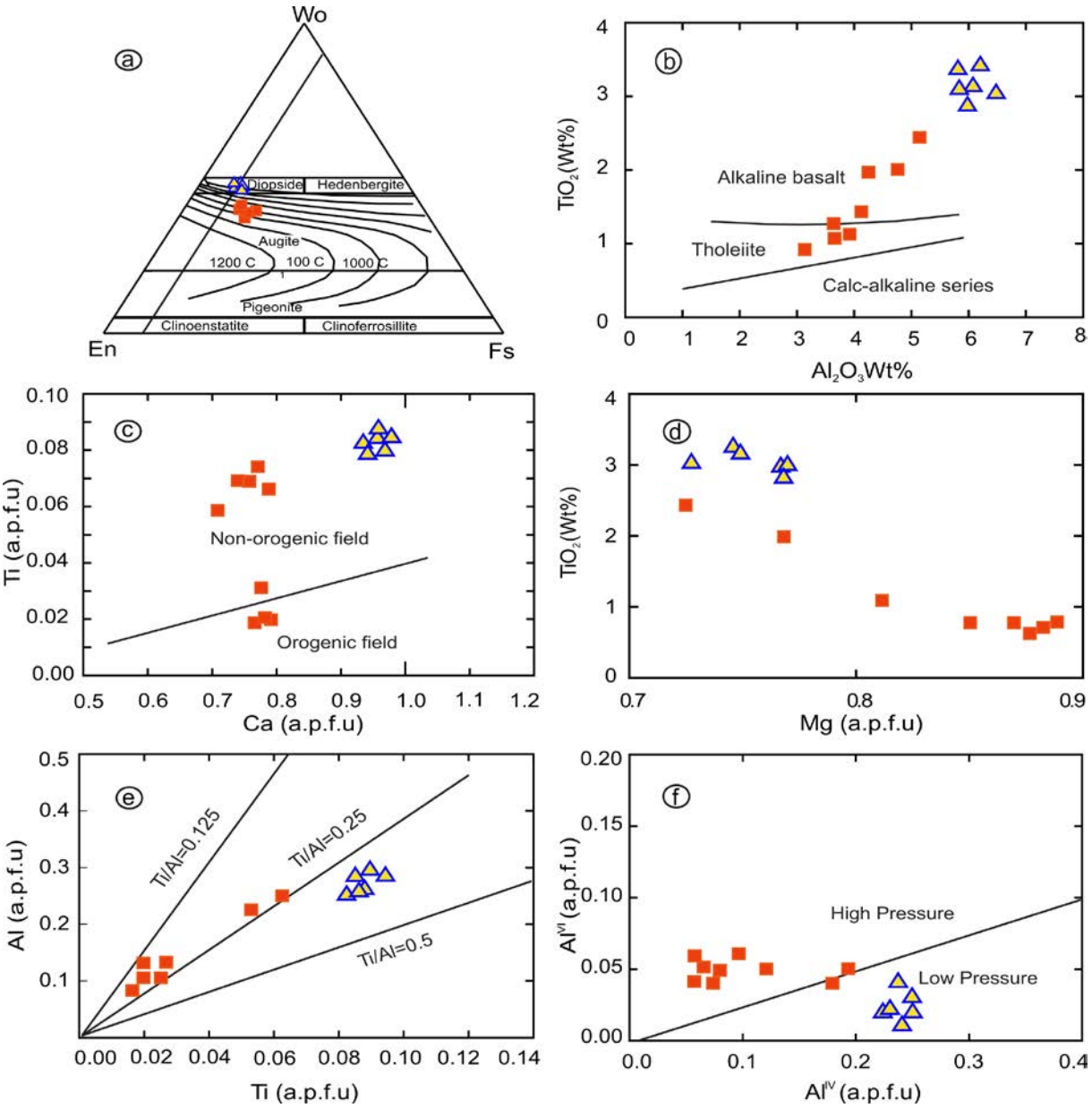

Fig. 3.5. Composiiton of pyroxene from ultramafic lamprophyre and alkaline basalt: (a) En–Wo–Fs diagram after Morimoto (1988); (b) TiO_2 v. Al_2O_3 binary diagram after Le Bas (1962); (c) Ca vs. Ti binary diagrams after Letterrier et al. (1982) modified by Sun and Bertrand (1991); (d) TiO_2 vs Mg; (e) Ti vs. total Al; and (f) Al^{vi} vs. Al^{iv} diagram of Aoki and Kushiro (1968) and Wass (1979). a.p.f.u – atoms per formula unit.

Table 3.1
Representative electron microprobe analyses of phlogopite and clinopyroxene from ultramafic lamprophyre and alkaline basalt.

	Phlogopite								Clinopyroxene										
	Ultramafic lamprophyre								Alkaline basalt					Ultramafic lamprophyre					
SiO_2	37.7	36.5	35.9	35.8	36.5	36.1	35.7	36.4	52.1	50.3	52.5	51.1	52.3	52.0	47.1	46.7	46.5	47.2	46.8	46.8
TiO_2	3.9	4.4	4.6	4.6	4.4	4.4	4.3	4.5	0.71	1.09	0.63	0.86	0.69	0.68	3.02	3.19	3.28	3.10	3.15	3.16
Al_2O_3	15.2	15.9	16.7	16.7	16.3	16.1	16.4	16.3	2.52	4.05	2.78	3.74	2.46	2.63	5.72	6.33	6.25	5.71	5.71	5.94
Cr_2O_3	na	na	na	na	na	na	na	na	0.020	0.023	0.040	0.000	0.04	0.03	0.005	0.020	0.023	0.03	0.04	0.04
MgO	20.1	19.2	19.7	19.4	19.0	19.9	19.4	19.5	16.1	14.6	15.96	15.3	15.8	16	13.9	13.1	13.44	13.7	13.9	13.77
CaO	0.1	0.2	0.1	0.2	0.2	0.0	0.1	0.1	19.6	20.1	19.7	20	19.7	19.9	24.6	24.2	24.3	24	24.4	24.3
MnO	0.2	0.2	0.1	0.0	0.1	0.1	0.1	0.1	0.16	0.23	0.19	0.14	0.28	0.24	0.10	0.07	0.03	0.04	0.03	0.03
FeO	8.7	8.7	8.1	7.8	9.2	7.9	8.3	8.4	8.55	9.17	7.64	8.12	8.23	8.55	5.46	5.22	5.24	5.17	4.97	5.33
Na_2O	0.2	0.2	0.2	0.2	0.2	0.3	0.2	0.2	0.26	0.34	0.29	0.27	0.33	0.3	0.26	0.24	0.21	0.23	0.25	0.28
K_2O	9.7	9.7	9.5	9.5	9.5	9.6	9.5	9.7	0.01	0.00	0.00	0.03	0	0.014	0.01	0.00	0.01	0.00	0.00	0.00
Total	96.0	95.4	95.9	95.5	96.2	94.9	95.0	95.9	99.9	99.9	99.7	99.7	99.8	100.4	100.1	99.1	99.2	99.2	99.2	99.6
Si	2.7	2.7	2.6	2.6	2.7	2.6	2.6	2.6	1.93	1.88	1.94	1.90	1.935	1.920	1.76	1.76	1.75	1.77	1.76	1.75
Ti	0.2	0.2	0.3	0.3	0.2	0.2	0.2	0.2	0.02	0.03	0.02	0.02	0.019	0.019	0.08	0.09	0.09	0.09	0.09	0.09
Al	1.3	1.4	1.4	1.4	1.4	1.4	1.4	1.4	0.11	0.18	0.12	0.16	0.107	0.114	0.25	0.28	0.28	0.25	0.25	0.26
Mg	2.2	2.1	2.1	2.1	2.1	2.2	2.1	2.1	0.89	0.81	0.88	0.85	0.870	0.881	0.77	0.73	0.75	0.77	0.77	0.77
Ca	0.0	0.0	0.0	0.0	0.0	0.0	0.0	0.0	0.78	0.80	0.78	0.80	0.783	0.785	0.98	0.98	0.98	0.97	0.98	0.98
Mn	0.0	0.0	0.0	0.0	0.0	0.0	0.0	0.0	0.00	0.01	0.01	0.00	0.009	0.007	0.00	0.00	0.00	0.00	0.00	0.00
Fe^{2+}	0.5	0.5	0.5	0.5	0.6	0.5	0.5	0.5	0.26	0.29	0.24	0.25	0.255	0.264	0.17	0.16	0.16	0.16	0.16	0.17
Na	0.0	0.0	0.0	0.0	0.0	0.0	0.0	0.0	0.02	0.02	0.02	0.02	0.023	0.021	0.02	0.02	0.02	0.02	0.02	0.02
K	0.9	0.9	0.9	0.9	0.9	0.9	0.9	0.9	0.000	0.000	0.000	0.001	0.000	0.001	0.00	0.00	0.00	0.00	0.00	0.00
Al^{IV}	1.3	1.3	1.4	1.4	1.3	1.4	1.4	1.4	0.07	0.12	0.06	0.10	0.065	0.080	0.24	0.24	0.25	0.23	0.24	0.25
Al^{VI}	0.0	0.0	0.0	0.1	0.1	0.0	0.0	0.0	0.04	0.05	0.06	0.06	0.042	0.035	0.01	0.04	0.02	0.02	0.01	0.02
Mg#	80	80	81	82	79	82	81	81	77	74	79	77	77	77	82	82	82	83	83	82
K/K+Na	0.96	0.97	0.96	0.97	0.97	0.96	0.96	0.96												
Na/Na+K	0.04	0.03	0.04	0.03	0.03	0.04	0.04	0.04												
Wo									37.8	38.6	37.0	37.7	38.2	38.6	49.11	47.77	48.36	47.91	49.04	48.74
En									47.9	45.4	49.7	48.0	47.8	47.3	41.70	42.70	42.38	42.99	42.40	42.08
Fs									14.3	16.0	13.3	14.3	14.0	14.1	9.20	9.53	9.26	9.11	8.56	9.18

Cation calculated on the basis of 6 O for pyroxene, and 12 O for phlogopite, na: not analyzed. Mg#: 100*Mg/ ($Mg+Fe^{+2}$), Wo: Wollastonite: En: Enstatite, Fs: Ferrosilite.

3.4.2. Whole rock geochemistry

Major and trace element concentrations and CIPW norms of the ultramafic lamprophyre and alkaline basalt are presented in Table 3.2. The ultramafic lamprophyre has high and variable volatile contents (9-18 wt %). The samples contain between 5.9 and 14.3 wt % CO_2 and between 2.6 and 3.8 wt % H_2O. High CO_2 is manifested in the rocks as abundant primary calcite and secondary carbonate in the altered phenocrysts and groundmass. The ultramafic lamprophyres contain 29.3–38.5 wt % SiO_2, 6.7–16.4 wt % MgO, a Mg-number between 58 and 80, and high Cr as well as Ni contents (222–974 ppm Cr and 111–410 ppm Ni). The high contents of Mg, Cr, and Ni suggest that these rocks represent primary mantle melt (Frey et al., 1978; Hess, 1992; Price et al 2000). Concentration of TiO_2 and Fe_2O_3t are high and range between 2.4 and 3.4 wt % and 9.5 and 11.2 wt %, respectively. The CaO content is high and variable (9.6–16.8 wt %), largely reflecting the high calcite content. Moderately high K_2O concentrations (1.8–3.2 wt %) and extremely variable Na_2O (0.45–3.2 wt %) are characteristic.

The alkaline basalt has higher SiO_2 (45.9–49.2 wt %), and Al_2O_3 (12.3–16.8 wt %). MgO varies between 4.6 and 13.1 wt % (Fig. 3.6), yielding a wide range of Mg-numbers (40–68), and reflecting fractionation. The highest Fe_2O_3t concentrations (up to 15.0 wt %) result from high contents of needle shaped magnetite, a feature also observed for alkaline basalt from other localities (e.g., Milovanović et al., 2005). For classification, we used the Nb/Y vs Zr/TiO_2 diagram (Fig. 3.7a), which is widely used for classification of lamprophyres (e.g., Hauser et al., 2010) and other basaltic rocks. In this diagram, the basaltic dikes can be described as alkaline basalt; only two samples have sub-alkaline affinity. The ultramafic lamprophyres fall in basanites/nephelinites field. Based on SiO_2 vs Zr/TiO_2 (Winchester and Floyd, 1977), all of the basaltic dikes fall into the alkali basalts field (Fig. 3.7b). Similar major element trends (Fig. 3.6) suggest that the alkaline basalt and ultramafic lamprophyres may be cognate.

The major and trace elements of the late Variscan calc-alkaline lamprophyres from Lusatia (325–335 Ma) have been discussed in detail in Abdelfadil et al. (2012). These rocks have high Mg# (52–61), MgO (5.1–8.0 wt%), Cr (85–321 ppm), and Ni (22–187 ppm) and moderate contents of Al_2O_3 (14.3–16.9 wt %), TiO_2 (1.0–2.5 wt %), and CaO (5.7–9.1) and high contents of K_2O (0.9–3.2 wt %). Furthermore, these rocks have high Rb (24–111 ppm), Zr (105–360 ppm), Nb (11–20.8 ppm), Ba (173–1662 ppm), Pb (3–15 ppm), Th (2–15 ppm), and Sr (273–625 ppm).

Table 3.2

Geochemical data of alkaline basalt and ultramafic lamprophyre from Lusatia.

	Ultramafic lamprophyre				Alkaline basalt						
No.	KE 1	KE 2	KE 3	KE 4	VG B1	VG B2	KE B3	KE B4	VG B5	NU B6	P B7
SiO_2 Wt%	38.5	29.3	32.2	32.1	45.9	47.6	50.6	49.2	46.1	43.3	43.3
TiO_2	2.44	2.49	3.36	3.24	1.51	3.14	1.58	1.24	3.72	2.35	2.47
Al_2O_3	11.3	5.7	6.5	7.5	12.5	14.3	16.8	16.4	13.8	12.5	12.3
FeO_t	10.1	8.5	9.5	9.6	11.3	12.4	8.2	8.1	13.5	12.2	11.9
MnO	0.16	0.16	0.19	0.18	0.17	0.17	0.14	0.15	0.29	0.16	0.15
MgO	6.7	16.5	15.8	13.6	13.1	5.2	4.9	5.1	4.6	11.8	12.2
CaO	9.7	13.3	15.3	16.8	8.5	8.6	7.1	8.4	6.8	8.6	9.3
Na_2O	3.15	0.45	0.63	0.47	2.14	2.96	2.98	2.61	2.34	1.6	2.2
K_2O	1.82	2.33	3.14	3.21	0.64	0.98	2.44	1.47	1.39	1.5	0.8
P_2O_5	0.62	1.01	1.18	1.21	0.22	0.40	0.50	0.24	0.48	0.33	0.38
CO_2	9.9	14.3	6.2	5.9	0.57	0.42	0.08	2.44	1.13	0.49	1.32
H_2O	2.6	3.83	3.34	3.39	1.81	1.81	3.33	3.08	2.72	3.68	3.06
Sum	98.2	98.9	98.4	98.3	99.5	99.4	99.6	99.4	98.4	98.9	99.9
Mg#	58.1	80.3	77.8	74.8	70.8	46.9	55.9	56.9	41.7	67.1	68.1
Sc ppm	21.9	23.5	29.1	23.8	22.5	23.5	30.0	28.7	25.1	22.0	22.0
V	266	213	259	309	211	256	215	196	282	240	247
Cr	222	974	880	650	520	38	70	100	59	390	479
Co	37	54	55	50	60	41	25	28	45	61	55
Ni	111	410	384	292	416	78	23	35	91	325	408
Cu	31	50	37	47	67	30	15	19	41	64	78
Zn	77	71	88	113	94	125	78	72	179	98	100
Rb	51	71	77	89	1	17	92	61	63	87	23
Sr	670	1001	1440	1671	248	373	384	366	934	453	388
Y	27	19	21	25	17	31	32	26	30	17	19
Zr	277	282	354	401	120	270	242	169	305	164	155
Nb	61	112	141	139	17	23	13	8	27	27	40
Cs	5.0	4.0	2.3	2.7	0.45	1.6	0.99	5.2	14	19	4.9
Ba	538	847	1198	1023	149	177	829	548	2823	329	227
Lu	0.34	0.17	0.19	0.23	0.23	0.40	0.50	0.44	0.40	0.19	0.21
Pb	12	6.3	6.0	7.4	2.0	2.2	10	7.5	22	1.9	2.7
Th	4.8	9.2	11.2	9.0	1.7	2.3	10	5.4	2.3	2.6	3.6
U	2.2	2.6	3.2	3.3	0.4	0.50	1.5	1.1	0.48	0.71	0.89
La	47	100	101	100	13	22	28	21	21	20	23
Ce	91	195	211	197	29	51	62	45	50	45	49
Pr	10	22	24	22	4	7	8	6	7	6	6
Nd	41	78	87	81	15	31	36	23	31	24	24
Sm	8.0	12	14	14	3.6	7.4	7.7	5.1	7.8	5.3	5.2
Eu	2.3	3.1	3.5	3.5	1.2	2.5	1.9	1.4	2.5	1.7	1.7
Gd	7.6	9.1	11	11	3.9	7.8	7.3	5.3	8.0	5.3	5.3
Tb	1.3	1.3	1.5	1.6	0.7	1.3	1.3	1.0	0.0	0.8	0.8
Dy	6.0	5.2	6.0	6.4	3.7	6.9	6.6	5.2	6.9	4.2	4.3
Ho	1.1	0.8	0.9	1.0	0.7	1.3	1.3	1.0	1.2	0.7	0.8
Er	2.9	1.8	2.0	2.4	1.9	3.5	3.8	3.1	3.4	1.8	2.0
Tm	0.43	0.00	0.00	0.35	0.26	0.48	0.54	0.46	0.00	0.24	0.27
Yb	2.5	1.3	1.5	1.8	1.7	3.0	3.5	3.1	2.9	1.6	1.7
Lu	0.34	0.17	0.19	0.23	0.23	0.40	0.50	0.44	0.40	0.19	0.21
Y/Nb	0.44	0.17	0.15	0.18	1.00	1.35	2.46	3.13	1.11	0.63	0.48
Nd/Sm	5.13	6.50	6.21	5.79	4.17	4.19	4.68	4.51	3.97	4.53	4.62
Ba/La	11.4	8.5	11.9	10.2	11.5	8	29	26	134	16	10

Zr/Nb	4.5	2.5	2.5	2.9	7.1	11.7	18.6	20.4	11.3	6.1	3.9
Ce/Pb	7.3	30.8	35.4	26.7	14.2	23.5	6.0	6.0	2.2	23.7	18.1
Nb/U	28.2	43.1	43.7	42.0	41.8	46.0	8.9	7.9	56.3	38.0	44.9

Locations: Samples VG1, VG2, and VG5 from Valtengrund; KE 1, KE 2, KE 3, KE 4, KE B3 and KE B4 from Klunst Ebersbach; NUB6 from Nucknitz; PB7 from Pichow.

In mantle-normalized multi-element variation diagrams, alkaline basalt and ultramafic lamprophyre from Lusatia show a strong enrichment relative to primitive mantle (Fig. 3.8a). Although the alkaline basalt and the ultramafic lamprophyre show similar trends, the incompatible HFSE elements (i.e., U, Th, Ti, Zr, and Nb) and the LREE are clearly more enriched in the ultramafic lamprophyre. The alkaline basalt shows a slightly higher enrichment in Cs, Pb, and Ba than the ultramafic lamprophyre. The samples show no Nb and Ti anomalies except two samples of alkaline basalt that show a weak negative Nb and Rb anomaly. In the trace-element pattern normalized to continental crust (Fig. 3.8b), these rocks show nearly parallel and flat trends, resembling continental crust except for a depletion in Pb and Rb and an enrichment in Cs, Ba, and most HFSE. The ultramafic lamprophyre presents similar trends as richterite minette from SW Poland, which were interpreted to be derived from a depleted asthenospheric source that had been re-enriched before melt extraction (Awdankiewicz, 2007). These rocks show a slight depletion in Sr and a strong Pb peak (Fig. 3.8a). Similar trace element pattern with a significant Sr trough and Pb peak were also observed from the late-Variscan calc-alkaline lamprophyre from Lusatia (Abdelfadil et al., 2012).

The ultramafic lamprophyres have highly fractionated REE with highly enriched LREE and depleted HREE, whereas the alkaline basalts show less fractionated LREE and less depleted HREE. The REE pattern for calc-alkaline lamprophyres from Lusatia are also strongly fractionated with $(La/Yb)_N$= 3.3–11 (Abdelfadil et al., 2012). Although these rocks have similar REE pattern to the alkaline basalt and ultramafic lamprophyre, their LREE are less enriched than ultramafic lamprophyre and slightly more enriched than alkaline basalt (Fig. 3.9). The ultramafic lamprophyres exhibit chondrite-normalized La and Ce values up to 350 and 300, whereas Yb and Lu contents are about 14 times chondrite. They also exhibit a wide range of fractionation $(La/Yb)_N$ = 12–52) whereas alkaline basalt $(La/Yb)_N$ = 5–11) which may result from the diverse mode of REE bearing phases (Tappe et al., 2006). The pattern does not have negative Eu anomalies (Fig. 3.9).

The Nd, Sr, and Pb isotopic composition of the ultramafic lamprophyre and alkaline basalt are reported in Table 3.3. The Sr and Nd isotopic compositions of these rocks have

overlapping ranges (Fig. 3.10a, b). The ultramafic lamprophyres exhibit a narrow range of measured Sr and

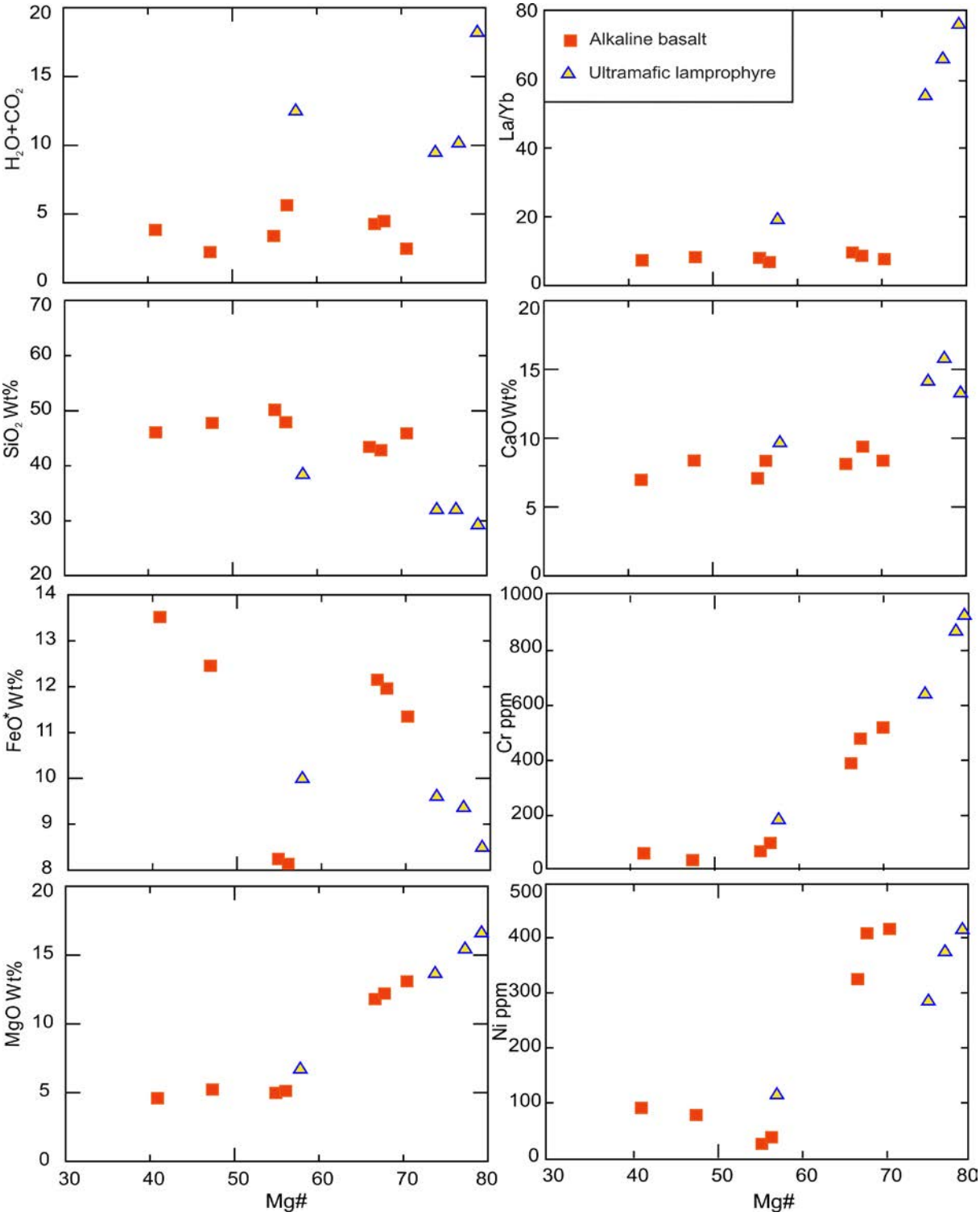

Fig. 3.6. *Plot of major and trace elements composition versus Mg# of Lusatian alkaline basalt and ultramafic lamprophyres.*

Nd isotopic compositions from 0.7042 to 0.7069 and 0.51255 to 0.51269 respectively, whereas the alkaline basalt shows wider range from 0.70385 to 0.71145 and 0.51244 to

0.51275, respectively. The initial Pb isotopic compositions of alkaline basalt and ultramafic lamprophyres show relatively wide variations, with $^{206}Pb/^{204}Pb$= 17.77–18.76, $^{207}Pb/^{204}Pb$ = 15.55–15.59, and $^{208}Pb/^{204}Pb$ = 37.57–38.84 (Table 3.3). The ultramafic lamprophyres have higher $^{206}Pb/^{204}Pb$ and $^{207}Pb/^{204}Pb$ ratios than the alkaline basalt (Fig. 3.10b); indicating a higher contribution of crustal Pb to the source of the ultramafic lamprophyres than to the source of the alkaline basalt.

Calc-alkaline lamprophyres from Lusatia show a narrow range of Nd isotopic compositions (0.51198 to 0.51234), and a more distinct crustal input. The crustal signature is isotopically most distinctly indicated by the broad range of Sr isotopic composition (0.7046 to 0.7079) and the relatively radiogenic Pb isotopis composition of the calc-alkaline lamprophyres ($^{206}Pb/^{204}Pb$= 17.80–18.25, $^{207}Pb/^{204}Pb$ = 15.54–15.59, and $^{208}Pb/^{204}Pb$ = 37.70–38.17) (Abdelfadil et al., 2012).

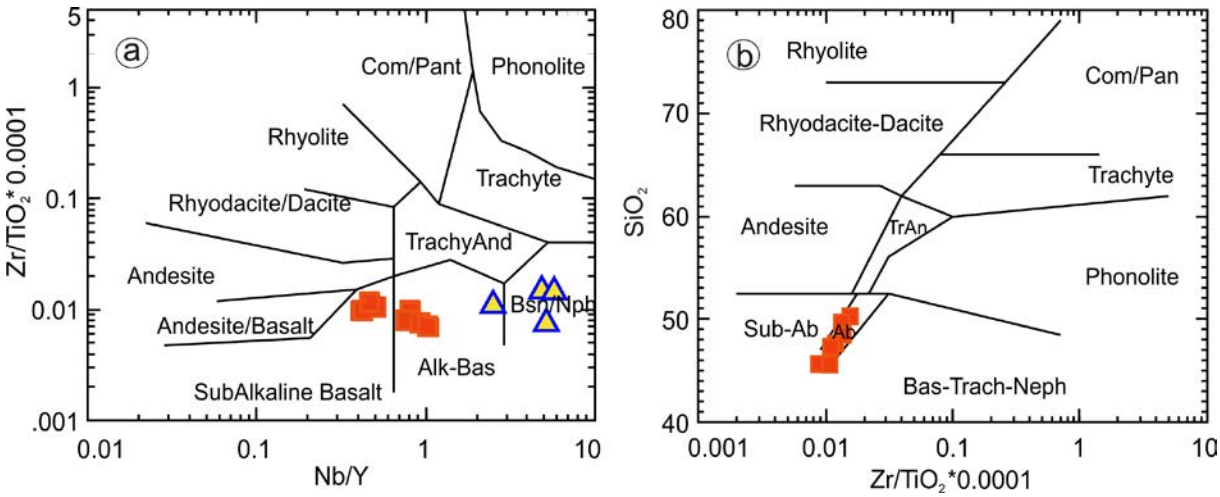

*Fig. 3.7. Geochemical classification. a) Nb/Y vs Zr/TiO_2*0.0001 diagram after (Winchester and Floyd, 1977); and b) Zr/TiO_2 vs. SiO_2 diagram (Winchester and Floyd, 1977). Symbols as in Fig. 3.6. Com/Pan: comendite/pantellerite; Alk-Bas: alkali basalt; Bsn/Nph: basanite/nephelinite; TrAn: trachyandesite; Ab: alkali basalt; Sub-Ab: subalkaline basalt.*

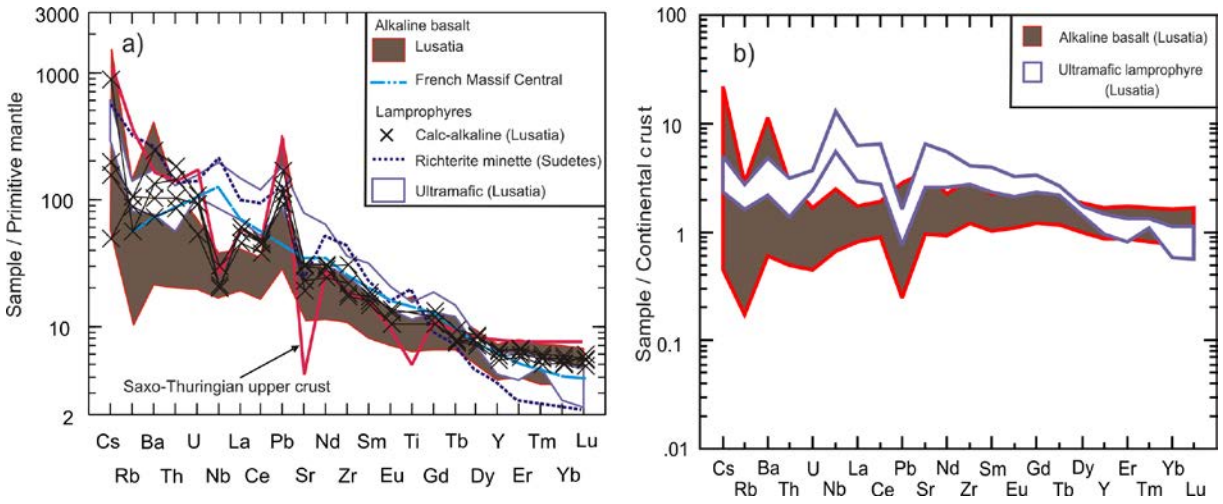

Fig. 3.8. a) Element pattern normalized to Primitive Mantle (Sun and McDonough, 1989) and b) element pattern normalized to Continental Crust (Taylor and McLennan, 1985) of Lusatian alkaline basalts and ultramafic lamprophyres. Corresponding rocks from adjacent regions are shown for comparison. Data sources: lamprophyres from the Sudetes (Awdankiewicz, 2007); alkaline basalts from Massive Central France (Chauvel and Jahn, 1984); Saxo-Thuringian upper crust (Romer and Hahne, 2010).

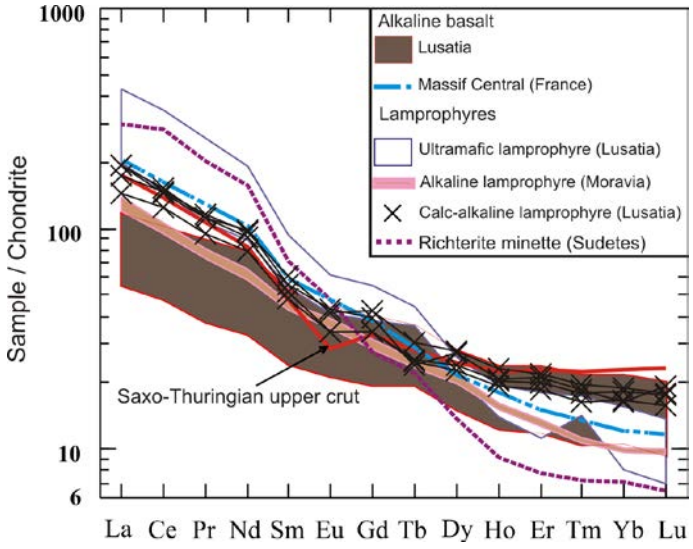

Fig. 3.9. Chondrite-normalized (after Taylor and McLennan, 1985) element patterns of alkaline basalts and ultramafic lamprophyres in comparison with corresponding rocks from adjacent regions. Data sources; Lamprophyres of southwestern Poland (Awdankiewicz., 2007), Saxo-Thuringian upper crust (Romer and Hahne, 2010) French Massive Central (Chauvel and Jahn, 1984), Moravian alkaline lamprophyres (Dostal and Owen, 1998).

Table 3.3
Whole-rock Sr, Nd, and Pb isotope data of alkaline basalt and ultramafic lamprophyres from Lusatia, Germany.

	Sample[a]	Age (Ma)	$^{87}Sr/^{86}Sr$ [b]	$^{87}Sr_{(T)}/^{86}Sr$ [c]	$^{143}Nd/^{144}Nd$ [b]	$\varepsilon Nd_{(T)}$ [c]	$^{206}Pb/^{204}Pb$ [d]	$^{207}Pb/^{204}Pb$ [d]	$^{208}Pb/^{204}Pb$ [d]	$^{206}Pb/^{204}Pb$ [e]	$^{207}Pb/^{204}Pb$ [e]	$^{208}Pb/^{204}Pb$ [e]
1	KE 1	120	0.706492±5	0.70649	0.512677±6	2.0	18.492	15.573	38.500	18.29	15.56	38.36
2	KE 2	120	0.70421±5	0.70421	0.51255±4	-0.1	18.256	15.618	38.215	17.77	15.59	37.65
3	KE 3	120	0.704322±3	0.70432	0.512694±4	2.6	19.282	15.624	38.296	18.64	15.59	37.57
4	KE 4	120	0.705251±4	0.70525	0.512543±3	-0.4	18.971	15.594	38.892	18.43	15.57	38.41
5	KE B3	120	0.711345±5	0.71022	0.512612±6	0.5	18.494	15.561	39.234	18.31	15.55	38.84
6	KE B4	120	0.709324±5	0.70854	0.512440±4	-2.9	18.340	15.598	38.786	18.16	15.59	38.50
7	NU B6	120	0.705841±3	0.70529	0.512753±4	3.2	18.573	15.562	38.677	18.36	15.55	38.35
8	P B7	120	0.703853±5	0.70360	0.512747±6	3.1	18.507	15.567	38.672	18.15	15.55	38.32
9	VG B1	120	0.703911±5	0.70387	0.512727±4	2.5	18.526	15.569	38.748	18.28	15.56	38.41
10	VG B2	120	0.704043±5	0.70382	0.512759±5	3.2	19.038	15.605	39.100	18.76	15.59	38.68

a Sr, Nd and Pb isotopic compositions were analyzed at Deutsches GeoForschungsZentrum GFZ (Potsdam). The samples were dissolved with concentrated HF for four days at 160°C on the hot plate. The digested samples were dried, taken up in 2N HNO_3 and slowly dried. Then the samples were taken up in 6N HCl.

b $^{87}Sr/^{86}Sr$ and $^{143}Nd/^{144}Nd$, normalized to $^{86}Sr/^{88}Sr = 0.1194$ and $^{146}Nd/^{144}Nd = 0.7219$, respectively, were obtained on a Thermo Triton and a Finnigan MAT262 multi-collector mass-spectrometer, respectively, using dynamic multi-collection. Analytical uncertainties are given at $2\sigma_m$ level.

c $^{87}Sr/^{86}Sr_{(T)}$ and $\varepsilon Nd_{(T)}$ were calculated for the emplacement age using $\lambda^{87}Rb = 1.42E\text{-}11\ y^{-1}$ and $\lambda^{147}Sm = 6.54E\text{-}12\ y^{-1}$, $(^{147}Sm/^{144}Nd)^0_{CHUR} = 0.1967$, and $(^{143}Nd/^{144}Nd)^0_{CHUR} = 0.512638$, respectively, and the concentration data given in Table 3.2.

d Pb was separated and purified using ion-exchange chromatography as described in Romer et al. (2005). The Pb isotopic composition was determined on a Finnigan MAT262 multi-collector mass-spectrometer using static multicollection. Lead isotope data corrected for mass discrimination with 0.1% / A.M.U. as estimated from the repeated measurement of lead reference material NBS 981. Reproducibility at 2σ level is better than 0.1%.

e Lead isotope data recalculated to the emplacement age using the contents of Pb, Th, and U (Table 3.2) and the constants recommended by IUGS ($\lambda^{232}Th = 4.9475E\text{-}11\ y^{-1}$, $\lambda^{235}U = 9.8485E\text{-}10\ y^{-1}$, and $\lambda^{238}U = 1.55125E\text{-}10\ y^{-1}$).

italics are anomalously low due to post-emplacement Pb, U, and/or Th mobility related to alteration.

3.5. Discussion

3.5.1 Characterization of mantle components

The geochemical characteristics (e.g., high MgO, FeO, Mg value, Cr, and Ni; Table 3.2) of the c. 120 Ma old ultramafic lamprophyres and alkaline basalt and the c. 330 Ma old calc-alkaline lamprophyres indicate derivation from a mantle source. The trace element signature (high LILE and strong LREE enrichment) and isotopic composition of these rocks, however, is inconsistent with the derivation of these magmas from a depleted or primitive mantle source. The extremely high incompatible trace elements cannot be accounted for by partial melting of a normal peridotite upper mantle (Hoch et al., 2001). It is notable that these signatures are similar to the pattern of continental crust (Taylor and McLennan, 1985). In this section, we highlight the mantle and crustal signatures of the late/post Variscan melts.

Nb/U and Ce/Pb ratios are constant in mantle basalts derived over a large range in melting extent (Hoffmann, 1986; van Keken et al., 2002). The Nb/U and Ce/Pb ratios of our data (Fig. 3.11) show that most of these samples are shifted toward continental values, i.e., are highly enriched in both ratios. Such a shift in the Nb/U and Ce/Pb ratios is also found in lamprophyres from the adjacent areas of southwestern Poland (Awdankiewicz, 2007) and the Erzgebirge (Seifert, 2008). Contribution of crustal material to the mantle source is also recorded in other highly incompatible elements ratios (e.g., Ba/La and Nb/La) that are not significantly affected by fractional crystallization and reflect their original concentrations in the source magmas (Saunders et al., 1988). These rocks have lower Zr/Nb and Y/Nb and higher La/Yb and Sm/Nd (Fig. 3.11) than continental crust (e.g., Zr/Nb ~ 9.09, Y/Nb ~ 1.81, La/Yb ~ 7.27, and Nd/Sm ~ 4.5; Taylor and Mclennan, 1985) and have similar trace element pattern as upper continental crust (Fig. 3.11d, 3.11e, and 3.11f). The Th/La ratio has been used as indicator for the contribution of subducted sediments by dehydration/melting of the subducted slab in a subduction zone (Plank, 2005). As this ratio is likely not to be changed during alteration and metamorphism (Kelly et al., 2003; Spandler et al., 2003), Th/La close to the values for lower and upper crust (Rudnick and Fountain, 1995) indicate an mantle source enriched by crustal material for the ultramafic lamprophyre and alkaline basalt.

The crustal source as identified by the trace element characteristics is also apparent from the Sr, Nd, and Pb isotopic compositions of post-Variscan alkaline basalts and ultramafic lamprophyres and late-Variscan calc-alkaline lamprophyres of Lusatia. These rocks have Pb isotope compositions similar to the enriched mantle (EMII; Zindler and Hart, 1986). In $^{87}Sr/^{86}Sr$ vs. $^{143}Nd/^{144}Nd$ binary diagram, the isotope data scatter and show variable deviations to high $^{87}Sr/^{86}Sr$ (Fig. 3.10). The alkaline basalts have Nd isotopic compositions close to the mantle end member. The metasomatic signature may have been introduced by both melts (variations along the two-component mixing trend) and fluids (offset of $^{87}Sr/^{86}Sr$ to the right of the mixing trend). Two alkaline basalt samples from Klunst Ebersbach (KE B3 and KE B4) display in addition to high $^{87}Sr/^{86}Sr$ and low $^{143}Nd/^{144}Nd$ ratios also high Rb/Sr ratios that may reflect reaction with the granodiorite wall-rocks. Alkaline basalt from other locations do not show such Rb/Sr ratios. The crustal Pb isotopic compositions and the high initial $^{87}Sr/^{86}Sr$ values of alkaline basalt and ultramafic lamprophyre at essentially constant initial $^{143}Nd/^{144}Nd$ values are accounted for by a metasomatic fluid (Ionov et al., 2002).

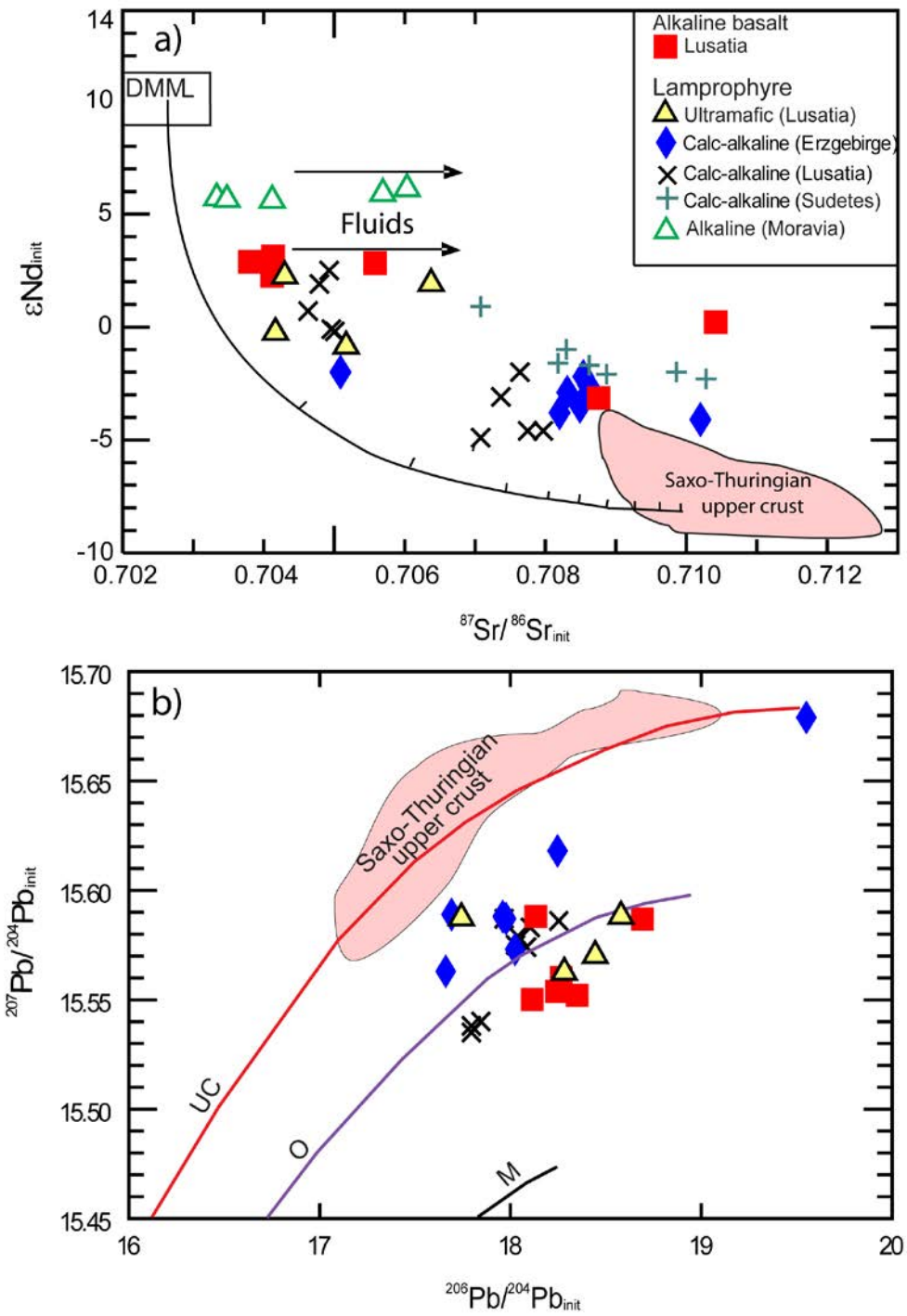

Fig. 3.10. a) The εNd_{init} versus $^{87}Sr/^{86}Sr_{init}$ and b) initial Pb isotopic composition of Lusatian alkaline basalts and ultramafic lamprophyres compared with late and post-Variscan lamprophyres from the Sudetes (Awdankiewicz, 2007), Lusatia (Abdelfadil et al., 2012), the Erzgebirge (Seifert, 2008), and the French Massif Central (Chauvel and Jahn, 1984). Saxo-Thuringian upper crust are taken from Romer and Hahne (2010) and Depleted MORB mantle (DMM) from Zindler and Hart (1986). Mixing line end member ($^{143}Nd/^{144}Nd$= 0.5131, 5122; $^{87}Sr/^{86}Sr$= 0.7025, 0.710; Nd= 1.2, 39 pmm; Sr=11.3, 39 ppm). Mantle (M), orogene (O) and upper crust (UC) Pb evolution curves are after Zartman and Doe (1981).

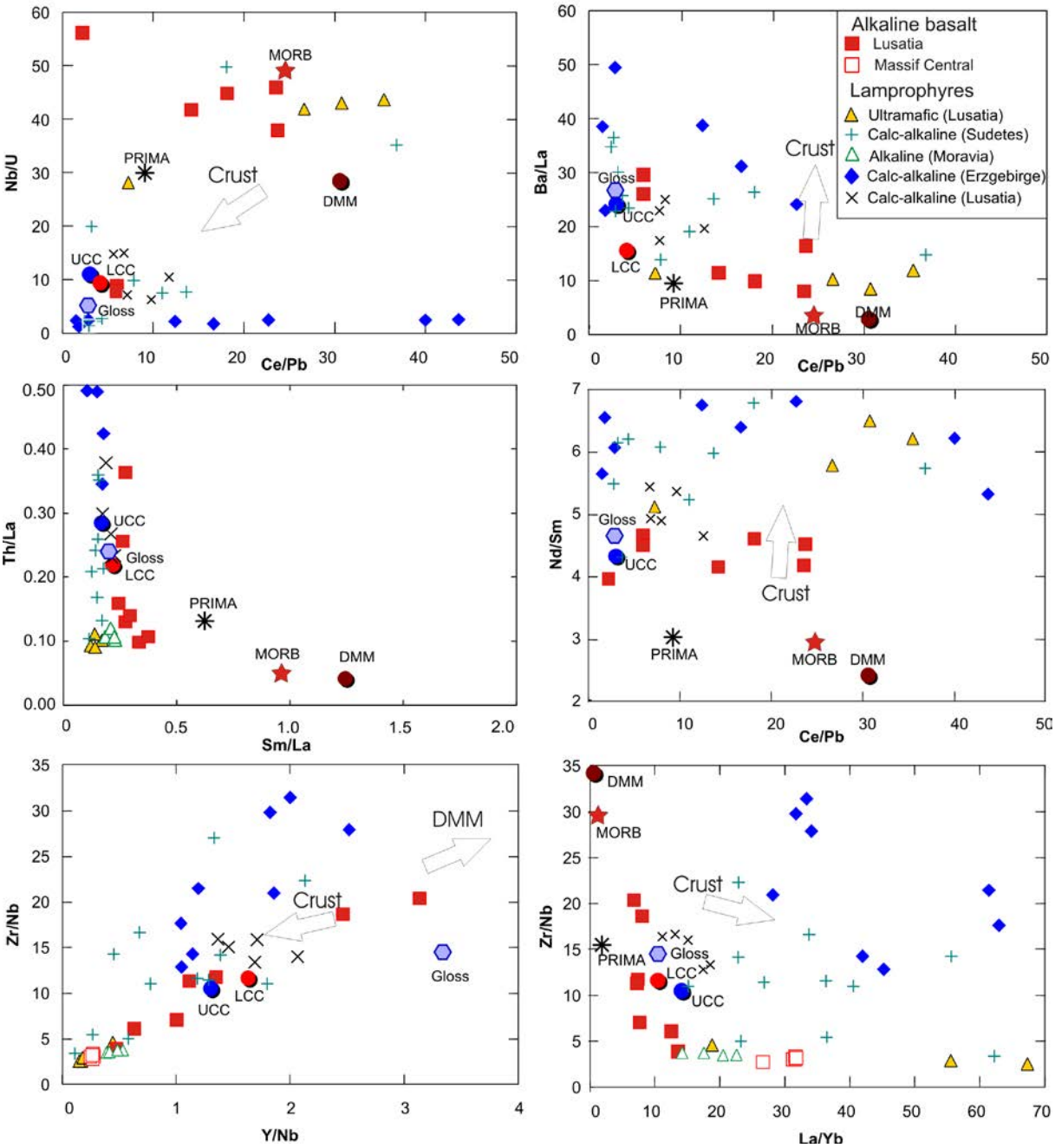

Fig. 3.11. Nb/U vs Ce/Pb; Ba/La vs Ce/Pb; Zr/Nb vs Y/Nb; Zr/Nb vs La/Yb; and Nd/Sm vs Ce/Pb of the alkaline basalt and ultramafic compared to post-Variscan lamprophyres and alkaline basalt from adjacent regions. Data sources: lamprophyres from the Sudetes (Awdankiewicz, 2007); lamprophyres from the Erzgebirge (Seifert, 2008); lamprophyres from Lusatia (Abdelfadil et al., 2012); alkaline lamprophyre from Moravia (Dostal and Owen, 1998); and tertiary alkaline basalt from the French Massif Central (Chauvel and Jahn, 1984). Average compositions of lower (LCC) and upper (UCC) continental crustal are from Rudnick and Fountain (1995); primitive mantle (PM) from (Hofmann, 1988); global subducting sediment (GLOSS) from Plank and Langmuir (1998), and average depleted MORB mantle (DMM) from Workman and Hart (2005).

3.5.2 Source of the mantle enrichment

The late-Variscan calc-alkaline lamprophyres from Lusatia were extracted from a mantle source that has been metasomatised during the Variscan orogeny (Abdelfadil et al., 2012). Melts derived from this metasomatically overprinted mantle have Ba/Nb (14.4–118), Nb/U (6.35–22.6), Th/U (3.8–8.2), Th/Nb (0.17–1.08), and Ce/Pb (4–12) that are typical for continental crust and their trace element pattern resembles Saxo-Thuringian upper crust (Abdelfadil et al., 2012). The Th/La, Sm/Nd, Y/Nb, La/Yb, Zr/Nb ratios of the calc-alkaline lamprophyres resembles those of the post-Variscan ultramafic lamprophyre and alkaline basalt (Fig. 3.11). The striking similarity of the trace elements pattern of the alkaline basalts, ultramafic lamprophyres, and late-Variscan calc-alkaline lamprophyres (Fig. 3.8a) indicates that these rocks were derived from same mantle source. As Ti and V are not affected by hydrothermal alteration and metamorphism (Shervais, 1982), the coherence of Ti and V (Fig. 3.12) indicates that the late-Variscan and post-Variscan melts are derived from a similar source. As the alkaline basalts, the ultramafic lamprophyres, and the late-Variscan calc-alkaline lamprophyres from Lusatia have the same metasomatic fingerprints (Figs. 3.9–3.12), the metasomatic components in the alkaline basalts and ultramafic lamprophyres are related to the Variscan orogeny, i.e., have been introduced to the mantle by an event entirely unrelated with the extraction of the alkaline basalts and the ultramafic lamprophyres.

3.5.3 Geodynamic significance

Cretaceous lamprophyres, similar to the ones from Lusatia, are also known from the adjacent areas of the Western Carpathians and Moravia (Dostal and Owen, 1998; Lucinska-Anczkiewicz et al., 2002) and farther to the southeast in Hungary (e.g., Harangi, 1994; Harangi et al., 2003). On the larger scale, 100-130 Ma old Cretaceous dikes are abundant throughout the entire North Atlantic Ocean region. For instance, c. 130 Ma old nephelinite, basanite, and phonolite dikes have been found in the present North Sea (Miller and Mohr, 1964; Harrison et al., 1977; Dixon et al., 1981) and c. 85-113 Ma old lamprophyres and trachytes are known from North Pyrenean Rift Zone and off the coast of NW Spain (Azambre et al., 1992; Rossy et al., 1992; Montigny et al., 1986). Corresponding early Cretaceous magmatism (monchiquites, spessartites, and ultramafic lamprophyres) related to the reactivation of old lineaments in conjunction with the opening of the North Atlantic Ocean

(McHone and Butler, 1984; Bedard, 1985), is also known from occur also in New England and Quebec (e.g., Philpotts, 1974; McHone, 1978).

The temporal coincidence of lamprophyric magmatic rocks over large part of western Europe indicates that the distribution of this magmatism is controlled by large-scale tectonic processes and changes in the stress field. In the late Jurassic and early Cretaceous, western Europe was affected by the incipient opening of the northern Atlantic and compression preceding the Alpine orogeny (Dewey and Windley, 1988; Golonka, 2004). The maximum tectonic activity occurred in the Aptian-Albian (c. 121-99 Ma), when break-up started (Ziegler, 1988). The magmatic episodes related to the opening of the Atlantic occurred at 135-125, 70-80, and 60-50 Ma (McIntyre, 1977). The c. 120 Ma post-Variscan ultramafic lamprophyre from Lusatia is representative of the early Cretaceous episode (135-125 Ma). Therefore, the opening of the North Atlantic and changes in the stress field are a major event which controlled a variety of widely dispersed Cretaceous magmatism in Eastern and Western Europe as well as North America provinces.

The similar geochemical fingerprint of late-Variscan calc-alkaline lamprophyres and post-Variscan alkaline basalt and ultramafic lamprophyre in Lusatia implies that (i) the same metasomatized mantle source may be sampled by repeated melt extraction; (ii) is not necessarily removed through time, and (iii) does not change character unless there is an additional metasomatic overprint. Importantly, melt extraction from the metasomatic mantle may be entirely unrelated to the metasomatic event. Instead, it is related to changes in the regional stress field and crustal thinning. Actually, because of extension and mantle upwelling, the same general source may be reactivated at different depths (e.g., Tappe et al., 2007). Extensive melting, however, may locally deplete the subcontinental mantle in fertile material and result in a different character later magmatism, as possibly reflected in the Tertiary magmatism of the Eger Graben (Haase and Renno, 2008), whose eastern end borders to Lusatia.

3.5.4 Genetic relation between alkaline basalts and ultramafic lamprophyres

The compositional variation between the alkaline basalt and the ultramafic lamprophyres cannot be explained in terms of fractional crystallization as the ultramafic lamprophyres that are supposed to be younger than alkaline basalt (Kramer and Andrehs, 2011) have higher MgO and FeO contents than the alkaline basalt. The variation in the mineralogical modes and trends result from different crystallization conditions, with different pressure and temperature

(Fig. 3.5). The slight depletion in HREE in the ultramafic lamprophyre relative to alkaline basalt (Fig. 3.8 and 3.9) reflects an existence of residual garnet (Polat et al., 1997; Furman and Graham, 1999). The similar Nd, Pb, and Sr isotopic compositions (Fig. 3.10) of the alkaline basalt and ultramafic lamprophyre (except KE B3 and KE B4) indicates similar mantle source. The alkaline basalt, however, seems to have crystallized over a greater temperature and pressure range than the ultramafic lamprophyre, as inferred from the clinopyroxene composition.

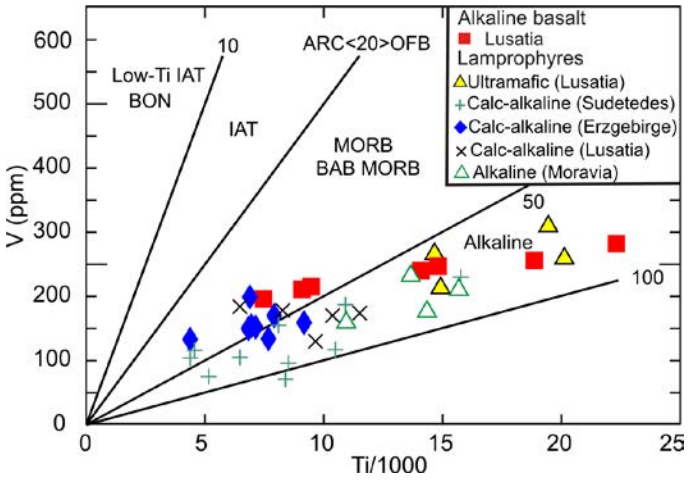

Fig. 3.12. Ti-V discrimination diagram after Shervais (1982). Symbols as in Fig.3.6.

3.6. Conclusions

The depleted mantle beneath Lusatia has been affected by metasomatism during the Variscan orogeny. This metasomatically enriched mantle has been sampled during late stages of the Variscan orogeny by c. 330 Ma old calc-alkaline lamprophyres that demonstrate (i) strong enrichment of the LREE and LILE, (ii) radiogenic Sr and Pb isotopic compositions, and (iii) striking similarity of the trace elements pattern of these rocks with Saxo-Thuringian upper crust. The c. 120 Ma old ultramafic lamprophyres and alkaline basalts were emplaced in the same general area and sampled the post-Variscan metasomatized mantle that was inherited from the Variscan orogeny. The late-Variscan calc-alkaline lamprophyre and post-Variscan alkaline basalt and ultramafic lamprophyre were derived from same mantle source, but melted at different pressure and temperature conditions. The Lusatian Block was repeatedly reactivated during reorganizations in the regional stress field allowing for the multiple melt extraction from the metasomatized mantle. The melt extraction itself is not related to the metasomatic event, but it is related to changes in the stress field and crustal thinning, which

results in mantle upwelling and preferential melting of metasomatic domains in the preciously enriched mantle.

Acknowledgments

We thank R. Naumann (GFZ-Potsdam) for the XRF analysis, K. Hahne (GFZ-Potsdam) for trace element analysis, S. Tonn (GFZ-Potsdam) for the REE data, and O. Appelt (GFZ-Potsdam) for support with the microprobe work. KMA thanks W. Kramer for guidance in the field.

4. Fate of subducted Li – the lamprophyre connection

Abstract

Variscan orogenic lamprophyres from the northeastern part of the Bohemian Massif (Erzgebirge, Lusatia, Sudetes) have δ^7Li values ranging from -5.5 to 1.9 ‰, i.e., values that are lower than the compositional range of depleted mantle. Correlations of δ^7Li with Li, Li/MgO, Li/Rb, and Li/Cs, demonstrate that these low values are not due to processes related to emplacement or surface-near low-temperature alterations, but represent genuine signatures from the mantle source of the lamprophyres. The low δ^7Li values of the lamprophyre source reflect Variscan metasomatism of the subcontinental mantle, whereas the regionally different correlations of δ^7Li with other elements (e.g., Li/Yb, Nb/Dy, Li/Cs) imply that this metasomatism shows regional differences that correlate with the nature of the subducted slab and its Palaeozoic sedimentary cover, which represents the source of the metasomatic component. The isotopic and geochemical composition of Variscan lamprophyres in part overlaps with the one of the Palaeozoic sedimentary rocks and in part falls in fields outlined by the composition of the depleted mantle and the compositional range of the Palaeozoic sedimentary rocks, depending whether the budget of respective element is dominated by the metasomatic component or has contributions from both components. These data demonstrate that the chemical and isotopic compositions of the subducted sedimentary rocks do not necessarily change during subduction. Our data demonstrate that crustal Li is reintroduced into the mantle. The virtual absence of this crustal signature in Oceanic Island Basalts implies that it is not reintroduced into the convecting mantle, but instead is transferred to the mantle wedge and thereafter remains in the subcontinental mantle.

4.1. Introduction

The Li isotopic composition of the convecting mantle is remarkably homogeneous (δ^7Li ~3 to 4) and seems to have varied little through time (e.g., Tomascak, 2004; Halama et al., 2007, 2008; Tomascak et al., 2008). In contrast, the Li isotopic composition of the crust is heterogeneous: Interaction with seawater shifts the Li isotopic composition of altered oceanic crust (AOC) to higher δ^7Li values (up to ~15), whereas weathering of the continental crust shifts the Li isotopic composition of siliciclastic debris to lower δ^7Li values (down to ~ –20) (e.g., Chan et al., 1992, 2002; Rudnik et al., 2004). Thus, Li entering a subduction zone is

isotopically heterogeneous. Field and experimental studies furthermore demonstrate that the Li isotopic composition of material entering the subduction zone is additionally affected by isotopic fractionation related to fluid loss during progressively higher-grade metamorphism (e.g., Zack et al., 2003; Elliott et al., 2004; Marschall et al., 2007). Thus, the isotopic composition of Li transferred back into the mantle may be highly variable depending both on the subducted material and on the mineralogically controlled partitioning and fractionation of Li between solid and fluids escaping during subduction. Dehydration or melting of subducted siliciclasting sediments or continental crust at mantle depth should bring along Li with relatively low δ^7Li values (e.g., Agostini et al., 2008) and add this material to the local mantle. Although mantle xenoliths display a broad range of Li contents and δ^7Li values (cf. Tomascak, 2004; Elliott et al., 2004; Nishio et al., 2004), mantle derived melts sampling larger mantle volumes show surprisingly small δ^7Li variations. For instance, OIB with different Sr-Nd-Pb isotope signatures, which should reflect the contrasting nature of subducted material, typically do not show a correlation between δ^7Li and the Sr-Nd-Pb isotope signatures. Instead, the δ^7Li values of OIB largely coincide with the compositional range known for MORB (e.g., Krienitz et al., 2012). This indicates that (i) if significant amounts of Li are introduced into the convecting mantle, its isotopic composition on average should be not too different from the average value of the mantle or (ii) Li is not introduced to a significant amount into the convecting mantle, but is mostly lost during subduction and resides in the crust or in non-convecting suprasubduction zone mantle wedges (e.g., Elliott et al., 2004; Krienitz et al., 2012).

Orogenic lamprophyres are samples from the metasomatized suprasubduction zone mantle wedge (e.g., Rock, 1987, 1991; Foley, 1992; Prelević et al., 2008, 2010a). They have a mixed geochemical signature with high MgO, FeO, Cr, and Ni contents and a high Mg# (Mg/(Mg+Fe) cation ratio), which demonstrates their derivation from a depleted mantle source, combined with high contents of LILE, HFSE, and REE and trace element pattern that resemble typical crustal rocks (e.g., Foley et al., 1987; Foley, 1992; Peccerillo and Marinotti, 2006; Prelevic et al., 2008, 2010a; Conticelli et al., 2009; Abdelfadil et al., 2012). The intensity of the crustal signature depends on (i) how prominent this signature is in the metasomatized mantle and (ii) on the relative portion of metasomatized and depleted mantle that are involved in the formation of these rocks. For instance, small amounts of melting will result in melts with a geochemical signature resembling the metasomatized mantle, whereas for large amounts of melting, the metasomatized mantle will be consumed and diluted by increasingly higher portions of depleted mantle. Note, this mixed origin of lamprophyres

results in a geochemical uncoupling of the elements that predominantly derive from the metasomatized mantle (e.g., alkaline elements, REE, and the isotopic compositions of Sr, Nd, and Pb) from those dominantly provided by the depleted mantle (e.g., Mg, Cr, and Ni). Furthermore, this uncoupling implies that the isotopic composition of Sr, Nd, and Pb does not provide age constraints on mantle metasomatism (cf. Rock, 1987, 1991; Prelevic et al., 2008). Instead, the crustal signature of the metasomatized mantle could be derived from the subducting slab and may – in the extreme case – be extracted from the wedge when subduction still is going on (e.g., Tonarini et al., 2005; Agostini et al., 2008; Prelević et al., 2010, 2012). Prelević et al., (2008, 2010a) demonstrated that the geochemical and isotopic composition of the metasomatic component of Mediterranean orogenic lamproites closely corresponds to the geochemical and isotopic signatures of sediments that enter the subduction zone. Thus, metasomatism of the wedge is directly related to subduction processes and the geochemical and isotopic composition of lamprophyres closely correspond the subducted material. Furthermore, lamprophyres occurring in the same area, but extracted at different time and under different conditions, use to show the same metasomatic signature (whereby the isotopic evolution of the metasomatic component has to be taken into account), implying that the metasomatized subcontinental mantle is not in taking part in mantle convection, but remains attached to the continental crust (e.g., Tappe et al., 2006, 2007). Thus, lamprophyres represent samples from the metasomatized mantle wedge that allow to trace the nature of the subducted material. Especially because of the spatial relation between geochemical signature of the subducted material and the lamproite and lamprophyre composition in young orogens (e.g., Prelević et al., 2008, 2010a), the nature of the crustal signature in orogenic lamprophyres may be used to distinguish and outline the extent of different mantle wedges in old orogens.

In this paper, we use late-Variscan lamprophyres from the Erzgebirge, Lusatia, and the Sudetes at the northern and eastern margins of the Bohemian Massif (Fig. 4.1) as samples of the Variscan subcontinental mantle to study the interaction of slab-derived material with the overlying mantle. As the subcontinental mantle of these three regions has been modified by material released from different kinds of subducting slabs and associated sedimentary rocks (e.g., Kroner and Romer, 2010, 2013; Abdelfadil et al., 2012), the geochemical and isotopic signature of late-Variscan lamprophyres should show regional differences that correspond to the contrasting nature of the subducted material. Our new Li isotope data from late-Variscan lamprophyres from the Erzgebirge, Lusatia, and the Sudetes – in particular in combination with Sr, Nd, and Pb isotope data and geochemical data – demonstrate regional differences

both in the importance and in the geochemical character of the metasomatic component that the subcontinenental mantle source of these lamprophyres shows. Furthermore, systematic relations between δ^7Li and, e.g., Li/Yb, Li/Sc, and Li/Nb indicate that Li in the lamprophyres is derived from the mantle and reflects the Variscan metasomatism of the subcontinental mantle and regional differences δ^7Li and its relation other chemical and isotopic fingerprints reflect the contrasting chemical and Sr-Nd-Pb isotopic composition of material released from the different subducted slabs.

4.2. Geological setting

The convergence and subsequent collision of Laurussia and Gondwana, i.e., the Variscan orogeny of central and western Europe, resulted in the formation of several short-lived subduction zones within the complex plate boundary zone between these two plates (Kroner and Romer, 2010, 2013). The position and behavior of these subduction zones is controlled by the spatial distribution of thick crustal blocks (Fig. 4.2), which are not subductable, and thinned continental crust together with its volcanosedimentary cover, which is subductable (Kroner et al., 2007; Kroner and Romer, 2013). During the convergence of the two continents, oceanic crust of the Rheic Ocean was consumed in a subduction system sustaining a magmatic arc, whose remains are preserved in the Mid-German Crystalline Zone (Fig. 4.1; Anthes and Reischmann, 2001; Zeh and Will, 2010). With the consumption of the oceanic crust of the Rheic ocean, the continental fragment of Armorica collided with the Midland craton at c. 400 Ma, displacing it to the northeast and resulting in extensional tectonics and mafic magmatism in the area of the Rhenohercynian Zone (Kroner and Romer, 2013). Farther to the east, the Teplá-Barrandian Unit collided with Laurussia and was thrust upon the Bohemian Massif (Figs. 4.1 and 4.2). The combined Teplá-Barrandian Unit and Bohemian Massif indented into Laurussia, forming the Sudetes orogenic belt. A new subduction zone developed behind the Bohemian Massif (Fig. 4.2), allowing for continued convergence between Laurussia and Gondwana. In this younger subduction system, thinned continental crust with its volcanosedimentary cover was subducted beneath the Bohemian Massif. Parts of the subducted thinned continental crust eventually resurfaced by lateral escape in the metamorphic belts to the northwest and southeast of the Bohemian Massif (i.e., the Erzgebirge and the Gföhl area). Peak metamorphism in the high-grade rocks of these three belts was reached at c. 340 Ma (e.g., Kröner and Willner, 1998; Willner et al., 2000), whereas peak metamorphism in the Sudetes was reached slightly earlier (i.e., 345 Ma, Marheine et al.,

2002), as this belt in genetically linked with the arrest of the older subduction system (Kroner and Romer, 2013).

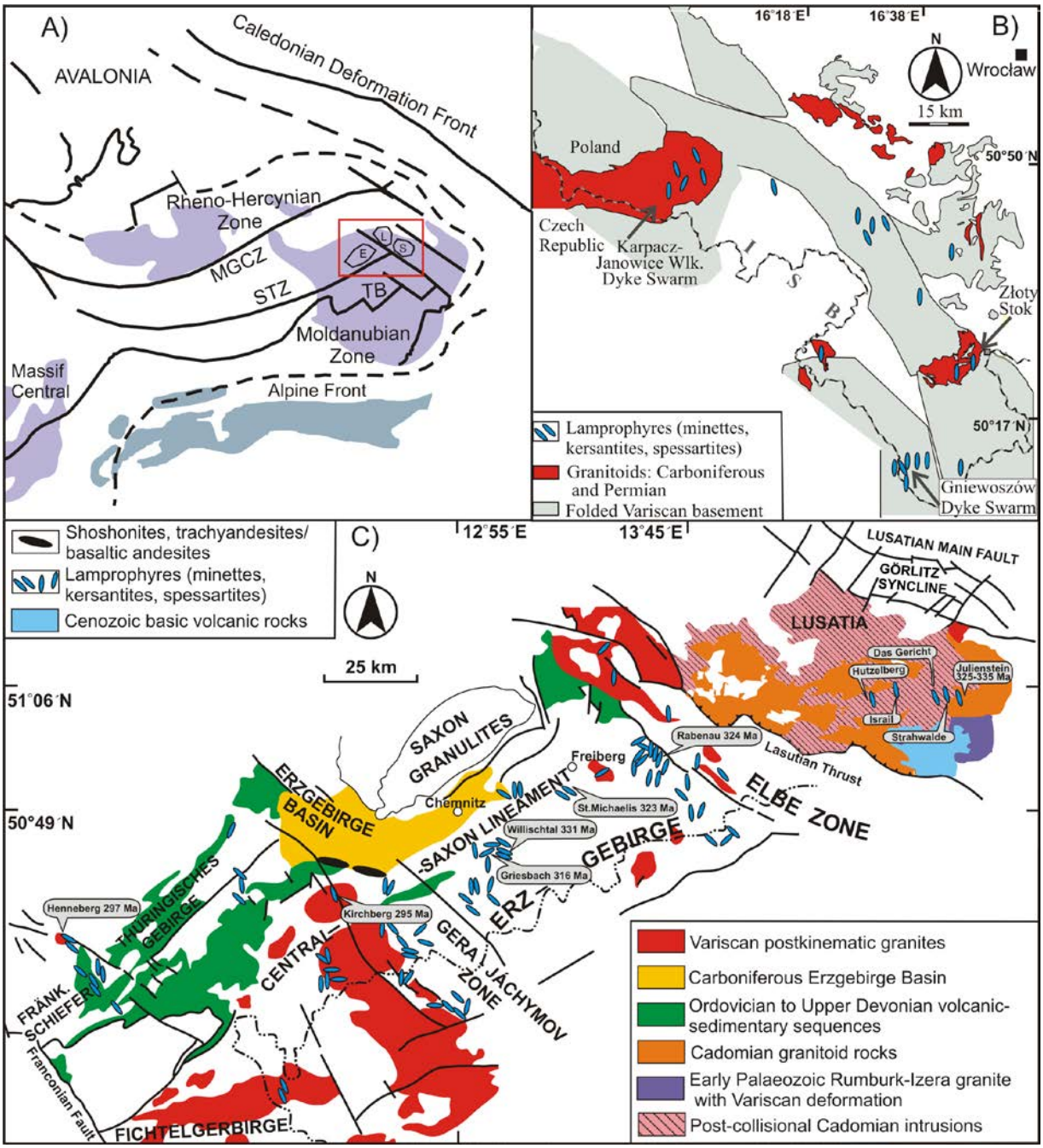

Fig. 4.1. a) Simplified map showing the distribution of Palaeozoic Massifs (blue), in part overprinted during the Alpine orogeny (green) and the major structural boundaries. Note the position of the Erzgebirge (E), Lusatia (L), and the Sudetes (S) in the northern part of the Bohemian Massif. Abbreviations: RHZ = Rheon-Hercynian Zone, STZ = Saxo-Thuringian Zone, MZ = Moldanubian Zone; TBU = Teplá-Barandian Unit, MGCZ = Mid-German Crystalline Zone. Simplified after Walter (2007). b) Geological map of Sudetes showing the

localities of calc-alkaline lamprophyre (simplified after Awdankiewicz, 2007). c) Geological map of Saxo-Thuringian Zone showing the setting of the dated lamprophyres dikes in the Erzgebirge and Lusatia (modified after Schust, 2000; von Seckendorf et al., 2004; Kemnitz, 2007).

The position of the Bohemian Massif within the Variscan orogen is specific as the upper mantle beneath has been affected by material released from several different subduction zones, whereas the mantle beneath Lusatia, which has been slid along the northern limit of the Bohemian Massif to its present position (Fig. 4.2), has been affected by this subduction-related metasomatism to a lesser extent (Abdelfadil et al., 2012). Lamprophyres emplaced soon after the emplacement of the metamorphic rocks in the tectonic nappes of the Erzgebirge and the Sudetes sampled the mantle along the northern and eastern margin of the Bohemian Massif and, thus, should record both contrasting signatures and contrasting extent of metasomatism related to the Variscan orogeny. In such a scenario, lamprophyres from the Erzgebirge should show strong mantle metasomatism by crustal material, whereas those from Lusatia should reflect less strongly metasomatized mantle that possibly was affected by oceanic crust and sedimentary material deposited on it. In contrast, lamprophyres from the Sudetes are expected to be more heterogeneous in their metasomatic signature, as this mantle was affected by oceanic crust and its cover and subsequently by thinned continental crust and its volcanosedimentary cover.

Lamprophyres of the Erzgebirge fall in two age groups, one around 325 Ma and a younger one around 300 Ma (e.g., von Seckendorf et al., 2004). Lamprophyres from Lusatia were emplaced around 335 Ma (Abdelfadil et al., 2012), whereas those from the Sudetes fall in the age range from 335 to 310 Ma (Awdankiewicz, 2007). The lamprophyres from all three areas show broadly overlapping fields of initial Sr, Nd, and Pb isotopic compositions, with minor, but notable differences (Fig. 4.3). In the εNd_{330} *vs.* $^{87}Sr/^{86}Sr_{330}$ diagram, the lamprophyres define a continuous trend between Sr isotopic compositions typical for the depleted mantle and those typical for Saxo-Thuringian upper crust (mostly sedimentary rocks). This crustal end-member is isotopically similar to the high-grade metamorphic rocks of the Erzgebirge, which in turn demonstrates that these sedimentary rocks have been subducted deep into the mantle (e.g., Rötzler et al., 1998; Kroner and Romer, 2010, 2013) and, thus, represent an upper crustal component that may have been involved in the metasomatism of the mantle beneath the Bohemian Massif. It is notable that the samples from the Sudetes encompass a much broader range than lamprophyres from the Erzgebirge and Lusatia (Fig. 4.3). The εNd_{330} and $^{87}Sr/^{86}Sr_{330}$ values of the lamprophyres from Lusatia seem

to fall in two groups of contrasting involvement of crustal material. The εNd_{330} and $^{87}Sr/^{86}Sr_{330}$ values of the lamprophyres from the Erzgebirge (and its low-grade continuations in Thuringia) form a relatively homogeneous group with compositions indicative for a strong crustal input. Three samples of the Erzgebirge suite (Table 4.1) fall of this common trend and have apparent initial $^{87}Sr/^{86}Sr$ values that are too low for their εNd_{330} values. These low values indicate that a secondary increase of $^{87}Rb/^{86}Sr$ took place, which eventually lead to an overcorrection of in situ ^{87}Sr ingrowth in these samples. Such a disturbance is also known from high Rb/Sr granitic rocks of the Erzgebirge and is related to Mesozoic reactivation of Erzgebirge-transverse structures (cf. Romer et al., 2012).

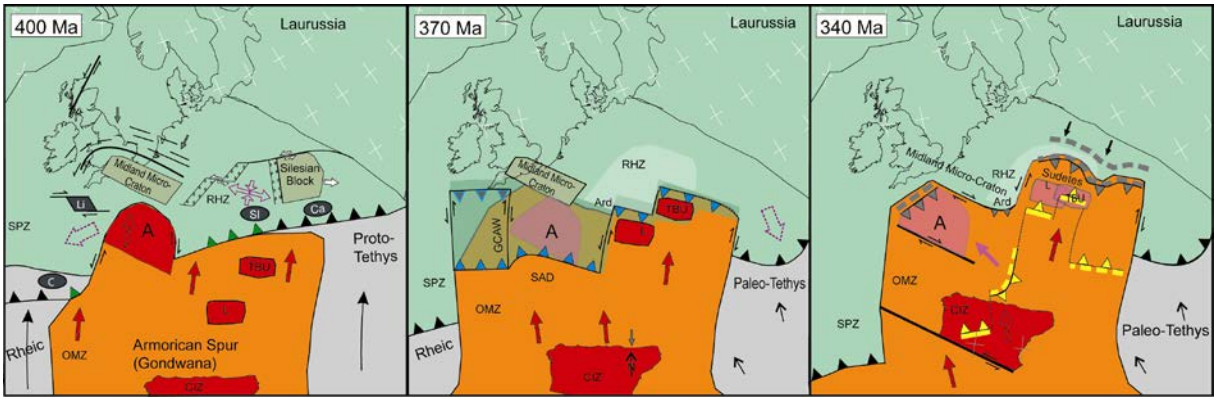

Fig. 4.2. Plate tectonic model illustrating the collision between the Armorican Spur as integral part of Gondwana and Laurussia between 400 and 340 Ma (Kroner and Romer, 2013).

The Pb isotopic composition of lamprophyres from all three regions shows a crustal fingerprint, plotting between the Orogenic and Upper Crust Pb growth curves of Zartman and Doe (1981). The Pb isotopic composition of lamprophyres from Lusatia and the Sudetes show the same compositional range, whereas the Pb isotopic composition of lamprophyres from the Erzgebirge show a broader compositional range and reach higher $^{207}Pb/^{204}Pb$ values than those from the other areas (Fig. 4.3). The compositional range of Pb from the lamprophyres may reflect contributions of crustal Pb from two different crustal Pb sources, with the lamprophyres from the Erzgebirge having a higher contribution of Pb from a source similar to Saxo-Thuriningina Palaeozoic shales.

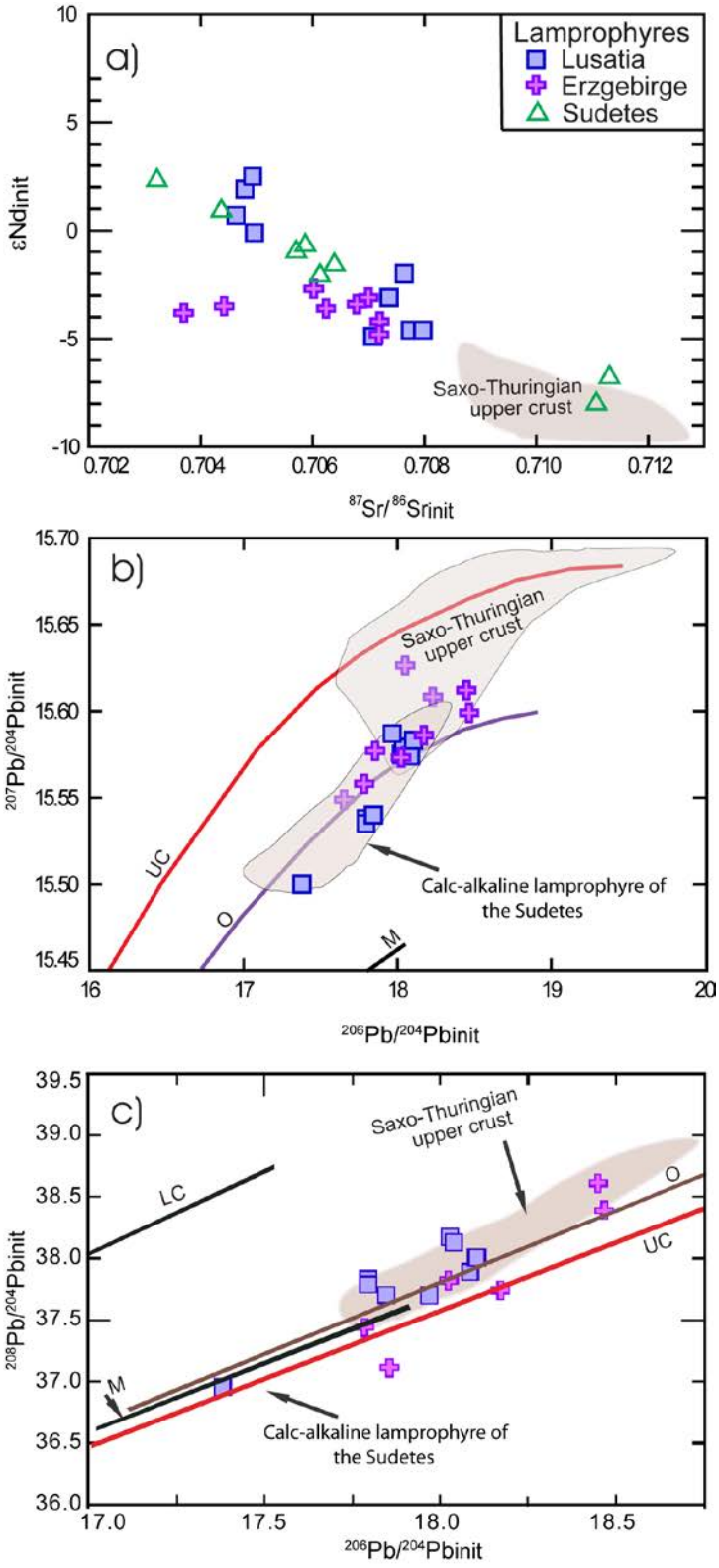

Fig. 4.3. Sr-Nd-Pb isotopic composition of late Variscan calc-alkaline lamprophyres from the Erzgebirge, Lusatia, and the Sudetes. All isotope ratios are calculated for the age of lamprophyre emplacement. a) εNd vs. $^{87}Sr/^{86}Sr_{init}$. b) $^{207}Pb/^{204}Pb_{init}$ vs. $^{206}Pb/^{204}Pb_{init}$. c) $^{208}Pb/^{204}Pb_{init}$ vs. $^{206}Pb/^{204}Pb_{init}$. Data sources for lamprophyres: Awdankiewicz (2007), Lusatia (Abdelfadil et al. (2012), and this work (Table 4.1). Reference fields: Saxo-

Thuringian Upper Crust: Romer and Hahne, 2010). Mantle (M), Orogenic Crust (O), and Upper Crust (UC) Pb evolution curves after Zartman and Doe (1981).

The crustal signature in these mantle-derived rocks is also apparent in the mixed geochemical composition of the lamprophyres (Fig. 4.4). The mantle signature is obvious from the high MgO, Cr, and Ni contents and the high Mg#, whereas the crustal signature is most prominent in incompatible trace elements (Fig. 4.4). Trace-element pattern normalized to primitive mantle show a distinct enrichment in Pb, U, Th, alkaline and alkaline earth elements, and the LREE (Fig. 4.4c), the latter also is obvious in steep chondrite-normalized REE patterns (Fig. 4.4d). Although the lamprophyres from the three regions are predominantly calc-alkaline lamprophyres and have overlapping ranges of MgO and Cr abundances (Fig. 4.4b), they differ both in the pattern and the intensity of the crustal signature. For instance, lamprophyres from Lusatia have a lower LREE enrichment than those from the Erzgebirge and the Sudetes. Similarly, lamprophyres from Lusatia have a less pronounced enrichment of alkaline and alkaline earth elements and LREE than lamprophyres from the adjacent two areas. The compositional range of lamprophyres from the Sudetes is larger than the one of lamprophyres from the Erzgebirge and Lusatia and overlaps with the compositional range of these lamprophyres.

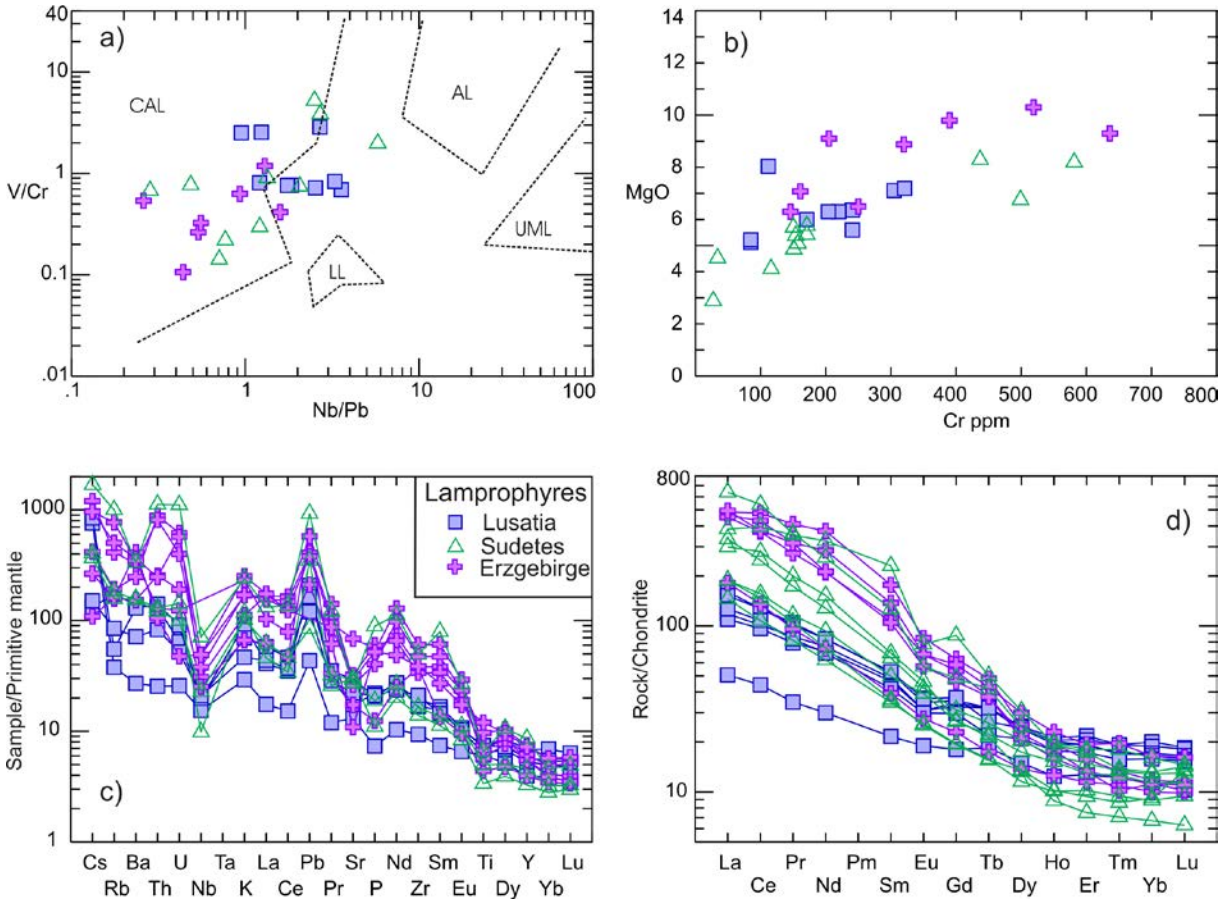

Fig. 4.4. Chemical characterization of late Variscan calc-alkaline lamprophyres from the Erzgebirge, Lusatia, and the Sudetes. a) V/Cr vs. Nb/Pb discrimination diagram of lamprophyres (Rock, 1991). CAL – calc-alkaline lamprophyres; AL – alkaline lamprophyres; UML – ultramafic lamprophyres; LL – Lamproites. Note that most of the investigated lamprophyres fall in the CAL field. b) MgO vs. Cr showing the mantle signature. c) Primitive-mantle-normalized (Sun and McDonough, 1989) element pattern of lamprophyres. d) Chondrite-normalized REE patterns of lamprophyres (Sun and McDonough, 1989). Note the contrasting crustal signatures of lamprophyres from the various areas. Data sources for lamprophyres: Kramer (1988), von Seckendorf et al. (2004), Awdankiewicz (2007), Abdelfadil et al. (2012).

4.3. Analytical methods

The chemical data presented in the Electronic Supplementary Materials (Table A1) have largely been published before and analytical details are given in the original work. For some older analyses from the literature, rare earth element (REE) and trace element contents had not been reported. For these samples, the original chemical analyses have been complemented on aliquots of the originally used sample powders. Analytical procedures and long-time reproducibility of international reference materials are given in detail in Romer and Hahne (2010).

For determination of the Sr, Nd, and Pb isotopic composition, samples were digested using concentrated HF on a hot plate. The fluorides were converted first to nitrates and then to chlorides. Standard procedures for the separation of Sr, Nd, and Pb are described in detail in Romer et al., (2001, 2005) and Romer and Hahne (2010). The Sr and Nd isotope ratios were determined on a Thermo Element Triton and a Finnigan MAT262 TIMS multi-collector mass-spectrometer, respectively, operated in dynamic multicollection mode. For analytical details, blanks, and long-time reproducibility of reference materials see Table 4.1. The Pb isotope ratios were determined on a Finnigan Mat262 mass-spectrometer using static multicollection. For details see Table 4.1.

Li-isotope ratios were determined using a Thermo Element Neptune MC-ICP-MS. For the lithium isotope determination, between 18 and 45 mg of the sample material were digested in a mixture of concentrated hydrofluoric and nitric acid. Sample preparation, rock standards, operating conditions, and measurement procedures are identical to those reported by Wunder et al. (2006, 2007) using the ion exchange techniques described by Tomascak et al. (1999) and

Jeffcoate et al. (2004). To check for possible loss of lithium during the separation procedures, we collected pre-Li eluate and post-Li eluate. Loss of lithium was less than 0.1% of the total Li in the samples and procedural blanks ranged from 10 to 280 pg Li. They had no significant effect on the lithium isotopic composition in the samples. All the samples were measured repeatedly in the standard/sample/standard mode using a 2% HNO_3 solution closely adjusted to 25 ppb Li (±5%).

4.4 Results

The isotopic compositions of Li, Sr, Nd, and Pb and the contents of Li in late-Variscan calc-alkaline lamprophyres from the Erzgebirge, Lusatia, and the Sudetes are listed in Table 4.1 and shown on Figs. 4.5 to 4.7. The major, trace, and rare earth element contents of the complete sample suite, which have been published before (Kramer, 1976, 1988; von Seckendorff et al., 2004; Awdankiewicz, 2007; Abdelfadil et al., 2012), are presented in Table A1 in the Electronic Supplementary Material.

The late-Variscan calc-alkaline lamprophyres of Lusatia show a relatively restricted range in Li isotopic composition (-1.3 to 1.8 ‰) and concentration (8.4 to 17 ppm). In contrast, the late-Variscan calc-alkaline lamprophyres from the Erzgebirge have generally lower δ^7Li values and higher lithium concentrations that range from -5.5 to 0.2 ‰ and 29 to 141 ppm, respectively. One sample has a δ^7Li value of -9.9 ‰ (147 ppm). As this sample also has an anomalously low apparent initial $^{87}Sr/^{86}Sr$ value (Table 4.1) that is indicative for post-emplacement change of Rb/Sr, it is obvious that this sample must have experienced low temperature alteration, which also would have affected the Li isotopic composition. Therefore, this sample is left aside in the discussion below. The other two lamprophyre samples with potentially disturbed Sr isotope systematics (Fig. 4.3) do not show anomalous Li isotopic compositions (Table 4.1). The lamprophyres from the Sudetes have Li isotopic compositions (-5.5 to 1.9 ‰) and Li contents (6.6 to 35.7 ppm) that encompass the ranges of both Lusatia and the Erzgebirge (Fig. 4.5). For each region, there is weak correlation between concentration and isotopic composition of lithium (Fig. 4.5b).

Variations between δ^7Li values and Li contents of lamprophyres from the three areas are systematic, but not coherent. For lamprophyres from the Sudetes and Lusatia, δ^7Li values and Li contents are slightly negatively correlated (Fig. 4.5) and define a trend that points toward the signatures of altered oceanic crust (AOC) and MORB (Tomascak et al., 2008; Marshall et al., 2007), whereas for lamprophyres from the Erzgebirge, δ^7Li varies little and Li

contents are highly variable, largely overlapping with the range obtained for Saxo-Thuringian Paleaozoic shales (Figs. 4.5, 4.6, and 4.7). The contents and isotopic compositions of Li correlates with other fluid-mobile elements (e.g, Sr, Ba, Rb, and Cs), although these correlations are not very distinct and differ among the three regions (Figs. 4.7a and 4.7b). For instance, lamprophyres from the Erzgebirge have high Li/Cs values that are negatively correlated with δ^7Li, whereas lamprophyres from Lusatia have low Li/Cs values that are positively correlated with δ^7Li. Lamprophyres from the Sudetes have even lower Li/Cs values that are negatively correlated with δ^7Li (Fig. 4.7b). A similar, regionally controlled relation is also observed for Li/Rb *vs.* δ^7Li (Fig. 4.7a), although in this diagram the samples from the all three trends show negative correlations (Fig. 4.7a). Note, all three trends converge toward the field of average upper continental crust and do not point toward the composition of MORB or AOC (Fig. 4.7).

The Li isotopic compositions and concentrations of the lamprophyres show – similar to the fluid-mobile elements (e.g., Sr, Ba, Rb, and Cs) – systematic variations with fluid-immobile elements (e.g., Yb, Nb, MgO, and Dy; Figs. 4.5, 4.6, and 4.7). Lamprophyres from Lusatia show a narrow range of Li/Yb ratios (3.5 to 10) and these values are negatively correlated with δ^7Li. The δ^7Li and Li/Yb ranges of lamprophyres from Lusatia and the Sudetes include the fields for upper crust (UC) and lower crust (LC) (Teng et al., 2004) and the trends point toward the fields for MORB and AOC (Tomascak et al., 2008, Marshall et al., 2007). In contrast, lamprophyres from the Erzgebirge show a broad range of Li/Yb values (12 to 59) without systematic relation to δ^7Li (Fig. 4.5) and overlap with the field defined by Saxo-Thuringian Palaeozoic shales (Fig. 4.5c; Romer and Hahne, 2010; Romer et al., subm.). It should be noted that both the Li/Yb ratios and δ^7Li values of lamprophyres from the Sudetes partially overlap with the fields defined by lamprophyres from the Erzgebirge and Lusatia (Fig. 4.5c). There is a similar relation between δ^7Li values and Li/MgO, Li/Sc, Li/Ce, and Li/Nb element ratios (Figs. 4.6 and 4.7), whereby lamprophyres from the Erzgebirge and Lusatia define largely separated fields and trends, whereas those from the Sudetes overlap with the compositional ranges of both areas in some diagrams and define a field of their own in other diagrams (Figs. 4.6 and 4.7).

The differences in the geochemical compositions of lamprophyres from the Erzgebirge, Lusatia, and the Sudetes are not restricted to the isotopic composition and contents of Li, as well as element ratios involving Li, but are also present in other isotope systems and in element ratios not involving Li (Figs. 4.6 and 4.7).

Table 4.1. Whole-rock Sr, Nd, Pb, and Li isotope data and Li contents of late-Variscan calc-alkaline lamprophyres from the Erzgebirge, Lusatia, and the Sudetes (Germany and Poland).

Sample [a]		Age (Ma)	^{87}Sr [b] / ^{86}Sr	$^{87}Sr_{(T)}$ [c] / ^{86}Sr	^{143}Nd [b] / ^{144}Nd	$\varepsilon Nd_{(T)}$ [c]	^{206}Pb [d] / ^{204}Pb	^{207}Pb [d] / ^{204}Pb	^{208}Pb [d] / ^{204}Pb	^{206}Pb [e] / ^{204}Pb	^{207}Pb [e] / ^{204}Pb	^{208}Pb [e] / ^{204}Pb	Li (ppm)	δ^7Li [f] (‰)
Erzgebirge														
1	2380	330	0.709520±5	0.70679	0.512242±6	-3.4	18.969	15.636	39.802	17.86	15.58	37.11	80	-5.5
2	2205	330	0.709733±3	0.70602	0.512275±7	-2.7	19.305	15.657	39.974	18.45	15.61	38.61	32	-1. 7
3	2174	330	0.708151±4	0.70442	0.512262±5	-3.5	18.489	15.595	38.679	17.78	15.56	37.44	29	-2.1
4	2217	330	0.711849±5	0.70720	0.512256±3	-4.2	18.468	15.621	38.459	18.25	15.61	38.22	61	0.2
5	2071.16	330	0.710150±4	0.70370	0.512224±6	-3.8	19.174	15.639	40.410	18.17	15.59	37.74	57	-1.5
6	3379	330	0.708154±4	0.70719	0.512193±7	-4.8	18.558	15.604	38.655	18.47	15.60	38.39	38	-1.8
7	2358	330	0.712663±6	0.70624	0.512248±5	-3.6	18.593	15.602	38.461	17.68	15.55	37.94	141	-3.1
8	2454	330	0.708252±5	0.70700	0.512266±6	-3.1	18.677	15.664	39.276	18.07	15.63	38.28	53	-1.1
9	2223.2	330	0.724415±4	*0.69545*	0.512259±5	-3.7	18.605	15.604	38.616	18.02	15.57	37.82	147	-9.9
Lusatia														
10	DG12	330	0.711938±2	0.70775	0.512256±5	-4.6	18.334	15.591	38.991	18.03	15.58	38.17	12	1.8
11	DG13	330	0.711637±4	0.70797	0.512259±5	-4.6	18.47	15.602	39.218	18.04	15.58	38.13	12.9	n.d.
12	JS14	330	0.706119±5	0.70479	0.512608±4	1.9	18.368	15.568	38.541	17.80	15.54	37.83	17	-1.3
13	JS15	330	0.706116±6	0.70493	0.512651±3	2.5	18.379	15.566	38.548	17.80	15.54	37.79	16	-0.7
14	JS18	330	0.708408±5	0.70764	0.512356±6	-2.0	18.635	15.603	39.008	18.09	15.57	37.89	15.9	n.d.
15	SW19	330	0.707204±4	0.70496	0.512476±7	-0.1	18.860	15.594	39.160	17.85	15.54	37.71	16.2	-1.0
16	HB20	330	0.708766±4	0.70737	0.512299±6	-3.1	18.970	15.640	39.928	17.97	15.59	37.70	8.4	0.7
17	IS21	330	0.706213±5	0.70463	0.512514±5	0.7	18.534	15.606	38.904	18.10	15.58	38.01	15.3	-0.0
Sudetes														
18	Sw 327	330	0.708893±5	0.70322	0.512526±4	2.3							6.6	-2.0
19	Sw 468	330	0.709197±4	0.70587	0.512384±5	-0.7							8.3	1.9
20	Sw 394	330	0.708865±6	0.70613	0.51232±6	-2.1							25.1	-5.5
21	Sw 351	330	0.708296±7	0.70571	0.512381±6	-1.0							12.4	0.5
22	Sw 382	330	0.707080±4	0.70437	0.512486±5	0.9							35.7	-3.4
23	Sw 305	330	0.708179±6	0.70639	0.512371±4	-1.6							19.1	-3.8
24	Sw 465	330	0.726209±4	0.71114	0.512102±6	-8.1							15.8	-0.3
25	Sw 470	330	0.721759±5	0.71128	0.512075±5	-6.8							16.1	-1.0

a The Sr, Nd, and Pb isotopic compositions were analyzed at Deutsches GeoForschungsZentrum (GFZ), Potsdam.

Data sources for Sr, Nd, and Pb isotope data: Samples 1-9 this study; samples 10 to 17: Abdelfadil et al. (2012); samples 18 to 25: Awdankiewicz (2007).

Sample locations as indicated in Fig. 4.1:

Lusatia (all samples are spessartites): DG12, DG13 (Das Gericht), JS14, JS15, JS18 (Julienstein), SW19 (Strahwalde), HB20 (Hutzelberg), IS21 (Israel).

Erzgebirge; 2380 (minette from Schwarzbach), 2205 (kersanite from Rabenauer Grund, eastern Erzgebirge), 2174 (spessartite from Elde Krone near Tharandt

eastern Erzgebirge), 2217 (kersantite from Henneberg quarry, Thuringian Slate Belt); 2071.16 (minette from St. Michaelis, Brand-Erbisdorf, eastern Erzgebirge), 3379 (shoshonite from Zwickau-Reinsdorf), 2358 (minette from Henneberg quarry, Thuringian Slate Belt), 2454 (kersantite from Marlesreuth, Thuringian Slate Belt), 2223.2 (kersantite from Hirschfeld near Kirchberg, western Erzgebirge).

Sudetes: Sw 327 (richterite minette from Karpacz-Janowice Wlk); Sw 468 (kersantite from Gniewoszów Dyke Swarm), Sw 394 (spessartite from Karpacz-Janowice Wlk), Sw 351 (spessartite from Karpacz-Janowice Wlk), Sw 382 (micaceous lamprophyre from Intra-Sudetic Basin), Sw 305 (kersantite from Góry Sowie), Sw 465 (richterite minette from Gniewoszów Dyke Swarm), Sw 470 (minette from Gniewoszów Dyke Swarm).

b $^{87}Sr/^{86}Sr$ and $^{143}Nd/^{144}Nd$, normalized to $^{86}Sr/^{88}Sr = 0.1194$ and $^{146}Nd/^{144}Nd = 0.7219$, respectively, were obtained on a Thermo Triton and a Finnigan MAT262 multi-collector mass-spectrometer, respectively, using dynamic multi-collection. Analytical uncertainties are given at $2\sigma_m$ level. Repeated measurement of Sr reference material NBS 987 and Nd reference material La Jolla gave mean values of $^{87}Sr/^{86}Sr = 0.710249 \pm 0.000005$ (n = 20, 2σ) and $^{143}Nd/^{144}Nd = 0.511855 \pm 0.000006$ (n = 14; 2σ). Total procedural blanks for whole-rock samples during the measurement period were less than 50 pg for Sr and less than 30 pg for Nd. Value in italics: anomalously low recalculated $^{87}Sr/^{86}Sr$ due to secondary increase of Rb/Sr of the rock.

c $^{87}Sr/^{86}Sr_{(T)}$ and $\varepsilon Nd_{(T)}$ were calculated for the emplacement age using $\lambda^{87}Rb = 1.42E\text{-}11\ y^{-1}$ and $\lambda^{147}Sm = 6.54E\text{-}12\ y^{-1}$, $(^{147}Sm/^{144}Nd)^0_{CHUR} = 0.1967$, and $(^{143}Nd/^{144}Nd)^0_{CHUR} = 0.512638$, respectively, and the concentration data given in Table A1 in the Electronic Supplementary Material.

d Pb was separated and purified using ion-exchange chromatography as described in Romer et al. (2005). The Pb isotopic composition was determined on a Finnigan MAT262 multi-collector mass-spectrometer using static multi-collection. Based on the repeated measurement of lead reference-material NBS 981, instrumental mass discrimination was corrected with 0.1% / A.M.U. Accuracy of reported lead ratios is better than 0.1% at the 2σ level.

e Lead isotope data recalculated to the emplacement age using the contents of Pb, Th, and U (Table A1 in the Electronic Supplementary Material) and the constants recommended by IUGS (($\lambda^{232}Th = 4.9475E\text{-}11\ y^{-1}$, $\lambda^{235}U = 9.8485E\text{-}10\ y^{-1}$, and $\lambda^{238}U = 1.55125E\text{-}10\ y^{-1}$).

f Lithium contents were determined on aliquots of the sample solutions that were used for determination of the isotopic composition. The data of independently analyzed reference materials replicate within ±8% (2SD). Lithium isotopic compositions were determined by standard–sample–standard bracketing on a MC-ICP MS (Neptune) and are expressed in the delta notation relative to NIST8545 Li reference material. The uncertainties in δ^7Li are consistently lower than ±1‰ (2SD) for repeatedly analyzed sample solutions. For analytical details see Krienitz et al. (2012).

For instance, lamprophyres from the three areas define three distinct fields in the εNd_{330} *vs.* Nb/Dy diagram. The respective fields of lamprophyres from the Erzgebirge and Lusatia are well-defined and show only little overlap (Fig. 4.6a), whereas the field defined by lamprophyres from the Sudetes is more outspread and shows broad overlap with the fields of lamprophyres from the other areas. The lamprophyres from Lusatia define a linear trend with higher Nb/Dy at higher εNd_{330} values. Lamprophyres from the Erzgebirge define a trend that is distinct from the one for lamprophyres from Lusatia and that is parallel to the field of Saxo-Thuringian Palaeozoic shales, but offset toward higher εNd_{330} values (Fig. 4.6a). A similar grouping is also seen in the εNd_{330} *vs.* Ba/Th diagram, where lamprophyres from the Erzgebirge fall on a trend that is essentially defined by the variation in Ba/Th, those from Lusatia show essentially no variation in Ba/Th, and those from the Sudetes show higher Ba/Th at higher εNd_{330} values (Fig. 4.6d). Finally, it should be noted that variation in εNd_{330}, which reflect the contrasting importance of crustal material introduced by Variscan subduction into the mantle source of the lamprophyres, also is associated with variations in δ^7Li (Fig. 4.6c). Calc-alkaline lamprophyres from the Erzgebirge show a significant variation in δ^7Li at little variation of εNd_{330}, whereas those from Lusatia show higher δ^7Li at lower εNd_{330}, and those from the Sudetes encompass the entire compositional range of the other two areas.

4.5. Discussions

4.5.1 Spatial variation of δ^7Li

The geochemical composition of lamprophyres from the three regions Erzgebirge, Lusatia, and Sudetes define – in particular in diagrams involving the Li isotopic composition – separate trends in different geochemical diagrams. In part, these trends overlap with each other, in part they are scattered. The trends converge toward the fields for depleted mantle (represented by MORB and altered oceaninc crust) and the field for Saxo-Thuringian Palaeozoic shales (Figs. 4.5, 4.6, and 4.7). The fields for average upper and lower continental crust fall into the same field as the lamprophyres, but do not represent end members. The geochemical and isotopic signature of all lamprophyres can be explained as two component mixtures between an end member from the depleted mantle and a crustal end member of comparable geochemical compositional range as the Saxo-Thuringian Palaeozoic shales.

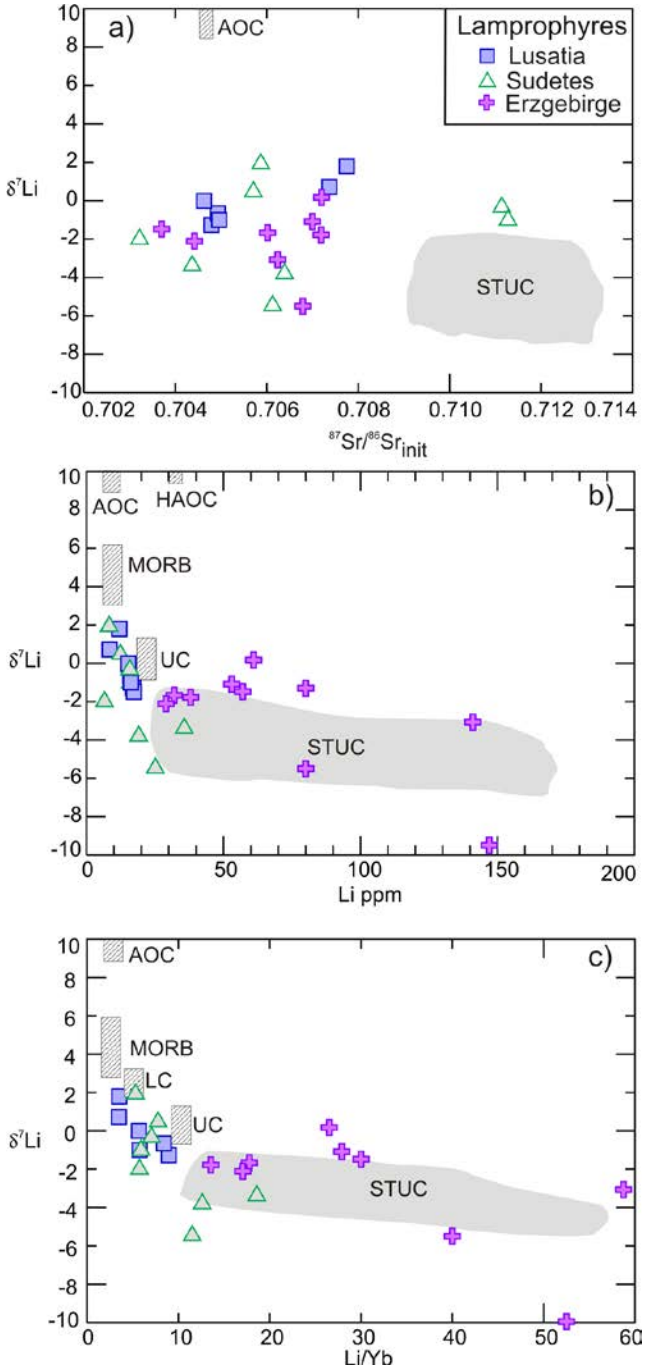

Fig. 4.5. Li isotopic composition of late Variscan calc-alkaline lamprophyres from the Erzgebirge, Lusatia, and the Sudetes. a) $^{87}Sr/^{86}Sr_{init}$ vs. δ^7Li; b) δ^7Li vs. Li; c) δ^7Li vs. Li/Yb of the studied lamprophyres. Data from Table 4.1. Reference fields: Saxo-Thuringian Upper Crust (STUC; Romer and Hahne, 2010), average compositions for lower continental crust (LC) and upper continental crust (UC) (Taylor and McLennan, 1995), Mid-Ocean Ridge Basalts (MORB; Hofmann, 1988), Altered Oceanic Crust and Highly Altered Oceanic Crust (AOC and HAOC; Staudigel et al., 1995). Li and δ^7Li of UC (Teng et al., 2004), LC (Teng et al., 2004), MORB (Tomascak et al., 2008), STUC (Romer et al., subm.), and AOC and HAOC (Marschall et al., 2007).

For such a two–component mixture, there are three different kinds of data arrangement that are best illustrated on behalf of the lamprophyres from the Erzgebirge. (i) Lamprophyre data fall between the data fields defined by the two end members. Examples for this kind of data pattern are the εNd_{330} *vs.* Nb/Dy and the εNd_{330} *vs.* $^{87}Sr/^{86}Sr_{330}$ diagrams (Figs. 4.3 and 4.6). This data pattern reflects that both end-members contribute in a variable, but similar extent to the element budget and isotope signature of the lamprophyres. (ii) Lamprophyre data fall entirely into the field defined by the Saxo-Thuringian Palaeozoic shales. Examples for this kind of data pattern are the δ^7Li *vs.* Li/Yb and the δ^7Li *vs.* Li diagram (Figs. 4.5b and 4.5c). In these diagrams the measured geochemical and isotopic composition is dominated by the crustal end-member, i.e., the Saxo-Thuringian Palaeozoic shales, whereas contributions from the mantle are subordinate only. (iii) Lamprophyre data define trends parallel to the field of the Saxo-Thuringian Palaeozoic shales, but are offset toward the mantle end member. Examples for this kind of data pattern are the εNd_{330} *vs.* Li/Yb and Ba/Th, respectively, diagrams and the $^{87}Sr/^{86}Sr_{330}$ *vs.* Li/Yb and Ba/Th, respectively, diagrams (Fig. 4.6). This third pattern is a combination of the first two, with the variation along one axis reflecting a mixture with similar contributions and the variation along the other axis being entirely dominated by one end member. Thus, these three different data pattern are caused by one single process and their contrasting appearance only reflects the contrasting concentration of the various elements in the two end members.

At low temperatures, alkaline and earth alkaline elements are highly mobile in fluids and are readily affected by secondary alteration. The coherent mixing trends for fluid-immobile and fluid-mobile elements with δ^7Li demonstrate that fluid-immobile and fluid-mobile elements did not behave differently after the mixing trends were established. As the trends between fluid-mobile and fluid-immobile elements reflect the mantle source, the correlation of εNd_{330} with δ^7Li also reflects a mantle signature. The same applies also for all other correlation trends. Thus, the coherent behavior of both fluid-immobile and fluid-mobile elements (cf. Figs. 4.6a, 4.7a, 4.7b) indicates that the observed δ^7Li isotopic variation is not related to secondary processes, but reflects the source of the lamprophyres, with the exception of above mentioned samples with anomalously low apparent $^{87}Sr/^{86}Sr_{330}$ isotopic compositions.

The compositional variation of the lamprophyres from Lusatia and the Sudetes also can be explained by such two components mixing between a mantle end member and a crustal end member. The separate trends of lamprophyres from these latter two regions, however, indicate that their crustal end member not necessarily is the same as the one for the

lamprophyres from the Erzgebirge. Instead, the smaller range in Li/Yb and Ba/Th in the lamprophyres indicates that the crustal end member has a narrower (and lower) range for these ratios (Figs. 4.5, 4.6, and 4.7). Similarly, the more prominent nature of the mantle end member in these lamprophyres indicates that the overall contribution of the metasomatic end member (derived from a crustal source) is smaller or that the contents of incompatible elements in this end member are smaller. Both, the narrower concentration range and the possibility of lower contents of incompatible elements in this end member do not exclude the possibility that the metasomatic component of the lamprophyre in Lusatia and the Sudetes is derived from a different source than the one in the lamprophyres of the Erzgebirge.

Tectonic models demonstrate that the different types of crust were subducted beneath the various segments of the present Bohemian Massif (Kroner and Romer, 2010, 2013). Thus, the regional difference in the metasomatic component in the postorogenic Variscan lamprophyres reflects the highly heterogeneous mantle beneath the Bohemian Massif, which is also obvious from the regional variability of mantle xenotliths (e.g., Medaris et al., 1995). The regional variations of the metasomatic component seem to correspond to areas of contrasting Variscan subduction history. The lamprophyres from the Erzgebirge have a metasomatized mantle end member that was modified by subducted Palaeozoic sedimentary rocks and its substratum of thinned continental crust. The variability of the lamprophyres in term of Li/Yb and Ba/Th may reflect the compositional variability of these sediments. The lamprophyres of Lusatia have the least pronounced involvement of a metasomatic component, which may reflect that subduction for most of the time was beneath the Laurussian plate and the mantle beneath Lusatia was affected only after a late subduction flip. The lamprophyres of the Sudetes broadly overlap with the lamprophyres from the Erzgebirge and Lusatia, possibly reflecting both the effect of subducted oceanic crust and Paleozoic sedimentary rocks deposited on this crust.

4.5.2 Transfer of Li from the slab to the mantle wedge

During low-temperature fluid–rock interaction the ratios Li/Yb and Ba/Th may vary significantly, as Li and Ba are mobile in fluids and Yb and Th are relatively immobile (Brenan et al., 1998; Elliott, 2003). At high temperatures and high pressures, as reached during subduction of crustal rocks in the lower crust and at mantle depth, differences between fluids and melts and their solubilities may have vanished (e.g., Tatsumi et al., 1986; Stalder et al., 1998). Thus, material loss from the subducting slab may not result in changes in the Li/Yb

and Ba/Th ratio. Large variations in the Li/Yb and Ba/Th ratio, as observed for the lamprophyres from the Erzgebirge, therefore were inherited from the subducted protoliths, as indicated by the comparable compositional range of Saxo-Thuringian Palaeozoic shales, or were acquired during the low-temperature stages of subduction, when metamorphism of sedimentary rocks release significant amounts of fluid.

The similarity of the crust-derived metasomatic end member with the Saxo-Thuringian Palaeozoic shales actually may indicate that the geochemical signature of the metasomatized mantle is inherited from the protolith, which in turn would imply that fluid-mediated changes of element ratios and fractionation of the Li isotopic composition during subduction – although possible – are not necessary to generate the geochemical fingerprint of the lamprophyres.

4.5.3 Lamprophyres and the Li budget of the mantle

Subduction introduces Li from the crust into the mantle. This has been documented by Li isotope studies on magmatic arcs (e.g., Leeman et al., 2004), mantle xenoliths (e.g., Nishio et al., 2004), and lamprophyres (e.g., Agostini et al., 2008). The Li isotope data from the lamprophyres of the Erzgebirge, Lusatia, and the Sudetes with their low δ^7Li values (Table 4.1) are in line with these earlier studies. These rocks sample and xenoliths sample the mantle wedge above the subducting slab. Thus, it is safe to say that crustal Li is present in the mantle wedge. It is, however, unclear which composition this Li has and whether Li also is introduced into the convecting mantle. The first open question is related to the isotopic variability of Li entering the subduction zone, altered oceanic crust having higher δ^7Li values and siliciclastic material derived from the continental crust having lower δ^7Li values than the mantle (e.g., Tomascak, 2004; Teng et al., 2004; Elliott et al., 2004), and the loss of Li and fractionation of the Li isotopic composition related to progressively higher grade metamorphism during subduction. Field studies indicate that some high-grade metamorphic rocks have very low δ^7Li values (e.g., Zack et al., 2003; Marschall et al., 2007) and experimental data and *ab initio* modeling demonstrate that Li lost to the fluid typically has higher δ^7Li values than the residual material, which during progressive Li loss should acquire increasingly lower δ^7Li values (e.g., Wunder et al., 2006, 2007, 2011; Kowalski and Jahn, 2011). Such fluid loss would result in increasingly lower δ^7Li values with increasing distance from the subduction zone (Agostini et al., 2008). The loss of Li during progressively higher grade of metamorphism, however, is controlled by the mineralogy of the rock, in particular

the stability of Li-rich phases, and whether Li released during the breakdown of one phase is sequestered by another phase (e.g., Marschall et al., 2006; Romer et al., subm.). Lithium loss controlled by mineral stability is likely to yield smaller effects on the Li isotopic composition than Rayleigh fractionation, which describes continuous loss with continuous re-equilibration. The second open question addresses the mass balance of Li in the deep part of the subduction zone, as it is unclear whether Li is mostly transferred to the mantle wedge above the subduction zone or there is Li transferred to the convecting mantle.

The lamprophyres from the Erzgebirge show the broadest compositional range and the most distinct crustal signatures (εNd_{330} and $^{87}Sr/^{86}Sr_{330}$ values) and relatively low δ^7Li values (Figs. 4.5, 4.6, and 4.7). The variation of δ^7Li with Ba/Th and Li, Yb encompasses the same ranges as Palaeozoic shales from the Saxo-Thuringian Zone (Figs. 4.5, 4.6, and 4.7). As equivalents of these Palaeozoic sedimentary and volcanosedimentary rocks have been subducted beneath the Bohemian Massif (e.g., Mingram, 1996, 1998; Kroner et al., 2007; Kroner and Romer, 2010, 2013) this geochemical signature has been brought to mantle depth during the Variscan orogeny. The close correspondence of the geochemical ranges of the sedimentary rocks and the lamprophyres of the Erzgebirge indicates that the metasomatic component in the mantle is dominated by material ultimately derived from the subducted sedimentary rocks. Some element ratios, for instance Li/Yb and Ba/Th, involve a soluble and a relatively insoluble element and show a very large range (Fig. 4.7). Because of the contrasting geochemical behavior of the involved elements, such a large range typically is interpreted to reflect the involvement of fluid-mediated rather than melt-mediated element mobility. The overlap of the fields for the Erzgebirge lamprophyres and the Palaeozoic sedimentary rocks demonstrates that the large range in Li/Yb and Ba/Th values does not have to be related to fluid-mediated element mobility within the subduction or at mantle depth, but may equally well represent a primary signature derived from the protoliths of the metasomatic component. In the particular case of the Palaeozoic Saxo-Thuringian sedimentary rocks, this fractionation of Li from Yb and Ba from Th is related to the weathering history of the source of the sediments and the mineralogical composition of the sediments (cf. Romer and Hahne, 2010; Romer et al., subm.). Finally, the overlap of the geochemical fingerprints of the lamprophyres from the Erzgebirge and the Palaeozoic Saxo-Thuringain sedimentary rocks indicates that progressive metamorphism during subduction not necessarily results in major Li loss and associated Li isotopic fractionation.

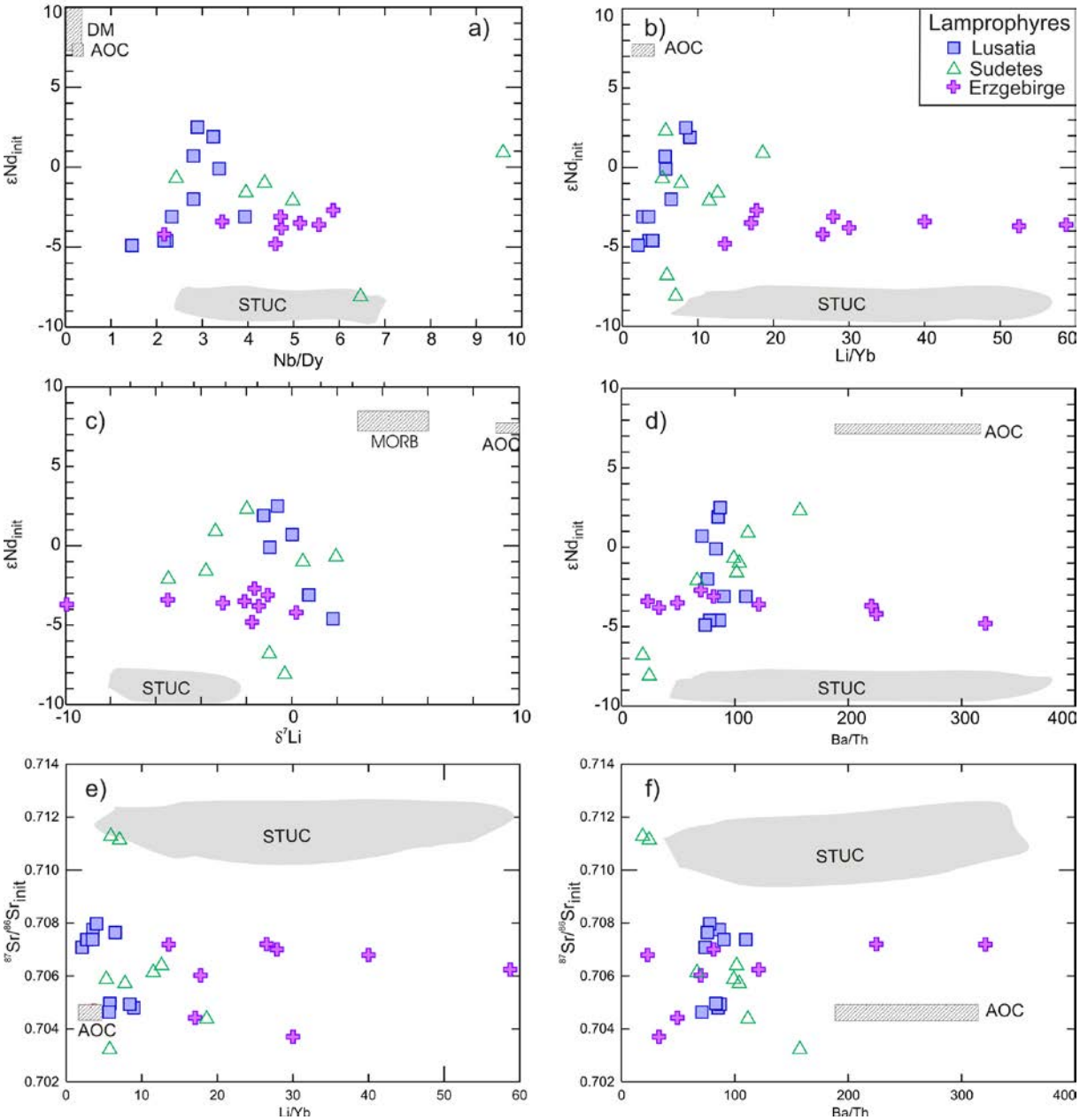

Fig. 4.6. Geochemical and isotopic signatures of late Variscan calc-alkaline lamprophyres from the Erzgebirge, Lusatia, and the Sudetes. a) Nb/Dy vs. εNd_{init}. b) εNd_{init} vs. Li/Yb. c) εNd_{init} vs. $\delta^7 Li$. d) εNd_{init} vs. Ba/Th. e) $^{87}Sr/^{86}Sr_{init}$ vs. Li/Yb; and f) $^{87}Sr/^{86}Sr_{init}$ vs. Ba/Th. Data sources: Kramer (1988), von Seckendorf et al. (2004), Awdankiewicz (2007), and Table 4.1. Reference fields as in Fig. 4.4; Depleted Mantle (DM; Workman and Hart, 2005). Note, the lamprophyres from the Erzgebirge, Lusatia, and the Sudetes define distinctly different fields.

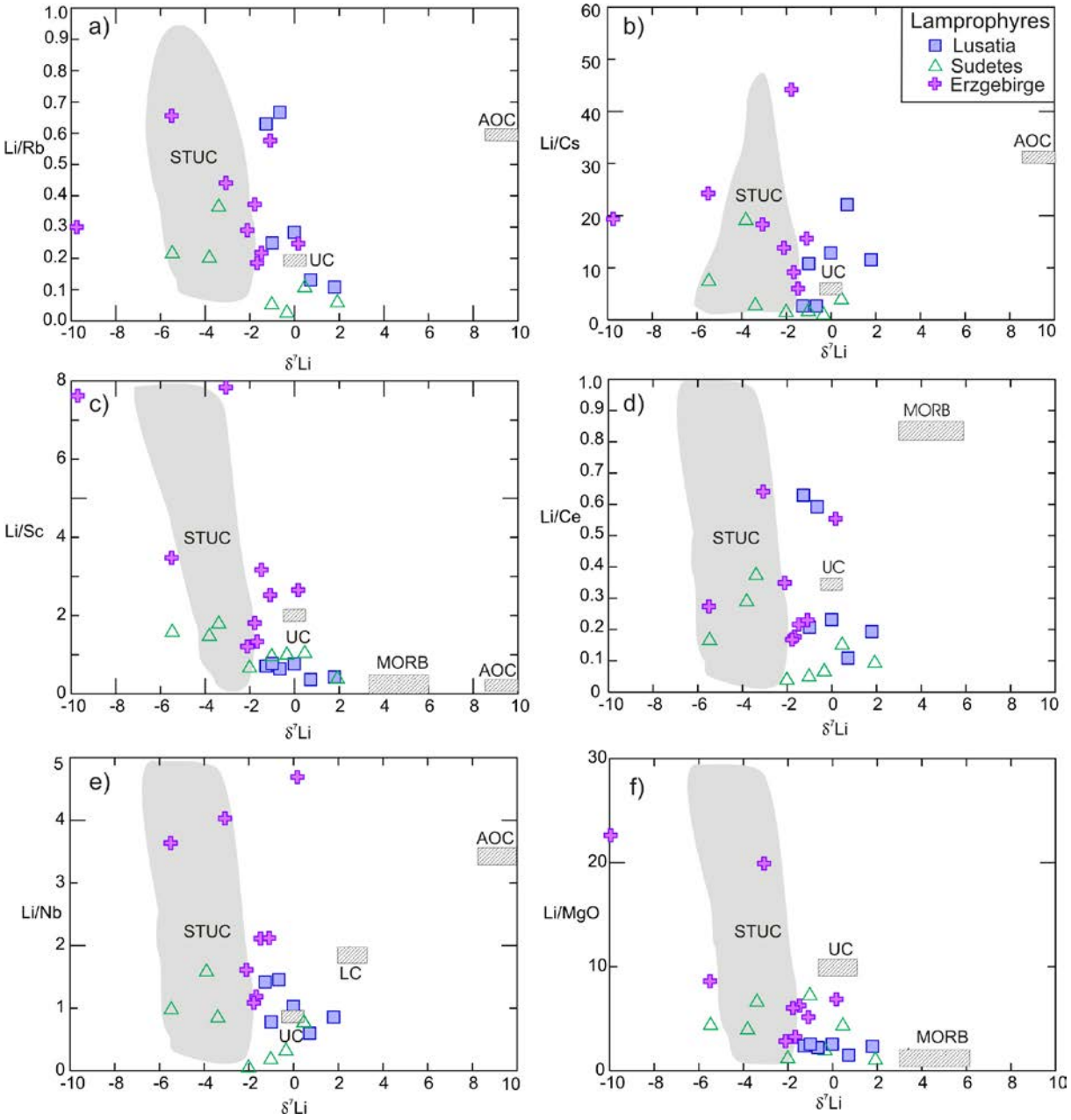

Fig. 4.7. Abundances and isotopic compositions a) Li/Rb vs. δ^7Li; b) Li/Cs vs. δ^7Li; c) Li/Sc vs. δ^7Li; d) Li/Ce vs. δ^7Li; e) Li/Nb vs. δ^7Li; f) Li/MgO vs. δ^7Li of the studied lamprophyres. Data sources are as in figures 4.4 and 4.5.

Subduction modifies the convecting mantle and gives rise to the isotopic and geochemical fingerprints of the EMI and EMII enriched mantle reservoirs. If significant portions of Li are brought into the convective mantle and this Li is isotopically distinct from mantle Li, mantle-derived melt with pronounced EMI and EMII Sr and Nd isotopic fingerprints also should have Li contents and isotopic composition that differ from those of the depleted mantle. As Oceanic Island Basalts (OIB) with a pronounced EMI and EMII

signature do not show Li isotopic signature that differ from MORB rocks with isotopic rocks from the convective mantle, it is quite possible that subducted Li is not introduced to a significant extent into the convecting mantle, but is largely transferred into the mantle wedge above the subducting plate (for discussion see Krienitz et al., 2012). Subducted Li would remain in the mantle wedge and subcontinental lithospheric mantle and contribute to the Li isotopic of rocks derived from the subcontinental mantle. This in turn implies, that not only Variscan lamprophyres, but also younger magmatism derived from the metasomatiszed subcontinental mantle – such as the Tertiary alkaline basalts of the Central European Volcanic Province – is likely to carry the Li isotopic signature introduced by the Variscan orogeny into the mantle, in analogy to sublithospheric mantle worldwide (see also Ionov and Seitz, 2008; Su et al., 2012; Magna et al., 2013).

4.6 Conclusions

A systematic difference of Li isotopic and content was observed between calc alkaline lamprophyres from Lusatia (1.8 to -1.3 ‰; 8.4 to 17 ppm), Erzgebirge (0.2 to -5.5 ‰; 29 to 141 ppm) and the Sudetes (+1.92 to -5.47 ‰; 6.6 to 36 ppm). In analogue, there are strong systematic variations of Li content and Li isotopic composition with Sr-Nd-Pb isotope composition of calc-alkaline lamprophyres from Lusatia and Erzgebirge, indicating that the Li elemental and isotopic composition reflect mantle source signature. This is also confirmed by strong variations of Li/Yb, Ba/Th, Li/Rb, Nb/Dy ratios, and other LILE with Li- Nd isotopic composition. In addition, the coherent behavior of fluid-immobile and fluid-mobile elements with Li-Nd-Sr isotope composition indicates that the observed variation of δ^7Li is not related to secondary processes, but reflects the source of the lamprophyres. Thus the mantle source of the calc-alkaline lamprophyres from the Erzgebirge, Lusatia, and the Sudetes are quite different. The compositional variations in the investigated lamprophyres are attributed to different subducting material beneath during Variscan orogeny. This study indicates that the δ^7Li budget from the subducted components to the mantle wedge is not strongly modified to a significant extent during subduction.

Acknowledgements. We gratefully acknowledge the extensive help of B. Hübner with the separation of Li. We thank R. Naumann, H. Rothe, S. Tonn, and K. Hahne for the geochemical data. K.M.A. gratefully thanks W. Kramer, R. Kryza, and M. Awdankiewicz for guidance in the field.

5. Conclusions

This study contributes to a better understanding of the local scale mantle signature and to differences between mantle signatures underneath different Variscan Domains i.e., Erzgebirge, Lusatia, and Sudetes. Geochemical signatures correlate with contrast tectonic evolutions and with contrast in the composition of material subducted during Variscan orogeny.

The pre-Variscan gabbros (c. 400 Ma) from Lusatia have trace element ratios and content characteristic for the involvement of crustal material in their mantle source. The crustal Pb isotopic compositions and the high initial $^{87}Sr/^{86}Sr$ values of the gabbros at essentially constant initial $^{143}Nd/^{144}Nd$ values indicate fluid-mediated uncoupling of Pb and Sr from Nd. The clinopyroxene composition of gabbros indicates crystallization temperatures that range from 1000°C to ~1200°C and tectonic setting along the line separating the orogenic and non-orogenic fields.

The Lusatian gabbros have distinct initial Sr and Nd isotopic composition in contrast to the c. 400 Ma old gabbros from the adjacent Sudetes that show N-MORB affinity as indicated from their initial Nd and Sr isotopic composition and considered to be a part of an ophiolite complex.

The calc-alkaline lamprophyres from Lusatia are emplaced at c. 330 Ma as indicated from their $^{40}Ar–^{39}Ar$ hornblende ages. This age is consistent with the emplacement age of calc-alkaline lamprophyres from adjacent areas and other parts of Variscan Europe, e.g., the Sudetes, the Black Forest, the Erzgebirge, and the French Massif Central.

The late-Variscan calc-alkaline lamprophyres from Lusatia are mantle derived rocks as reflected from their high MgO, Cr, and Ni contents. These rocks, however, have distinctly higher LILE, $^{87}Sr/^{86}Sr$, and $^{206}Pb/^{204}Pb$ ratios, and lower $^{143}Nd/^{144}Nd$ ratios relative to pre-Variscan gabbros. The clinopyroxene composition of these rocks indicates crystallization temperatures that range from 900°C to ~1200°C and subduction-related tectonic setting.

The late-Variscan calc-alkaline lamprophyres and pre-Variscan gabbros from Lusatia have similar Cr, MgO, Mg#, the trace-element pattern and Th/La, Sm/La, and Ce/Pb ratios indicates that these rocks have been extracted from a similar mantle source.

The effect of assimilation and fractional crystallization during ascending as a source for the mantle enrichment beneath Lusatia may be limited and cannot account for the observed variation between gabbros and late Variscan calc-alkaline lamprophyres from Lusatia.

The variable enrichment extent between pre-Variscan gabbros and late-Variscan calc-alkaline lamprophyre has been explained as following: Melting of the pre-Variscan mantle that has been metasomatised during Cadomian subduction to produce the gabbros will result in preferential melting of the metasomatised domains leaving behind a mantle that is depleted in incompatible elements. As the metasomatized parts of the mantle have been consumed during the melting of the gabbro source, renewing small-scale melting of this mantle would not produce a melt that is highly enriched in incompatible elements (similar to late-Variscan calc-alkaline lamprophyre). Accordingly, the late-Variscan lamprophyres require a second enrichment of the mantle after the extraction of gabbroic melts (during Variscan) and imply a repeatedly enriched mantle source. Thus the pre-Variscan mantle beneath Lusatia was modified by Cadomian (c. 600–570 Ma) and the metasomatic signature of this mantle was inherited by intra-plate magmatism at c. 400 Ma (gabbros) whereas the late-Variscan mantle was modified by Variscan and sampled by late-Variscan calc-alkaline lamprophyre.

The calc-alkaline lamprophyres from Lusatia show an extent of crustal enrichment differs from lamprophyres in different domains in Central Europe. The different extent of enrichment between late-Variscan lamprophyres in different domains in Central Europe reflects the regionally heterogeneous effect of the Variscan orogeny.

Combination of Li-Sr-Pb-Nd isotopic composition with lithium content of the late-Variscan calc-alkaline lamprophyres from the Erzgebirge, Lusatia, and the Sudetes indicate a systematic difference between the investigated rocks.

The systematic variations of Li content and Li isotopic composition with Sr-Nd-Pb isotope composition indicate that the Li elemental and isotopic composition reflects mantle source signature. The fluid-mobile and fluid-immobile element ratios define different trends following mostly the geographic distribution of these lamprophyres which together with the spatial differences in Sr, Nd, and Pb isotopic compositions confirm different mantle sources.

The effect of low temperature posteruption and weathering processes as a source of variability of Li isotopic and content between the investigated rocks is negligible. Thus the Li isotopic and content combined with Sr-Nb-Pb isotopic composition reflects different mantle sources.

The compositional variations in the investigated lamprophyres from the Erzgebirge, Lusatia, and the Sudetes are attributed to different subducting material during Variscan orogeny as well as different modes of its transportation/metasomatism (crust via melt, fluid). The δ^7Li and Li contents of the calc-alkaline lamprophyre from Lusatia and Erzgebirge are

consistent with recycling of oceanic crust and sediment to the mantle wedge, respectively, whereas the lamprophyres from Sudetes define mixed end member.

Regarding variation of Variscan mantle signatures in time on a local scale (in Lusatia), we used calc-alkaline lamprophyres that trace the late-Variscan mantle signature and post-Variscan ultramafic lamprophyre and alkaline basalt that trace the post-Variscan mantle signature. It is found that that the calc-alkaline lamprophyres and ultramafic lamprophyres and alkaline basaltic rocks were derived from same mantle source and the metasomatic components in these rocks are related to the Variscan orogeny. These rocks have similar trace-element signatures as well as isotopic compositions indicating that melts have been repeatedly extracted from the same metasomatized mantle source. As melt extraction in Lusatia is coeval with geochemically corresponding magmatism in other parts of Europe, melting of metasomatized mantle may be directly related to large-scale reorganization of the stress field and the partial melting of the metasomatized mantle source due to crustal thinning and mantle upwelling.

6. Appendix –Analytical methods

All the analytical work has been done at the GeoForschungsZentrum (GFZ) Potsdam except the Ar-Ar analyses at university of Potsdam. The complete results of analyses are presented within this thesis in Tables 2.1, 2.2, 2.3, 2.4, 3.1, 3.2, 3.4, and 3.5.

Microprobe analyses

The chemical composition of minerals was performed using a CAMECA SX100 electron microprobe operated at 15 kV accelerating voltage, a beam current of 20 nA, and a variable beam diameter of 1 to 15 μm. Peak counting times were 10-20 s for major and 30 s for minor elements; backgrounds were counted for 5-15 s. Data reduction used the PAP correction procedure implemented in the CAMECA software.

Ar-Ar analysis

Amphibole Ar-Ar dating was performed at the geochronology laboratory of the University of Potsdam. Amphibole was separated from the 250 to 200 μm fraction and purified by hand-picking under a binocular microscope. The samples were irradiated at the Geesthacht Neutron Facility (GeNF), GKSS Research Center, Germany, for 96 h with a fast neutron flux of 1x1012 n/cm^2/s. As monitors for the neutron flux and the production of Ar from Ca and K, we used Fish Canyon tuff sanidine and crystals of CaF_2 and K_2SO_4, respectively. For the Fish Canyon tuff sanidine, we used an age of 27.5 Ma (Uto et al., 1997; Ishizuka, 1988; Ishizuka et al., 2002), which agrees with the one obtained by Lanphere and Baadsgaard (2001). The samples were analyzed by stepwise heating until total fusion, using a 50W CO_2 laser operated at a wavelength of 10.6 μm involved in the Dual Wave laser ablation system. The extracted gas was purified using cold traps and Zr-Al SEALS alloy getters and analyzed using a Micromass 5400 noble gas mass spectrometer with high sensitivity and low background. System blanks were measured after every three samples. The measured isotopic ratios were corrected for blank measurements, mass discrimination, interference of Ar isotopes derived from Ca and K by irradiation, and post irradiation decay of ^{37}Ar and ^{39}Ar. The final age calculation and errors follow the procedure of Uto et al (1997). The following three criteria were used to define a plateau for the dated samples; (1) The plateau has to include a series of adjacent steps that together comprise more than 50% of the released ^{39}Ar, (2) the ages of the steps should agree within two sigma (2σ) error, (3) each degassing step included in the plateau should have more than 3 % of the total ^{39}Ar released.

Whole rock geochemistry

Whole-rock major element composition and selected trace elements (Zn, Zr, Ba, Cr, Nb, Ni, Sr and V) were measured with X-ray fluorescence spectrometry at the GeoForschungsZentrum Potsdam. H_2O and CO_2 were determined by high-temperature catalytic combustion with a Vario EL III instrument. Additional trace elements (Nb, Mo, Cd, Cs, Ti, Pb, Th, U, Sc, Co, Cu, Ga, Sb, and Sn) were analyzed using ELEMENT 2XR ICP-MS. Sample powders were decomposed using HF, aqua regia, and $HClO_4$. The dissolved samples were dried and redissolved in HNO_3 and then diluted with H_2O for analysis. Rare earth elements (REE) and Y were analyzed with inductively coupled plasma-atomic emission spectroscopy (ICP-AES) following the procedure of Zuleger and Erzinger (1988). These samples were decomposed using Na_2O_2 fusion and the REE were separated and concentrated chromatographically using ion-exchange methods.

Sr-Nd-Pb-Li isotope analysis

Li-Sr-Nd-Pb isotope compositions of the samples were determined at Deutsches GeoForschung Zentrum GFZ, Potsdam (Germany). For the lithium isotope, between 18 and 45 mg of the sample material were digested in a mixture of concentrated hydrofluoric and nitric acid. The digested samples were dried and taken up in a mixture of 6ml 1N nitric acid and 3ml methanol. For each series of Li separations, Li standards and procedural blanks were run as additional samples. Li was principally separated and purified using the ion exchange techniques described by Tomascak et al. (1999) and Jeffcoate et al. (2004). Li eluates with considerable Na contents were processed on a separate set of separation columns using 0.5N/1N HCL:80% methanol (Jeffcoate et al., 2004). To check for possible loss of lithium during the separation procedures, which would cause isotopic fractionation (Tomascak et al., 1999), we collected 12 ml pre-Li eluate and 5 ml post-Li eluate. The total loss of the lithium was less than 0.1% of the total Li in the samples and thus had an insignificant influence on the lithium isotopic composition in the samples. The estimated procedural blanks ranged from 10 to 280 pg Li and had insignificant effect on the lithium isotopic composition of the samples.

Li-isotope ratios were determined using a Thermo Finnigan NEPTUNE MC ICP-MS. Sample preparation, rock standard, operating conditions, and measurement procedures are identical to those reported by Wunder et al. (2006, 2007). All the samples were measured repeatedly in the standard/sample/standard mode. Both samples and standard were dissolved in 2% HNO_3 and closely adjusted to 25 ppb Li (±5%). Lithium isotopic compositions are expressed as δ^7Li ($\delta^7Li=\{[(^7Li/^6Li)_{sample}/(^7Li/^6Li)_{standard}] - 1\}*1000$) relative to NIST SRM

8545 (L-SVEC) lithium carbonate standard. Repeated isotopic analysis of various reference materials give an external reproducibility of better than 1 per mil at the 2σ level.

For Nd-Sr-Pb isotope, the whole-rock sample powders were digested with concentrated HF for four days at 160° C on a hot plate. In order to transfer fluorides into nitrates, the dissolved samples were dried and then leached in HNO3 to transfer fluorides into nitrates and dried again. The dried samples were taken up in 6N HCl overnight and splitted for Pb and Sr-Nd ion-chromatographic separation. Sr and Nd were separated and purified using cation-exchange chromatography procedures. The Sr and Nd isotope ratio measurements were carried out on a Triton and a Finnigan MAT262 multi-collector mass-spectrometer, respectively, operated in dynamic multicollection mode. Isotopic composition values of Sr and Nd were corrected for mass fractionation using $^{86}Sr/^{88}Sr=0.1194$ and $^{146}Nd/^{144}Nd=0.7219$, respectively. Repeated measurement of the standards NBS 987 for Sr and La Jolla for Nd yielded mean values of $^{87}Sr/^{86}Sr = 0.710249 \pm 0.000005$ (n = 20) and $^{143}Nd/^{144}Nd = 0.511855 \pm 0.000006$ (n = 14; 2σ). Total procedural blanks for whole-rock samples during the measurement period were less than 50 pg for Sr and less than 30 pg for Nd. Lead from whole-rock samples was separated using the HCl-HBr ion exchange technique reported by Romer et al. (2005). On single Re-filaments, Pb was loaded with H_3PO_4 and silica-gel. The isotopic ratios of lead were analyzed at 1200-1250°C on a Finnigan Mat262 TIMS multi-collector mass spectrometer using static multicollection. Based on the repeated measurement of lead reference-material NBS 981, the instrumental mass fractionation was corrected with 0.1% per a.m.u. Uncertainty of reported lead ratios is better than 0.1% at the 2σ level.

7. Bibliography

Abdelfadil, Kh., Romer, R.L., Seifert, Th., Lobst, R., 2010. Geochemistry and petrology of alkaline basalt and ultramafic lamprophyre dikes from Lusatia (Lausitz), Germany. Mineralogia Special Papers 37, 17-18.

Abdelfadil, Kh., Romer, R.L., Seifert, Th., Lobst, R., 2012. Calc-alkaline lamprophyres from Lusatia (Germany) – evidence for a repeatedly enriched mantle source. Chemical Geology, in press. http://dx.doi.org/10.1016/j.chemgeo.2012.10.023.

Agostini, S., Ryan, J. G., Tonarini, S., Innocenti, F., 2008. Drying and dying of a subducted slab: Coupled Li and B isotope variations inWestern Anatolia Cenozoic Volcanism. Earth and Planetary Science Letters 272, 139-147.

Anthes, G., Reischmann, T., 2001. Timing of granitoid magmatism in the eastern Mid German Crystalline Rise. Journal of Geodynamics 31, 119-143.

Aoki, K., Kushiro, I., 1968. Some clinopyroxenes from ultramafic inclusions in Dreiser Weiher, Eifel. Contribution to Mineralogy and Petrology 18, 326-337

Arai, S., 1984. Pressure–temperature dependent compositional variation of phlogopitic micas in upper mantle peridotites. Contributions to Mineralogy and Petrology 87, 260-264.

Arai, S., 1986. K/Na variation in phlogopite and amphibole of upper mantle peridotites due to fractionation of the metasomatising fluids. Journal of Geology 94, 436-444.

Awdankiewicz, M., 2007. Late Palaeozoic lamprophyres and associated mafic subvolcanic rocks of the Sudetes (SW Poland): petrology, geochemistry and petrogenesis. Geologica Sudetica 39, 11-97.

Azambre, B., Rossy, M., Albarède F., 1992. Petrology of the alkaline magmatism from the Cretaceous North-Pyrenean Rift Zone (France and Spain). European Journal of Mineralogy 4, 813-834.

Bedard, J.H., 1985. The opening of the Atlantic, the Mesozoic New England igneous province, and mechanisms of continental breakup. Tectonophysics, 113, 209-232.

Bedard, J.H., 1994. Mesozoic east North American alkaline magmatism: Part 1. Evolution of Monteregian lamprophyres, Québec, Canada. Geochimica et Cosmochimica Acta 58, 95-112.

Brenan, J.M., Ryerson, F.J., Shaw, H.F., 1998. The role of aqueous fluids in the slab-to-mantle transfer of boron, beryllium, and lithium during subduction: Experiments and models. Geochimica et Cosmochimica Acta 62, 3337-3347.

Buzzi, L., Gaggero, L., Grozdanov, L., Yanev, S., Slejo, F., 2010. High-Mf potassic rocks in the Balkan segment of the Variscan Belt (Bulgaria); implications for the genesis of orogenic lamproite magmas. Geological Magazine 147, 434-450.

Chan, L.H., Edmond, J.M., Thompson, G., Gillis, K., 1992. Lithium isotopic composition of submarine basalts – implications for the lithium cycle in the oceans. Earth and Planetary Science Letters 108, 151-160.

Chan, L.H., Alt, J.C., Teagle, D.A.H., 2002. Lithium and lithium isotope profiles through the upper oceanic crust: a study of seawater-basalt exchange at ODP Sites 504B and 896A. Earth and Planetary Science Letters 201, 187-201.

Chauvel, C., Jahn, B.M., 1984. Nd–Sr isotope and REE geochemistry of alkali basalts from the Massif Central, France. Geochimica et Cosmochimica Acta 48, 93-110.

Condie, K.C., 1990. Growth and accretion of continental crust: Inferences based on Laurentia. Chemical Geology 93, 183-94.

Conticelli, S., Guarnieri, L., Farinelli, A., Mattei, M., Avanzinelli, R., Bianchini, G., Boari, E., Tommasini, S., Tiepolo, M., Prelevic, D., Venturelli, G., 2009. Trace elements and Sr-Nd-Pb isotopes of K-rich, shoshonitic, and calc-alkaline magmatism of the Western Mediterranean Region: genesis of ultrapotassic to calc-alkaline magmatic associations in a post-collisional geodynamic setting. Lithos, 107, 68-92.

Cribb, J.W., Barton, M., 1996. Geochemical effects of decoupled fractional crystallization and crustal assimilation. Lithos 37, 293-307.

Currie, K.L., Williams, P.R., 1993. An Archean calc-alkaline lamprophyre suite, northeastern Yilgarn block, Western Australia. Lithos 31, 33-50.

DePaolo, D.J., 1981. Trace element and isotopic effects of combined wallrock assimilation and fractional crystallization. Earth and Planetary Science Letters 53, 189-202.

Dewey, J.F., Windley, B.F., 1988. Palaeocene-Oligocene tectonics of NW Europe. In: Morton, A.C., Parson, L.M. (Eds.), Early Tertiary Volcanism and the Opening of the NE Atlantic. Geological Society, London, Special Publication 39, 25-31.

Dixon, J.E., Fitton, J.G., Frost, R.T.C., 1981. The tectonic significance of post-Carboniferous igneous activity in the North Sea Basin. In: Illing, L.V., Hobson, G.D. (eds): Petroleum Geology of the Continental Shelf of NW Europe. Heyden. London, 121-137.

Dobosi, G., Schultz-Gütler, R., Kurat, G., Kracher, A., 1991. Pyroxene chemistry and evolution of alkali basaltic rocks from Burgenland and Styria, Austria. Mineralogy and Petrology 43, 275-292

Dostal, J., Owen, J.V., 1998. Cretaceous alkaline lamprophyres from northeastern Czech Republic: geochemistry and petrogenesis. Geologische Rundschau 87, 67-77.

Eidam, J., Hammer, J., Korich, D., Bielicki, K.-H. 1995. Amphibole-bearing granites in the Lusatian Anticlinal Zone: Variscan I-type magmatism at the margin of the Bohemian Massif. Neues Jahrbuch fur Mineralogie. Abhandlungen 168, 259-281.

Eidam, J., Krauss, M., Hammer, J., Korich, D. 2001. Zur Ausbildung und zum Alter der zonalen kataklastisch-mylonitischen Deformation im Lausitzer Granodioritkomplex. Zeitschrift für Geologische Wissenschaften 29, 471-481.

Elliott, T., 2003. Tracers of the Slab, in Eiler, J. (ed.), Inside the Subduction Factory: Washington DC, American Geophysical Union, p. 23-45.

Elliott, T., Jeffcoate, A., Bouman, C. 2004. The terrestrial Li isotope cycle: light-weight constraints on mantle convection. Earth and Planetary Science Letters 220, 231-245.

Faerseth, R., Macintyre, R., Naterstad, J., 1976. Mesozoic alkaline dykes in the Sunnhordland region, western Norway: ages, geochemistry and regional significance. Lithos 9, 331-345.

Feng, G., Weiming, F., Yuejun, W., Ming, Z., 2004. Origin of the early Cretaceous cal-alkaline lamprophyres from the Sulu orogen ineastern China: implications for enrichments process beneath continental collision belts. Lithos 78, 291-305.

Finger, F., Roberts, M.B., Haunschmid, B., Schermaier, A., Steyrer, H.B., 1997. Variscan granitoids of central Europe: their typology, potential sources and tectonothermal relations. Petrology and Mineralogy 61, 67-96.

Förster, H-J., Romer, R.L., 2010. Carboniferous Magmatism, In: Linnemann, U., (Eds.), Pre-Mesozoic Geology of Saxo-Thuringia: From the Cadomian Active Margin to the Variscan Orogen, Schweizerbart, pp. 287-308.

Foley, S.F., 1992. Vein-plus-wall-rock melting mechanisms in the lithosphere and the origin of potassic alkaline magmas. Lithos 28, 435-453.

Foley, S.F., Venturelli, G., Green, D.H., Toscani, L., 1987. The ultrapotassic rocks: characteristics, classification and constraints for petrogenetic models. Earth-Science Reviews 24, 81-134.

Franke, W., 2000. The mid-European segment of the Variscides: tectonostratigraphic units, terrane boundaries and plate tectonic evolution. In: Franke, W., Haak, V., Oncken, O. and Tanner, D. (Eds.). Orogenic Processes: Quantification and modelling in the Variscan belt. Geological Society London Special Publications 179, 35–61.

Frey, F.A., Green, D.H., Roy, S.D., 1978. Integrated models of basalt petrogenesis. A Study of quartz tholeiites to olivine melilities from south eastern Australia utilizing geochemical and experimental petrological data. Journal of Petrology 19, 463-513.

Furman, T., Graham D., 1999. Erosion of lithospheric mantle beneath the east African rift system; geochemical evidence from the Kivu volcanic province. Lithos 48, 237-262.

Gerstenberger, H., Haase, G., 1997. A highly effective emitter substance for mass spectrometric Pb isotope ratio determinations. Chemical Geology 136, 309-312.

Golonka, J., 2004. Plate tectonic evolution of the southern margin of Eurasia in the Mesozoic and Cenozoic. Tectonophysics 381, 235-273.

Haase, K.M., Renno, A.D., 2008. Variation of magma generation and mantle sources during continental rifting observed in Cenozoic lavas from the Eger Rift, Central Europe. Chemical Geology 257, 192-202.

Halama, R., McDonough, W. F., Rudnick, R. L., Keller, J., Klaudius, J., 2007. The Li isotopic composition of Oldoinyo Lengai: Nature of the mantle sources and lack of isotopic fractionation during carbonatite petrogenesis. Earth and Planetary Science Letters 254, 77-89.

Halama, R., McDonough, W. F., Rudnick, R. L., Bell, K., 2008. Tracking the Li isotopic evolution of the mantle sources using carbonatites. Earth and Planetary Science Letters 265, 726-742.

Harangi, S., 1994. Geochemistry and petrogenesis of the Early Cretaceous continental rift-type volcanic rocks of the Mecsek Mountains, South Hungary. Lithos 33, 303-321.

Harangi, S., Tonarini, S., Vaselli, O., Manetti, P., 2003. Geochemistry and petrogenesis of the Early Cretaceous alkaline igneous rocks in Central Europe: implications for a long-lived EAR-type mantle component beneath Europe. Acta Geologica Hungarica 46, 77-44.

Harrison, R.K., Snelling, N.J., Merriman, R.J., Morgan, G.E., Goode, A.J, 1977. The Wolf Rock, Cornwall: new chemical, isotopic age and palaeomagnetic data." Geological Magazine 114, 249-264.

Hawthorne, FC., Oberti, R., 2007. Amphiboles: Crystal chemistry. Reviws in Mineralogy and Geochemistry 67, 1-54.

Hauri, E.H., Hart, S.R., 1997. Rhenium abundances and systematics in oceanic basalts. Chemical Geology 139, 185-205.

Hauser, N., Matteini, M., Omarini, H.R., Pimentel, M.M., 2010. Constraints on metasomatized mantle under Central South America: evidence from Jurassic alkaline

lamprophyre dykes from the Eastern Cordillera, NM Argentina. Mineralogy and Petrology 100, 153-184.

Hegner, E., Kolbl-Ebert, M., Loeschke, J., 1998. Post collisional Variscan lamprophyres (Black Forest, Germany). $^{40}Ar/^{39}Ar$ phlogopite dating, Nd, Pb, Sr isotope and trace element characteristics. Lithos 45, 395-411.

Heinrich, C., 1993. Hydrothermalmetamorphose und Geoschemie der Lausitzer Gabbronorit-Gabbro-Diorit Serie. Dissertation, Karlsruhe; 190 S.

Hess, P.C., 1992. Phase equilibria constraints on the origin of ocean floor basalts. In: Morgan, J.P., Blackman, D.K., Sinton, J.M. (eds), Mantle flow and melt generation at mid-ocean ridges. Geophysical Monograph, American Geophysical Union 71, 67-102.

Heuse, T., Blumenstengel, H., Elicki, O., Geyer, G., Hansch, W., Maletz, J., Sarmiento, G.N., Weyer, D., 2010. Biostratigraphy- The faunal province of the southern margin of the Rheic ocean. In: Linnemann, U., Romer, R.L. (Eds.), Pre-Mesozoic Geology of Saxo-Thuringia. From the Cadomian Active Margin to the Variscan Orogen Schweizerbart, Stuttgart, pp. 99-170.

Hoch, M., Rehkamper, M., Tobschall, H.J., 2001. Sr, Nd, Pb and O isotopes of minettes from Schirmacher Oasis, East Antarctica. A case of mantle metasomatism involving subducted continental material. Journal of Petrology 42, 1387-1400.

Hofmann A.W., 1986. Nb in Hawaiian magmas: constraints on source composition and evolution. Chemical Geology 57, 17-30.

Hofmann, A.W., 1988. Chemical Differentiation of the Earth: the relationship between mantle, continental crust, and oceanic crust. Earth Planetary Science Letters 90, 297-314.

Ionov, D.A., Bodinier, J.L., Mukasa, S.B., Zanetti, A., 2002. Mechanisms and sources of mantle metasomatism: major and trace element compositions of peridotite xenoliths from Spitsbergen in the context of numerical modeling. Journal of Petrology 43, 2219-2259.

Ionov, D.A., Seitz, H.M., 2008. Lithium abundances and isotopic compositions in mantle xenoliths from subduction and intra-plate settings: mantle sources vs. eruption histories. Earth and Planetary Science Letters 266, 316-331.

Irvine, N., Baragar, W.R.A., 1971. A guide to chemical classification of the common volcanic rocks. Canadian Journal of Earth Sciences 8, 523-548.

Ishizuka, O., 1998. Vertical and horizontal variations of the fast neutron flux in a single irradiation capsule and their significance in the laser-heating $^{40}Ar/^{39}Ar$ analysis. Case study for the hydraulic rabbit facility of the JMTR reactor, Japan. Geochem. J. 32, 243-252.

Ishizuka, O., Uto, K., Yuasa, M., Hochstaedter, A.G., 2002. Volcanism in the earliest stage of back-arc rifting in the Izu-Bonin arc revealed by laser-heating $^{40}Ar/^{39}Ar$ dating. Journal of Volcanology and Geothermal Research 120, 71-85.

Ito, E., White, W.M., Göpel, C., 1987. The O, Sr, Nd and Pb isotope geochemistry of MORB. Chemical Geology 62, 157-179.

Janousek, V., Holub, F.V., 2007. The causal link between HP–HT metamorphism and ultrapotassic magmatism in collisional orogens: case study from the Moldanubian Zone of the Bohemian Massif. Proceedings of the Geologists' Association 118, 75-86.

Janoušek, V., Holub, F., Magna, T., Erban, V., 2010. Isotopic constraints on the petrogenesis of the Variscan Ultrapotassic magmas from Moldanubian Zone of the Bohemian massif. Mineralogia Special Papers 37, 32-36.

Jeffcoate, A.B., Elliott, T., Thomas, A., Bouman, C., 2004. Precise/small sample size determinations of lithium isotopic compositions of geological reference materials and modern seawater by MC-ICP-MS. Geostandards and Geoanalytical Research 28, 161-172.

Jones, A.P., Smith, J.V., 1983. Petrological significance of mineral chemistry in the Agaltha peak and the thumb minettes, Navajo volcanic field. Journal of Geology 91, 643-656.

Kelley, K.A., Plank, T., Ludden, J.N., Staudigel, H., 2003. The composition of altered oceanic crust at ODP sites 801 and 1149. Geochemistry Geophysics Geosystems 4, 1-22.

Kemnitz, H., 2007. The Lausitz graywackes, Saxo-Thuringia, Germany - witness to the Cadomian orogeny - In: Linnemann, U.; Nance, R.D.; Kraft, P.; Zulauf, G. (Eds.), The evolution of Rheic Ocean: from Avalonin-Cadomian active margin to Alleghenian-Variscan collision. Geological Society of America Special Papers 423, 97-141.

Kemnitz, H., Romer, R.L., Oncken, O., 2002. Gondwana break-up and the northern margin of the Saxothuringian belt (Variscides of Central Europe). International Journal of Earth Sciences 91, 246-259.

Kindermann, A., Fiedler, F., Seifert, T., Uhlig, S., 2003. Platinmetall-Führung der Ni-Cu-Sulfidmineralisationen im Bereich der Lausitzer Antiklinalzone. Zeitschrift für Angewandte Geologie 49, 43-47.

Kowalski, P.M., Jahn, S., 2011. Prediction of equilibrium Li isotope fractionation between minerals and aqueous solutions at high P and T: An efficient ab initio approach. Geochimica et Cosmochimica Acta 75, 6112-6123.

Kramer, W., 1976. Zur Petrologie und Metallogenetischen Bedeutung der Dolerite (Lamprophyre) des Lausitzer Massivs. Zeitschrift für Geologische Wissenschaften 4, 975-994.

Kramer, W., 1988. Magmengenetische Aspekte der Lithosphärenentwicklung- Geochemisch-petrologische Untersuchung basaltoider variszischer Gesteins-Formationen sowie mafischer und ultramafischer Xenolithe im nordöstlichen Zentraleuropa. Schriftenreihe für Geologische Wissenschaften 26, pp. 1-136.

Kramer, W., Andrehs, G., 2011. Basische Gangintrusionen im Oberlausitzer Bergland, Ostsachsen. Berichte der Naturforschenden Gesellschaft der Oberlausitz 19, 21-46.

Kramer, W., Müller, B., Peschel, A., 1977. Zur tektonischen und substantiellen Charakteristik der Basite des Lausitzer Antiklinoriums und deren Altersbeziehung. Zeitschrift für Geologische Wissenschaften 5, 95-100.

Krienitz, M.-S., Garbe-Schönberg, C.-D., Romer, R.L., Meixner, A., Haase, K.M., Stroncik, N.A., 2012. Lithium isotope variations in ocean island basalts - implications for the development of mantle heterogeneity. Journal of Petrology 53, 2381-2409.

Krmíček, L., 2010. Pre-Mesozoic lamprophyres and lamproites of the Bohemian Massif (Czech Republic, Poland, Germany, Austria). Mineralogia Special Papers 37, 37-46.

Kröner, A., Hegner, E., 1998. Geochemistry, single zircon ages and Sm-Nd systematics of granitoid rocks from the Gory Sowie (Owl Mts), Polish West Sudetes; evidence for early Palaeozoic arc-related plutonism. Journal of the Geological Society of London 155, 711-724.

Kröner, A., Willner, A.P., 1998. Time of formation and peak of Variscan HP-HT metamorphism of quartz-feldspathic rocks in the Central Erzgebirge, Saxony. Contributions to Mineralogy and Petrology 132, 1-20.

Kroner, U., Goerz, I., 2010. Variscan assembling of the Allochthonous Domain of the Saxo-Thuringian Zone– a tectonic model. In: Linnemann, U., Romer, R.L. (eds.) Pre-Mesozoic Geology of Saxo-Thuringia–From the Cadomian Active Margin to the Variscan Orogen, Schweizerbart, Stuttgart. pp 271-286.

Kroner, U., Romer, R.L. 2010. The Saxo-Thuringian Zone-tip of the Armorican Spur and part of the Gondwana plate. In: Linnemann, U., Romer, R.L. (eds.), Pre-Mesozoic Geology of Saxo-Thuringia. From the Cadomian Active Margin to the Variscan Orogen, Schweizerbart, pp 371-394.

Kroner, U., Romer, R.L., 2013. Two plates - many subduction zones: the Variscan orogeny reconsidered. Gondwana Research, 24: 298-329.

Kroner, U., Hahn, T., Romer, R.L., Linnemann, U., 2007. The Variscan orogeny in the Saxo-Thuringian Zone – Heterogenous overprint of Cadomian/Paleozoic Peri-Gondwana crust. Geological Society of America Special Papers 423, 153-172.

Kroner, U., Mansy, J.L., Mazur, S., Aleksandrowski, P., Hann, H.P., Huckriede, H., Lacquement, F., Lamarche, J., Ledru, P., Pharao, T.C., Zedler, H., Zeh, A., Zuulauf, G., 2008. Variscan tectonics. In McCann, T. (ed). The Geology of Central Europe. Geological Society, London, pp. 599-664.

Kroner, U., Romer, R.L., Linnemann, U., 2010. The Saxo-Thuringian Zone of the Variscan Orogen as part of Pangea. In: Linnemann, U., Romer, R.L. (Eds.), Pre-Mesozoic Geology of Saxo-Thuringia. From the Cadomian Active Margin to the Variscan Orogen Schweizerbart, Stuttgart, pp. 3-16.

Kryza, R., 2008. The Variscides in the West Sudetes: geological setting and review of tectonic models. Mineralogia – Special Papers 32, 21-27.

Kryza, R., Pin, C., 2010. The Central-Sudetic ophiolites (SW Poland): Petrogenetic issues, geochronology and palaeotectonic implications. Gondwana Research 17, 292-305.

Lanphere, M.A., Baadsgaard, H., 2001. Precise K-Ar, $^{40}Ar/^{39}Ar$, Rb-Sr, U/Pb mineral ages from the 27.5 Ma Fish Canyon Tuff reference standard. Chemical Geology 175, 653-671.

Leeman, W.P., Tonarini, S., Chan, L.H., Borg, L.E., 2004. Boron and lithium isotopic variations in a hot subduction zone — the southern Washington Cascades. Chemical Geology 212, 101-124.

Letterrier, J., Maury, R.C., Thonon, P., Girard, D., Marchal, M., 1982. Clinopyroxene composition as a method of identification of the magmatic affinities of paleo-volcanic series. Earth and Planetary Science Letters 59, 139-54.

Le Bas, M.J., 1962. The role of aluminum in igneous clinopyroxenes with relation to their parentage. American Journal of Science 260, 267-288.

Le Maitre, R. W., Bateman, P., Dudek, A., Keller, J., Lameyre, J., Le Bas, M. J., Sabine, P. A., Schmid, R., Sorensen, H., Streickeisen, A., Wooley, A. R., Zanetten, B., 2002. Igneous Rocks: a Classification and Glossary of Terms: Recommendations of the International Union of Geological Sciences Subcommission on the Systematics of Igneous Rocks. Cambridge: Cambridge University Press, 236 pp.

Lindsley, D.H., 1983. Pyroxene thermometry. American Mineralogist 68, 477-93.

Linnemann, U., Romer, R.L., 2002. The Cadomian orogeny in Saxo-Thuringia, Germany: Geochemical and Nd-Sr-Pb isotopic charachterization of marginal basins with constraints to geotectonic setting and provenance. Tectonophysics 352, 33-64.

Linnemann, U., Gehmlich, M., Tichomirowa, M., Buschmann, B., Nasdala, L., Jonas, P., Lützner, H., Bombach, K., 2000. From Cadomian subduction to Early Palaeozoic rifting. The evolution of Saxo-Thuringia at the margin of Gondwana in the light of single zircon

geochronology and basin development (central European Variscides, Germany). In Franke, W., Haak, V., Oncken, O., Tanner, D. (eds.) Orogenic Processes: Quantification and Modelling in the Variscan Belt. Geological Society London Special Publications. 179, 131-153.

Linnemann, U., McNaughton, N.J., Romer, R.L., Gehmlich, M., Drost, K., Tonk, C., 2004. West Africa Provenance for Saxo-Thuringia (Bohemia Massif): Did Armorica ever leave pre-Pangean Gondwana? – U/Pb-SHRIMP zircon evidence and the Nd-isotopic record. International Journal of Earth Sciences 93, 683-705

Linnemann, U., Pereira, F., Jeffries, T.E., Drost, K., Gerdes, A., 2008. The Cadomian Orogeny and the opening of the Rheic Ocean. The diacrony of geotectonic processes constrained by LA-ICP-MS U–Pb zircon dating (Ossa-Morena and Saxo-Thuringian Zones, Iberian and Bohemian Massifs). Tectonophysics 461, 21-43.

Linnemann, U., Romer, R.L., Gerdes, A., Jeffries, T.E., Drost, K., Ulrich, J., 2010a. The Cadomian Orogeny in the Saxo-Thuringian Zone. In: Linnemann, U., Romer, R.L. (eds.), Pre-Mesozoic Geology of Saxo-Thuringia. From the Cadomian Active Margin to the Variscan Orogen, Schweizerbart, pp 37-58.

Linnemann, U., Hofmann, M., Romer, R.L., Gerdes, A., 2010b. Transitional stages between the Cadomian and Variscan orogenies: Basin development and tectono-magmatic evolution of the southern margin of the Rheic Ocean at the Saxo-Thuringian Zone (North Gondwana shelf). In: Linnemann, U., Romer, R.L. (eds.), Pre-Mesozoic Geology of Saxo-Thuringia. From the Cadomian Active Margin to the Variscan Orogen, Schweizerbart, pp 59-99.

Lucinska-Anczkiewicz, A., Villa, I. M., Anczkiewicz, R., Slaczka, A., 2002. $^{40}Ar/^{39}Ar$ dating of alkaline lamprophyres from the Polish Western Carpathians. Geologica Carpathica 53, 45-52.

Macdonald, R., Thorpe, R.S., Gaskarth, J.W., Grindrod, A.R., 1985. Multi-component origin of Caledonian lamprophyres of northern England. Mineralogical Magazine 49, 485-494.

Magna, T., Ackerman, L., Špaček, P., 2013. Lithium isotope evidence for pervasive metasomatism of subcontinental lithospheric mantle in peridotitic xenoliths from the Upper Palatinate, Germany. Basalt 2013 – Cenozoic Magmatism in Central Europe, Abstract, 29-30.

Marheine, D., Kachlík, V., Maluski, H., Patočka, F., Żelaźniewicz, A., 2002. The $^{40}Ar/^{39}Ar$ ages from the West Sudetes (NE Bohemian Massif): constraints on the Variscan polyphase tectonothermal development. Geological Society, London, Special Publications 201, 133-155.

Marschall, H.R., Altherr, R., Ludwig, T., Kalt, A., Gméling, K., Kasztovszky, Z., 2006. Partitioning and budget of Li, Be and B in high-pressure metamorphism. Chemical Geology 239, 323-335.

Marschall, H., Pogge von Strandmann, P.A.E., Seitz, H.-M., Elliott,T., Niu,Y., 2007. The lithium isotopic composition of orogenic eclogites and deep subducted slabs. Earth and Planetary Science Letters 262, 563-580.

Matte, P., 1986. Tectonics and plate tectonics model for the Variscan belt of Europe. Tectonophysics 126, 329-374.

Matte, P., 1991. Accretionary history and crustal evolution of the Variscan belt in western Europe. Tectonophysics 196, 309-337.

Matte, P., 2001. The Variscan collage and orogeny (480-290 Ma) and the tectonic definition of the Armorica microplate: a review. Terra Nova 13, 122-128.

McHone, J.G., 1978. Distribution, orientations, and ages of mafic dikes in central New England. Geological Society of America Bulletin 89, 1645-1655.

McHone, J.G., Butler, J.R., 1984. Mesozoic igneous provinces of New England and the opening of the North Atlantic Ocean: Geological Society of America Bulletin 95, 757-765.

McIntyre, R.M., 1977. Anorogenic magmatism, plate motion and Atlantic evolution. Journal of the Geological Society of London 133, 375-384.

Medaris, L.G., Beard, B. L., Johnson C.M., Valley, J. W., Spicuzza, M.J., Jelinek, K., Misar, Z., 1995. Garnet pyroxenite and eclogite in the Bohemian Massif: geochemical evidence for Variscan recycling of subducted lithosphere. Geologische Rundschau 84, 489-505.

Miller, J.A., Mohr, P.A. 1964. Potassium-argon measurements on the granites and some associated rocks from south-west England. Geological Journal 4, 105-126.

Milovanovic, D., Karamata, S., Banjesevic, M., 2005. Petrology of alkali basalts of Zlot, Timok magmatic complex (Eastern Serbia). Tectonophysics 410, 501-509.

Mingram, B., 1996. Geochemische Signaturen der Metasedimente des erzgebirgischen Krustenstapels. Scientific Technical Report, GeoForschungsZentrum Potsdam, 104 pp.

Mingram, B., 1998. The Erzgebirge, Germany – a subducted part of northern Gondwana: geochemical evidence for repetition of early Paleozoic metasedimentary sequences in metamorphic thrust units. Geological Magazine 135, 785-801.

Mitchell, R.H., 1995. Kimberlites, Orangeites, and related rocks. Plenum Press, New York, 410 p.

Mitchell, R.H., Scott Smith, B.H., Larsen, L.M., 1999. Mineralogy of Ultramafic Dikes from the Sarfartoq, Sisimiut and Maniitsoq Areas, West Greenland. In: Gurney, J.J., Gurney, J.L.,

Pascoe, M.D., Richardson, S.H. (Eds.), Proceedings of the 7th Interna-tional Kimberlite Conference. University of Cape Town, Cape Town, pp. 574-583.

Montigny, R., Azambre, B., Rossy, M., Thuizat, R., 1986. K-Ar Study of Cretaceous magmatism and metamorphism in the Pyrenees: Age and length of rotation of the Iberian Peninsula. Tectonophysics 129, 257-273.

Morimoto, N., 1988. The nomenclature of pyroxenes. Mineralogical Magazine 52, 535-50.

Nédli, Zs., Tóth, T.M., 2007. Origin and geodynamic significance of Upper Cretaceous lamprophyres from the Villány Mts (Hungary). Mineralogy and Petrology 90, 73-107.

Nishio, Y., Nakai, S., Yamamoto, J., Sumino, H., Matsumoto, T., Prikhod'ko, V., Arai, S., 2004. Lithium isotopic systematics of the mantle-derived ultramafic xenoliths: implications for the EM1 origin. Earth and Planetary Science Letters 217, 245-261.

Oliver, G.J.H., Corfu F., Krogh T.E., 1993. U-Pb ages from SW Poland. Evidence for a Caledonian suture zone between Baltica and Gondwana. Journal of Geological Society, London 150, 355-369.

Peccerillo, A., Martinotti, G., 2006. The Western Mediterranean lamproitic magmatism: origin and geodynamic significance. Terra Nova 18, 109-117.

Peschel, A., Müller, B., Kramer, W., 1973. Die basischen Intrusivgesteine der Lausitz und ihre industrielle Nutzung. Freiberger Forschungshefte, C 283, 1-153.

Philpotts, A.R., 1974. The Monteregian province. In: Sorensen, H., (ed.), The Alkaline Rocks. Wiley, London, 293-310.

Pin, C., Majerowicz, A., Wojciechowska, I., 1988. Upper Paleozoic oceanic crust in the Polish Sudetes: Nd–Sr isotope and trace element evidence. Lithos 21, 195-209.

Plank, T., 2005. Constraints from Thorium/Lanthanum on sediment recycling at subduction zones and the evolution of the continents. Journal of Petrology 46, 921-944.

Plank, T., Langmuir., C.H., 1998. The chemical composition of subducting sediments and its consequences for the crust and mantle. Chemical Geology 145, 325-394.

Polat, A., Kerrich, R., Casey, J.F., 1997. Geochemistry of Quaternary basalts erupted along the East Anatolian and Dead Sea Fault zones of southern Turkey: Implications for mantle sources. Lithos 40, 55-68.

Prelević, D., Foley, S.F., Cvetković, V., Romer, R.L., 2004. Origin of minette by mixing of lamproite and dacite magmas in Veliki Majdan, Serbia. Journal of Petrology 45, 759-792.

Prelević, D., Foley, S.F., Romer, R.L., Cvetković, V., Downes, H., 2005. Tertiary ultrapotassic volcanism in Serbia: constraints on petrogenesis and mantle source characteristics. Journal of Petrology 46, 1443-1487.

Prelević, D., Foley, S.F., Cvetković, V., 2007. A review of petrogenesis of Mediterranean Tertiary lamproites: a perspective from the Serbian ultrapotassic province. In: Beccaluva, L., Bianchini, G., Wilson, M., (eds.), Cenozoic Volcanism in the Mediterranean Area: Geological Society of America Special Papers 418, 113-129.

Prelević, D. Foley, S.F., Romer R., Conticelli, S., 2008. Mediterranean Tertiary lamproites derived from multiple source components in postcollisional geodynamics. Geochimica et Cosmochimica Acta 72, 2125-2156.

Prelević, D., Akal, C., Romer, R.L., Foley, S.F., 2010. Lamproites as indicators of accretion and/or shallow subduction in the assembly of south-western Anatolia, Turkey. Terra Nova 22, 443-452.

Prelević, D., Stracke, A., Foley, S.F., Romer, R.L., Conticelli, S., 2010a. Hf isotope compositions of Mediterranean lamproites: mixing of melts from asthenosphere and crustally contaminated lithosphere. Lithos 119, 297-312.

Prelević, D., Akal, C. Foley, S.F., Romer, R.L., Stracke, A., van den Bogaard, P., 2012. Ultrapotassic mafic rocks as geochemical proxies for postcollisional mantle dynamics of lithosphere: the case of SW Anatolia, Turkey. Journal of Petrology 49, 1-37.

Price, S., Russell, J.K., Kopylova, M.K., 2000. Primitive magma from the Jericho pipe, N.W.T., Canada; Constraints on primary kimberlite melt chemistry. Journal of Petrology 41, 789-808.

Renno, A.D., Stanek, K.P., Lobst, R., Pushkarev, Y., 2003a. A new lamprophyre species from the Klunst quarry (Ebersbach, Lusatia, Germany) – geochemical and petrological implications. Zeitschrift für Geologische Wissenschaften 31, 1-20.

Renno, A.D., Hacker, B.R., Stanek, K.P., 2003b. An Early Cretaceous (126 Ma) utramafic alkaline lamprophyre from the Quarry Klunst (Ebersbach, Lusatia, Germany). Zeitschrift für Geologische Wissenschaften 31, 31-36.

Renno, A.D., Haser, S., Stanek, K.P., Götze, J., 2003c. Mineral chemistry and petrogenesis of ultramafic alkaline lamprophyre dyke from the Klunst Quary in Ebersbach (Lusatia, Germany). Geolines 15, 133-139.

Rötzler, K., Plessen, B., 2010. The Erzgebirge: a pile of ultrahigh- to low-pressure nappes of Early Palaeozoic rocks and their Cadomian basement. In: Linnemann, U., Romer, R. L. (Eds.), Pre-Mesozoic Geology of Saxo-Thuringia - From the Cadomian Active Margin to the Variscan Orogen, Schweizerbart, 253-270.

Rötzler, K., Schumacher, R., Maresch, W.V., Willner, A.P., 1998. Characterization and geodynamic implications of contrasting metamorphic evolution in juxtaposed high-pressure

units of the Western Erzgebirge (Saxony, Germany). European Journal of Mineralogy 10, 261-280.

Rock, N.M.S., 1977. The nature and origin of lamprophyres: some definitions, distinctions and derivations. Earth Science Reviews 13, 123-169.

Rock, N.M.S., 1987. The nature and origin of lamprophyres; an overview. The nature and origin of lamprophyres: an overview. In: Fitton, J.G., Upton, B.G.J. (Eds.) Alkaline Igneous Rocks. Geological Society, London, Special Publications 30, 191-226.

Rock, N.M.S., 1991. Lamprophyres. Blackie & Son, Glasgow, pp. 43-46.

Romer, R.L., Hahne, K., 2010. Life of the Rheic Ocean: Scrolling through the shale record. Gondwana Research 17, 236-253.

Romer, R.L., Förster, H. J., Breitkreuz, Chr., 2001. Intracontinental extensional magmatism with a subduction fingerprint: the late Carboniferous Halle Volcanic Complex (Germany). Contributions to Mineralogy and Petrology 141, 201-221.

Romer, R. L., Förster, H. J., Stemprok, M., 2010. Age constraints for the late-Variscan magmatism in the Altenberg-Teplice Caldera (Eastern Erzgebirge/Krusne Hory). Neues Jahrbuch für Mineralogie Abhandlungen 187, 289-305.

Romer, R.L., Heinrich W., Schröder-Smeibidl, B., Meixner, A., Fischer, C.-O., Schulz, C., 2005. Elemental dispersion and stable isotope fractionation during reactive fluid-flow and fluid immiscibility in the Bufa del Diente aureole, NE-Mexico: Evidence from radiographies and Li, B, Sr, Nd, and Pb isotope systematics. Contributions to Mineralogy and Petrology 149, 400-429.

Romer, R.L., Förster, H.-J., Hahne, K., 2012. Strontium isotopes – a persistent tracer for the recycling of Gondwana crust in the Variscan Orogen. Gondwana Research 22, 262-278.

Romer, R.L., Meixner, A., Hahne, K., (subm.). Lithium and boron in collisional orogens: 1. Isotopic variability of subducted sediments – the role of source history and depositional environment. Geochimica et Cosmochimica Acta.

Rossy, M., Azambre, B., Albarede, F., 1992. REE and Sr–Nd isotope geochemistry of the alkaline magmatism from the Cretaceous North Pyrenean Rift Zone (France-Spain). Chemical Geology 97, 33-46.

Rudnick, R.L., 1995. Making continental crust. Nature 378, 571-578.

Rudnick, R.L., Fountain, D.M., 1995. Nature and composition of the continental crust; a lower crustal perspective. Reviews of Geophysics 33, 267-309.

Rudnick, R.L., Tomascak, P.B., Heather, B.N., Gardner, L.R., 2004. Extreme lithium isotopic fractionation during continental weathering revealed in saprolites from South Carolina. Chemical Geology 212, 45-57.

Saunders, A.D., Norry, M. J., Tarney, J., 1988. Origin of MORB and chemically depleted mantle reservoirs: trace element constraints. Journal of Petrology, Special volume 1, 415-445.

Scarrow, J.H., Molina, J.F., Bea, F., Montero, P., Vaughan, A.P.M., 2011. Lamprophyre dikes as tectonic markers of late orogenic transtension timing and kinematics: A case study from the Central Iberian Zone. Tectonics 30, 1-22.

Schust, F., 2000. Zum magmengeologischen Bau und zur Altersdatierung des Lausitzer prävariszischen Granitoidkomplexes. Zeitschrift für Geologische Wissenschaften 28, 111-132.

Seifert, Th., 2008. Metallogeny and Petrogenesis of Lamprophyres in the Mid-European Variscides: Post-Collisional Magmatism and Its Relationship to Late-Varsican Ore Forming Processes (Bohemian Massif). IOS Press BV, Amsterdam, Netherlands, pp. 1-128.

Shervais, J. W., 1982. Ti-V plots and the petrogenesis of modern and ophiolitic lavas, Earth and Planetary Science Letters 59, 101-118.

Spandler, C., Hermann, J., Arculus, R., Mavrogenes, J., 2003. Redistribution of trace elements during prograde metamorphism from lawsonite blueschist to eclogite facies: implications for deep subduction-zone processes. Contributions to Mineralogy and Petrology 146, 205-222.

Stille, P., Oberhänsli, R., Wenger-Schenk, K., 1989. Hf-Nd isotopic and trace element constraints on the genesis of alkaline and calc-alkaline lamprophyres. Earth and Planetary Science Letters 96, 209-219.

Stosch, H.-G., Lugmair, G.W., 1990. Geochemistry and evolution of kyanite-bearing eclogites from the Münchberg massif, southern Germany. Earth and Planetary Science Letters 99, 230-249.

Stalder R., Foley S. F., Brey G. P., Horn I., 1998. Mineral-aqueous fluid partitioning of trace elements at 900–1200°C and 3.0–5.7 GPa: New experimental data for garnet, clinopyroxene, and rutile, and implications for mantle metasomatism. Geochimica et Cosmochimica Acta 62, 1781-1801.

Staudigel, H., Davies, G.R., Hart, S.R., Marchant, K.M., Smith, B.M., 1995. Large scale isotopic Sr, Nd and O isotopic anatomy of altered oceanic crust: DSDP/ODP sites 417/418. Earth and Planetary Science Letters 130, 169-185.

Stille, P., Oberhänsli, R., Wenger-Schenk, K., 1989. Hf-Nd isotopic and trace element constraints on the genesis of alkaline and calc-alkaline lamprophyres. Earth and Planetary Science Letters 96, 209-219.

Stosch, H.-G., Lugmair, G.W., 1990. Geochemistry and evolution of kyanite-bearing eclogites from the Münchberg massif, southern Germany. Earth and Planetary Science Letters 99, 230-249.

Su, B.-X., Zhang, H.-F., Deloule, E., Sakyi, P.A., Xiao, Y., Tang, Y.-J., Hu, Y., Ying, J.-F., Liu, P.P., 2012. Extremely high Li and low □7Li signatu Chemical Geology 292-293, 149-157.

Sun, C.M., Bertrand, J., 1991. Geochemistry of clinopyroxenes in plutonic and volcanic sequences from the Yanbian Proterozoic ophiolites (Sichuan Province, China): Petrogenetic and geotectonic implications. Schweizer Mineralogische und Petrographische Mitteilungen 71, 243-59.

Sun, S.S., McDonough, W.F., 1989. Chemical and isotopic systematics of oceanic basalts: Implications for the mantle composition and processes. In Saunders, A.D., and Norry, M.J. (Eds.). Magmatism in the Ocean Basins. Geological Society, London, Special Publications 42, 313-345.

Tappe, S., Foley, S.F., Jenner, G.A., Heaman, L.M., Kjarsgaard, B.A., Romer, R.L., Andreas Stracke, A., Hoefs, J., 2006. Genesis of utramafic lamprophyres and carbonatites at Aillik Bay, Labrador: A consequence of incipient lithospheric thinning beneath the North Atlantic craton. Journal of Petrology 47, 1261-1315.

Tappe, S., Foley, S.F., Stracke, A., Romer, R.L., Kjarsgaard, B.A., Heaman, L.M., Joyce, N., 2007. Craton reactivation on the Labrador Sea margins: 40Ar/39Ar age and Sr–Nd–Hf–Pb isotope constraints from alkaline and carbonatite intrusives. Earth and Planetary Science Letters 256, 433-454.

Tappe, S., Foley, S.F., Kjarsgaard, B.A., Romer, R.L., Heaman, L.M., Stracke, A., Jenner, G.A., 2008. Between carbonatite and lamproite - Diamondiferous Torngat ultramafic lamprophyres formed by carbonatefluxed melting of cratonic MARID-type metasomes. Geochimica et Cosmochimica Acta 72, 3258-3286.

Tatsumi Y., Hamilton D.L., Nesbitt R.W., 1986. Chemical characteristics of fluid phase released from a subducted lithosphere and origin of arc magmas: Evidence from high-pressure experiments and natural rocks. Journal of Volcanology and Geothermal Research 29, 293-309.

Taylor, S.R., McLennan S.M., 1985. The Continental Crust: Its Composition and Evolution. Blackwell, Oxford. 312 pp.

Taylor, S.R., McLennan, S.M., 1995. The geochemical evolution of the continental crust. Reviews of Geophysics 33, 241-265.

Teng, F.Z., McDonough, W.F., Rudnick, R.L., Dalpe, C., Tomascak, P.B., Chappell, B.W., Gao, S., 2004. Lithium isotopic composition and concentration of the upper continental crust. Geochimica et Cosmochimica Acta 68, 4167-4178.

Tomascak P.B., 2004. Developments in the understanding and application of lithium isotopes in the Earth and planetary sciences. In: Johnson CM., Beard BA., Albarede F. (eds), Geochemistry of Non-Traditional Isotope Systems, Reviews in Mineralogy and Geochemistry 55, 153-195.

Tomascak, P.B., Carlson, R.W, Shirey, S.B., 1999. Accurate and precise determination of Li isotopic compositions by multi-collector sector ICP-MS. Chemical Geology 158, 145-154.

Tomascak, P.B., Langmuir, C.H., le Roux, P.J., Shirey, S. B., 2008. Lithium isotopes in global mid-ocean ridge basalts. Geochimica et Cosmochimica Acta 72, 1626-1637.

Tonarini, S., Agostini, S., Innocenti, F., Piero Manetti, P., 2005. $\delta^{11}B$ as tracer of slab dehydration and mantle evolution in Western Anatolia Cenozoic Magmatism. Terra Nova, 17, 259-264.

Turpin, L., Cuney, M., Friedrich, M., Bouchez, J.L. and Aubertin, M., 1990. Meta-igneous origin of Hercynian peraluminous granites in N-W French Massif Central: implications for crustal history reconstructions. Contribution to Mineralogy and Petrology 104, 163-172.

Turpin, L., Velde, D., Pinte, G., 1988. Geochemical comparison between minettes and kersantites from the western European Hercynian orogen. trace element and Pb-Sr-Nd isotope constraints on their origin. Earth and Planetary Science Letters 87, 73-86.

Uto, K., Ishizuka, O., Matsumoto, A., Kamioka, H., Togashi, K., 1997. Laser-heating $^{40}Ar/^{39}Ar$ dating system of the Geological Survey of Japan. system outline and preliminary results. Bulletin of the Geological Survey of Japan 48, 23-46.

van Keken, P.E., Hauri, E. H., Ballentine, C. J., 2002. Mantle Mixing: The generation, preservation, and destruction of chemical heterogeneity. Annual Review of Earth and Planetary Sciences 30, 493-525.

von Seckendorf, V., Timmerman, M.J., Kramer, W., Wrobel, P., 2004. New $^{40}Ar/^{39}Ar$ ages and geochemistry of Late Carboniferous-early Permian lamprophyres and related volcanic rocks in the Saxothuringian Zone of the Variscan Orogen (Germany). In: Wilson M., Neumann E.R., Timmermann G.R., Heremans M., Larsen B.T. (eds), Permo-Carboniferous

Magmatism and Rifting in Europe. Geological Society, London, Special Publications 223, 335-359.

Wass, S. Y., 1979. Multiple origine of clinopyroxenes in alkali basaltic rocks. Lithos. 12, 115-132.

Walter, R., 2007. Geologie von Mitteleuropa. 7. Auflage, Schweizerbart'sche Verlagsbuchhandlung, Stuttgart, pp. 1-511.

Wenzel, T., Mercolli, I., Oberhänsli, R., 1991. The plutonic rocks of the Meissen Massif (Germany): evidence for open and closed system fractionation processes. Schweizer Mineralogische und Petrographische Mitteilungen 71, 371-390

Wenzel, Th., Mertz, F.D., Oberhänsli, R., Becker., T., 1997. Age, geodynamic setting, and mantle enrichment processes of a K-rich intrusion from the Meissen massif (northern Bohemian massif) and implications for related occurrences from the mid-European Hercynian. Geologische Rundschau 86, 556-570.

Willner, A.P., Krohe, A., Maresch, W.V., 2000. Interrelated PT-t-d Paths in the Variscan Erzgebirge Dome (Saxony, Germany): Constraints on the rapid Exhumation of High-Pressure Rocks form the Root Zone of a Collisional Orogen. International Geology Review 42, 64-85.

Winchester, J.A., Floyd, P.A., 1977. Geochemical discrimination of different magma series and their differentiation products using immobile elements. Chemical Geology 20, 325-343.

Wood, D.A., 1980. The application of a Th–Hf–Ta diagram to problems of tectonomagmatic classification and establishing the nature of crustal contamination of basaltic lavas of the British Tertiary volcanic province. Earth and Planetary Science Letters 50, 11-30.

Workman, R.K., Hart, S.R., 2005. Major and trace element composition of the depleted MORB mantle (DMM). Earth and Planetary Science Letters 231, 53-72.

Wunder, B., Meixner, A., Romer, R. L., Heinrich, W., 2006. Temperature-dependent isotopic fractionation of lithium between clinopyroxene and high-pressure hydrous fluids. Contributions to Mineralogy and Petrology 151, 112-120.

Wunder, B., Meixner, A., Romer, R. L., Feenstra, A., Schettler, G., Heinrich, W., 2007. Lithium isotope fractionation between Li-bearing staurolite, Li-mica and aqueous fluids: an experimental study. Chemical Geology 238, 277-290.

Wunder, B., Meixner, A., Romer, R.L., Jahn, S., 2011. Li-isotope fractionation between silicates and fluids: pressure dependence and influence of the bonding environment. European Journal of Mineralogy 23, 333-342.

Yagi, K., Onuma, K., 1967. The join $CaMgSi_2O_6$-$CaTiAl_2O_6$ and its bearing in titanaugites, Journal of the Faculty of Science. Hokkaido University Series IV 13, 117-138.

Zack, T., Tomascak, P.B., Rudnick, R.L., Dalpe, C., McDonough,W. F., 2003. Extremely light Li in orogenic eclogites; the role of isotope fractionation during dehydration in subducted oceanic crust. Earth and Planetary Science Letters 208, 279-290.

Zartman, R.L., Doe. B.R., 1981. Plumbotectonics-the model. Tectonophysics 75, 135-162.

Zeh, A., Will, T.M., 2010. The mid-German crystalline zone. In: Linnemann, U., Romer, R.L. (eds.), Pre-Mesozoic Geology of Saxo-Thuringia. From the Cadomian Active Margin to the Variscan Orogen, Schweizerbart, Stuttgart, pp 195-220.

Ziegler, P.A., 1988. Evolution of the Arctic-North Atlantic and the western Tethys. American Association of Petroleum Geologist, Memoir 43, 198pp.

Zindler, A., Hart, S., 1986. Chemical geodynamics. Annual Review of Earth and Planetary Sciences 14, 493- 571.

Zuleger, E., Erzinger, J., 1988. Determination of REE and Y in silicate materials with ICP-AES. Fresenius' Zeitschrift für analytische Chemie 332, 140-143.